Sustainability of groundwater resources in Kumasi, Ghana

Estimating potential groundwater recharge using a water-balance approach and remote-sensing data in Google Earth Engine.

E. Fernandes Potter

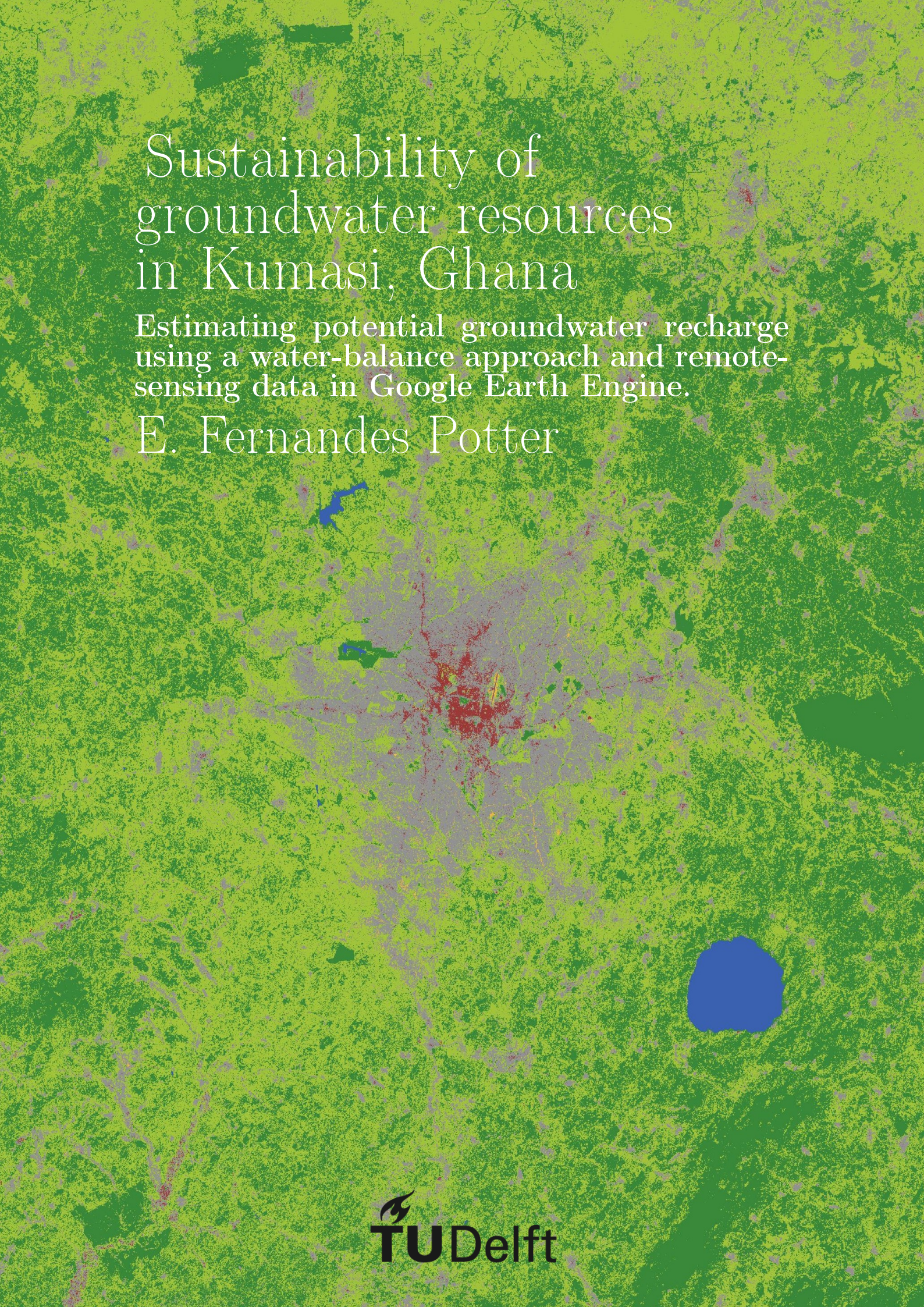

TU Delft

Sustainability of groundwater resources in Kumasi, Ghana

Estimating potential groundwater recharge using a water-balance approach and remote-sensing data in Google Earth Engine.

by

Estela Fernandes Potter

in partial fulfillment of the requirements for the degree of

Master of Science

in Water Management

at the Delft University of Technology,

to be defended publicly on Friday 8 October at 16:00.

Student number:	4554027	
Thesis committee:	Dr. ir. M. M. Rutten,	TU Delft, chair
	Dr. ir. D. van Halem,	TU Delft
	Dr. I. Monney,	AAMUSTED
	D. de Villiers,	AWC

An electronic version of this thesis is available at `http://repository.tudelft.nl/`.

Cover image: Land use classification of greater Kumasi in 2020.

TU Delft

Preface

Challenges in water management are tied to the complexity of hydrological studies alongside the importance of water for socio-economic well-being and environmental protection. The multi-disciplinary aspect of water management caught my attention during the first months of following this study. When choosing my thesis topic I knew this was something I wanted to do, which is how decided to do my thesis with the African Water Corridor. The freedom of choosing a topic allowed me to pursue something under my area of interest, making the whole process a challenging but very enjoyable endeavour.

Five years ago I stared my journey at TU Delft, which would not have been possible if not for my parents giving me the opportunity to pursue my education in the Netherlands. I am immensely grateful to them. Thank you to my girls (the potathoes) for being such an amazing friend group. To capoeira and my capoeirista friends, I am grateful for all the rodas, music, and laughter. My time in Delft has been so enjoyable, largely in part to the friends I have made. A special thanks goes out to Owen, who bared with me through every small challenge during this process. The conversations about our respective topics have helped me think deeper and work harder.

To my thesis committee: I would like to express my gratitude to Martine for the numerous meetings and detailed feedback. This made me challenge my way of thinking and moulded this thesis into what it is today. Thank you to Isaac, without whom I would have never come across this topic. I am grateful for his enthusiasm, insights and trust in me to carry out the project. I would also like to thank Didier for his feedback and our chats, which helped me understand what my results mean for real-life applications and future challenges. And of course, thank you to Doris who stepped in to save the day.

Writing my thesis has shown me how much I have learnt during this masters but also how much there is yet to learn. Methods to assess groundwater sustainability are continuously developing and changing. I am excited to see how this field of study will progress to adapt to major challenges such as urbanisaion and climate change.

Estela Fernandes Potter
Delft, 2021

Abstract

Groundwater use has seen a significant increase in the rapidly urbanising city of Kumasi, Ghana, due to its reliability, general good quality, and low-cost development. Conversion of vegetated to urban land along with the challenges of growing groundwater abstraction has put the groundwater system at risk. This study aims to assess how the urbanisation trends in Kumasi affect the availability of groundwater resources. Sustainability is investigated by comparing (multi-)annual groundwater withdrawals to long-term average annual replenishment. Groundwater recharge is estimated in Google Earth Engine using a water-balance approach and remote-sensing datasets to bridge the hydrological data gap. Runoff is determined using the Soil Conservation Service Curve-Number (SCS-CN) method requiring soil and land-cover maps. Land-cover maps are created for 1986, 2013, and 2020 using Sentinel-2 and Landsat 8 surface reflectance products. Evapotranspiration is derived from the MODIS evapotranspiration product and precipitation is retrieved from CHIRPS. Results indicate that groundwater recharge decreased by 80% from 1986 to 2020 ($124Mm^3$ to $28.9Mm^3$) attributed to a loss of permeable land (63 percentage point decrease) and intensification of urbanisation. Domestic and non-domestic groundwater consumption in 2020 is estimated to be $28.4Mm^3$ and $2.7Mm^3$ respectively. For 2020, long-term average groundwater recharge ($28.9Mm^3$) is less than the annual abstraction ($31.1Mm^3$) indicating current urbanisation trends are unsustainable for future groundwater availability. Under a "business as usual" scenario, population growth presents the largest challenge for the future by causing an estimated four-fold increase in groundwater consumption by 2050. Climate change and land-cover changes under the same scenario may reduce groundwater recharge by 10% and 55% respectively. This requires the implementation of policies to properly manage the groundwater resource, such as promoting low-impact development, monitoring groundwater use, and monitoring changes in the groundwater system. This study should be seen as a preliminary investigation into the components affecting groundwater sustainability. Further research is needed to assess the exact state of the groundwater system and its response to future challenges.

Contents

List of Figures

List of Tables

1 Introduction

1.1 Urbanisation and growing water demand

Urbanisation is a global phenomenon with 55% of the world's population currently residing in urban areas, a percentage which is expected to increase by two-thirds by 2050 (Abass et al., 2018). Nowhere is this growth as rapid as in Sub-Saharan Africa, where the urban population is expected to double within the next 20 years (Foster et al., 2020). This unprecedented growth has lead to great challenges for fresh water supply and availability emphasising the importance of sustainable management of water resources.

Ghana's urbanisation rates have outpaced West Africa's, with 51% of the population now living in towns and cities (Abass et al., 2018). Since 1960, Ghana has been experiencing high rates of urbanisation due to rural-urban migration and the transformation of rural settlements into towns (Ghana Statistical Service, 2013b). The country's current population growth rate is 2.5% with the fastest growth rate being seen in the city of Kumasi (Ghana Statistical Service, 2013b). According to the last population census in 2010, the population of the Kumasi Metropolitan Area (KMA) was 2,035,064 and the growth rate was at 5.5% contributing to 20% of the Ghana's urban growth (Ghana Statistical Service, 2013b). Urbanisation poses an enormous challenge for urban planning, water management, and sanitation services (Foster et al., 2020). It is therefore expected that as the population of Kumasi continues to grow, so will the demand for water resources and infrastructure.

In Kumasi the majority of the population relies on piped water access, however this access dropped from 83% in 2000 to 75% in 2010 (World Bank, 2015). This can be attributed to issues such as frequent system losses, ineffective maintenance, and insufficient investments from the water sector to meet the increasing demand in new communities (World Bank, 2015). To supplement this demand, residents have resorted to groundwater as an alternate source (Ewusi et al., 2016). Water wells in urban areas are prone to many challenges, the two largest hazards being degradation in quality and over-exploitation (Foster et al., 2020). The trend of increased groundwater usage in Kumasi is expected to continue due to its growing population, putting groundwater at the risk of pollution and over-exploitation.

1.2 Problem statement

The decreasing quality and availability of fresh water resources in urbanising areas worldwide has lead to a steady increase of non-renewable groundwater use and consequently high rates of aquifer depletion (Bierkens & Wada, 2019). Groundwater plays an important role in satisfying the water demand of areas with low availability of other water resources (Graaf et al., 2017). In cities where groundwater is available, utility wells can cheaply and rapidly be constructed in developing outer districts (Foster et al., 2020). This is what is being seen in the rapidly urbanising city of Kumasi. Groundwater is also important in rural communities as it has become a cost-effective water supply option (Gumma & Pavelic, 2013). In order to ensure the sustainable usage of groundwater resources, policies need to be put in place to control and manage the resources. However, this can only be done with sufficient comprehension of the current state of the resource. In Kumasi there is a lack of information regarding how much groundwater is being used annually for domestic and commercial users and how much groundwater is physically available.

Groundwater processes are difficult to measure and are not directly visible, making many studies involved highly uncertain (Fitts, 2013). MacDonald et al. (2021) explains that although there has been no recent evidence of a significant decline in groundwater storage in Africa, localised depletion has been observed in urban areas such as in Morocco and Kenya. When investigating the groundwater system in Kumasi only 13 search results in Scopus for "groundwater" and "Kumasi" are available, where the majority investigate groundwater quality. Hydrogeological assessments of the whole of Ghana do exist from the Africa Groundwater Atlas (see O'Dochartaigh et al. (2019) and Kortatsi (1994), but these are at a coarse scale and fail to provide details on local

aquifer conditions in and around Kumasi. Moreover, studies on recharge rates and temporal and spatial monitoring of groundwater variations are missing. All in all, there is no good overview available on the groundwater system in Kumasi. This is important to have if the effects of urbanisation on groundwater availability are to be well understood. Especially in the context of an increasingly large population resorting to groundwater use and urban growth, it is necessary to ensure sustainable groundwater use takes place. This requires investigating how much groundwater is available in Kumasi, how much is being used, and how groundwater will be affected by the population explosion. The focus of this study is on the challenge of Kumasi's urbanisation for the availability of groundwater resources.

Rapid urban growth is affecting sustainable groundwater usage on two fronts. Firstly in relation to population growth that increases water demand consequently increasing water abstraction. Secondly, land use changes are affecting infiltration that leads to recharge of the aquifers. A detailed comprehension of both aspects of sustainable groundwater usage is required to properly manage the resource and avoid consequences such as groundwater depletion.

1.3 Research questions and research approach

Urbanisation in Kumasi has come hand in hand with an increase in groundwater usage and a loss of permeable surfaces important for infiltration. As populations continue to grow and the urban area expands and intensifies, this brings up the research question:

To what extent are the urbanisation trends in Kumasi sustainable for the availability of the groundwater resources?

This research question consists of three parts: (1) availability of groundwater resources, (2) urbanisation trends, and (3) sustainability. Each part is investigated in order to answer the final research question.

The largest obstacle in this study is the scarcity of information on groundwater resources. In Kumasi, data on groundwater levels is not readily available and has not been monitored in the long term. Using Earth Observation technologies to estimate components of the water cycle can bridge this data gap. Remote sensing provides global datasets that can be used for purposes such as monitoring rainfall patterns or distinguishing land use categories (Meijerink, 2007). The aim of this study is therefore to use Earth Observation data to map groundwater recharge patterns in Kumasi and compare these to the urban water demand. However, working with large spatial datasets can be problematic for GIS programmes due to computational overload. Therefore, in this study all remote sensing based calculations are done in Google Earth Engine, which is a cloud-based geospatial analysis platform where satellite imagery is publicly stored to be used for visualisation and analysis. Recharge is calculated for each grid cell (30m x 30m) and each time step (monthly) in Kumasi. The aim of this study is therefore to use Earth Observation data to map groundwater recharge patterns in Kumasi and compare these to the urban water demand.

1.4 Collaborative approach

Kumasi is not alone in the challenges faced from urbanisation. According to Foster et al. (2020) 528 cities in Sub-Saharan Africa are growing at a rate of 3.9%, prompting the need for collaboration between different partners to create solutions for the increasing issues surrounding water. This is the aim of the African Water Corridor (AWC), which is striving to co-create projects focusing on different water issues together with African partners. Sustainable development is emphasised through co-creation of innovative, open-source technologies and sustainable implementation strategies.

One of these initiatives was introduced by Dr. Monney from Akenten Appiah-Menka University of Skills Training and Entrepreneurial Development (AAMUSTED) focusing on the sustainable utilisation of groundwater resources in the Kumasi Metropolis. The overall aim of the larger project is to provide baseline data on the available groundwater and its quality, and to quantify the extent of groundwater usage in Kumasi. The current scope of the greater project is divided into

two research topics: one is the focus of this study, and the other research will focus on determining the spatial distribution of groundwater use in Kumasi characterising how much water is used and for which purposes, eventually also assessing water quality. The focus of this study is in identifying important zones for recharge and how urbanisation has affected recharge in Kumasi. The project will mostly be carried out using GIS/remote-sensing tools, which is beneficial when carrying out research in data-sparse environments. As this study was conducted remotely, collaboration with local professors and students was important to promote an enhanced understanding of the local context. Methods developed here can eventually be applied to other rapidly growing cities in Africa. As case-specific information will differ, it will be important to create an open-source tool that can be adapted to different cities.

2 Background information

2.1 Groundwater availability

2.1.1 Natural groundwater availability

In order to understand sustainable groundwater use, the fluxes determining groundwater availability need to be well understood. The following section summarises the fluxes affecting groundwater and the natural processes governing groundwater availability as described by Fitts (2013), unless stated otherwise. Subsurface waters are categorised into the unsaturated zone close to the surface and the deeper saturated zone. In the unsaturated or vadose zone, pore water pressure is less than atmospheric pressure and pore spaces contain air and water. The saturated zone is where pore water pressures are higher than the atmospheric and pores are fully saturated with water, which is referred to as groundwater. The boundary between the two zones is called the phreatic surface or water table. Figure 2.1 shows the different zones and fluxes affecting groundwater.

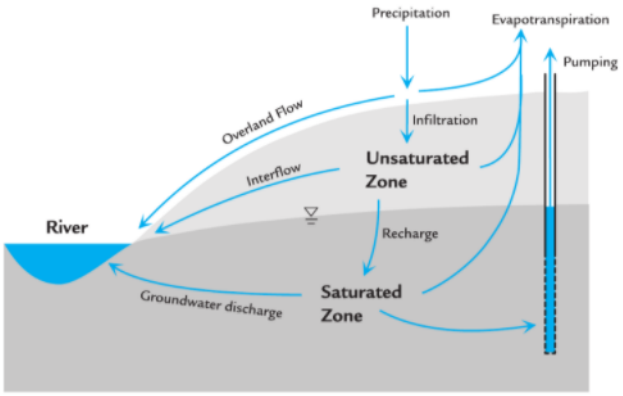

Figure 2.1: Fluxes affecting groundwater. Retrieved from (Fitts, 2013).

After a precipitation event water infiltrates the surface and flows through soil into the unsaturated zone. Water in the unsaturated zone can then seep through to the water table, leading to groundwater recharge. Water in the unsaturated zone may also flow towards surface water bodies as interflow. Therefore, not all water that infiltrates reaches the water table, which is a common conceptual problem when modelling groundwater (Vries & Simmers, 2002). Groundwater recharge can be a result of rainfall infiltration through soil to the water table, lateral or vertical movement from other groundwater bodies, or seepage from surface water bodies (Theis, 1940). It can result from a combination of these sources, which have been grouped as direct, localised, and indirect recharge respectively (Vries & Simmers, 2002). In the unsaturated zone water can be taken up by plant roots, leaving the subsurface through evapotranspiration. Sources of extraction of groundwater are discharge to surface water bodies, pumping, and water uptake of deep-rooted plants. In arid climates where the depth to the saturated zone is significant, water may also be drained from the surface water bodies to groundwater, this stream is defined as a losing stream (Bierkens & Wada, 2019). In humid climates such as in Kumasi, gaining streams exist where groundwater discharge contributes to streamflow.

Fitts (2013) explains there are five factors that affect groundwater recharge rates, namely precipitation, permeability, topography, vegetation, and urbanisation. The key governing factor is precipitation, as this determines the availability of water at the surface. Permeability is also important for recharge as a high permeability allows water to easily infiltrate the soil resulting in higher recharge rates. Topography affects recharge as steep slopes result in faster runoff allowing less water to infiltrate. Moreover, smaller-scale topographic depressions can accumulate water runoff leading to zones of high infiltration. Another governing factor is vegetation: highly vegetated

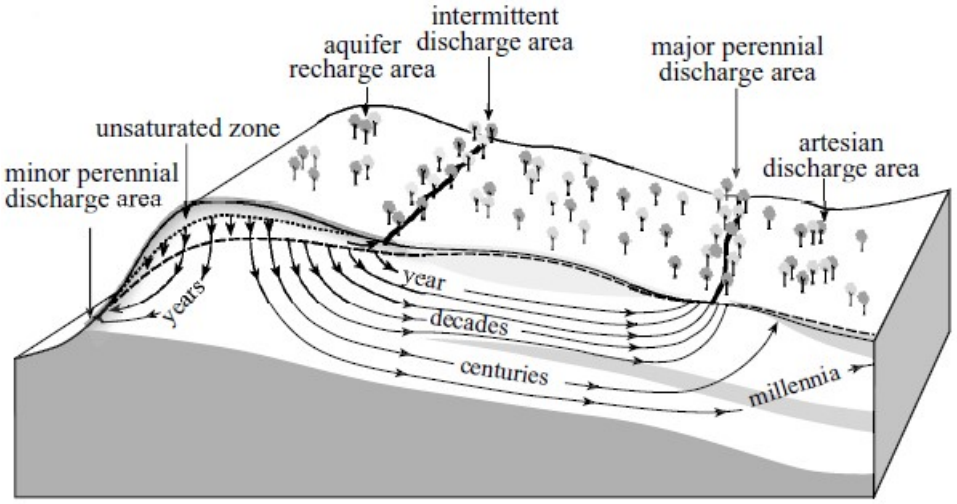

Figure 2.2: Typical groundwater systems in humid regions. Dotted line: groundwater, dashed line: piezometric level. Retrieved from Foster & Chilton (2003).

areas have more effective transpiration thus tend to have lower recharge rates than less vegetated areas as more water is extracted from the system. When looking at agricultural zones, an area experiencing irrigation may have enhanced recharge due to infiltration of excess water. Lastly, urbanisation alters the natural system and the increase in paved surfaced and built structures limit infiltration. Urbanisation can also enhance recharge, such as with the construction of reservoirs that lift the groundwater table over a large area or sewer systems and water pipes may leak creating new recharge sources. The storage of water in aquifers is important in the context of climate change and urbanisation, as inputs of water are buffered due to the duration of recharge Foster & Chilton (2003). Figure 2.2 shows the residence periods and typical duration of recharge from the source to point of discharge. Recharge is notably heavily dominated by infiltration. The volume of recharge depends on the availability of water and infiltration capacity of the soil. Infiltration capacity is consequently dependent on topography, surface and subsurface permeability.

2.1.2 Groundwater-surface water interaction

In groundwater recharge studies the groundwater-surface water interaction is often neglected (Bierkens & Wada, 2019). However, this is an important flux to consider due to the effect that surface water can have on groundwater recharge. In locations with intermittent streams, such as Kumasi, the conditions of the streams change rapidly in response to rain events (Vu et al., 2018). Whether the stream is a gaining or losing stream depends on climatic and topographic factors. Bierkens & Wada (2019) explains gaining streams are typical in (semi-)humid climates or at locations where infiltrated water converges to, such as lower parts of the catchment. Losing streams are dominant in dry climates and locations high in the catchment with permeable soils. Within the same catchment there may be different streams simultaneously present at different locations (Bierkens & Wada, 2019). In this study it is assumed that streams in Kumasi are gaining streams due to the humid climate and non-perennial nature of the streams, indicating they cannot contribute to the replenishment of the groundwater system during the dry season.

2.1.3 Urbanisation and groundwater

Naturally, aquifers are in state of dynamic equilibrium where fluctuations can occur that are generally balanced out over seasonal or climatic cycles (Theis, 1940). Urban environments can cause imbalances in this equilibrium, requiring the equilibrium to be retained by increasing recharge of the aquifer, decreasing old natural discharge, or storage loss of the aquifer (Theis, 1940). A simple analysis of the effects of urbanisation on groundwater is complex as urbanisation alters

all parts of the hydrological cycle (Lerner, 1990). Urbanisation alters the frequency, volume and quality of groundwater recharge by modifying existing mechanisms and introducing new ones (Foster & Chilton, 2003). An overview of the urban effects on groundwater recharge are shown in Figure 2.3 as explained by Lerner (1990). When focusing on groundwater availability, the urban environment influences both abstraction and recharge processes. Growing populations lead to an increase in water demand, hence increasing groundwater use. Concerning groundwater recharge, the most visible effect is infiltration reduction due to the increase of impermeable surfaces such as buildings, roads, and other paved surface coverings. Lerner (1990) explains this results in a reduction of direct recharge in urban areas. However, water is often imported from outside the urban boundary to supply water to the urban population. This water is subject to leakages and losses that can lead to increased recharge in the urban areas. Over-irrigation of parks and gardens can also be factor increasing recharge. The irrigation losses, wastewater returns and leakage losses are sources of artificial recharge (Hiscock et al., 2002). Conditions vary in every city, making it difficult to generalise about the net effect of urban areas on recharge. When looking at the effect of urbanisation on recharge in Kumasi, the previously mentioned factors should be investigated to determine whether they have been influential in determining local recharge characteristics.

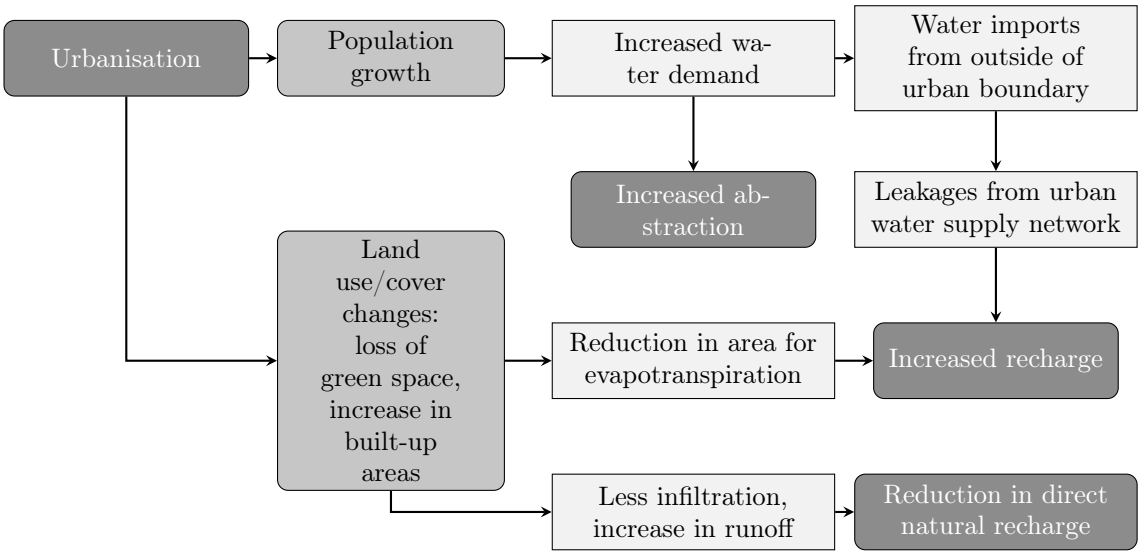

Figure 2.3: Effects of urbanisation groundwater recharge.

2.2 Sustainable groundwater resource development

Sustainable use of groundwater resources requires the balance of economic, environmental and human benefits against groundwater storage and the various recharge inputs (Hiscock et al., 2002). Groundwater abstraction supports the economy and society by providing water for agriculture, industry, and people. The low-cost development, generally good quality and drought-reliability of groundwater make it a beneficial and reliable source of water (Foster & Chilton, 2003; UNESCO, 2007). Groundwater is not only important for socio-economic reasons, but also for the environment as it supplies water to springs, surface waters, and wetlands (Hiscock et al., 2002). In many developing nations, groundwater has been regarded as a key for poverty alleviation by providing water and sanitation to those without access to other water sources (UNESCO, 2007). Due to its many benefits groundwater has become a widely used water source, but this has occurred without proper management resulting in uncontrolled exploitation and contamination of many aquifers (UNESCO, 2007). Some problems that arise with improper groundwater management are the inefficient use of groundwater, social inequities in access to groundwater, physically unsustainable abstraction rates, localised land subsidence, saline intrusion, reduction in baseflow to rivers and streams, and damage to ecosystems dependent on groundwater and pollution reducing natural quality (Foster & Chilton, 2003).

Groundwater management is important to prevent the occurrence of the adverse effects that arise from uncontrolled aquifer development. Locally, issues around groundwater management must be identified, such as declining water levels or pollution (UNESCO, 2007). The adoption of strategies for achieving sustainable groundwater development must deal with current scenarios as well as events that may result in future scenarios, such as climate change or rapid urbanisation (Hiscock et al., 2002).

Sustainability is often defined using indicators that can be used for the purposes of description of the state of a resource, to extract trends that may provide information on the functioning of the system, communicate policy objectives, as a tool for assessment, and finally as a tool to predict the future (UNESCO, 2007). In the context of sustainable development, a sustainability indicator should be able to give information on the resilience of a resource to a certain stress such as urbanisation, which affects groundwater extraction as well as groundwater recharge. One example from UNESCO (2007) is total groundwater abstraction divided by the groundwater recharge. Other indicators include groundwater depletion estimates dervied by subtracting groundwater abstraction rates from recharge rates (Bierkens & Wada, 2019; Wada et al., 2010). Wada et al. (2010) explains abstraction in excess of recharge can be used as an estimate of groundwater depletion, while negative values indicate abstraction is sustained by recharge. Bierkens & Wada (2019) explains the definition of "physically sustainable groundwater use" is the prolonged (multi-annual) withdrawal of groundwater from an aquifer in quantities not exceeding the average annual replenishment. Groundwater depletion is reached when this prolonged withdrawal exceeds the average annual replenishment (Bierkens & Wada, 2019). Using this definition for sustainable groundwater use, the indicator defined by Wada et al. (2010) fits as a suitable representation for sustainability.

2.3 Recharge estimation methods

Groundwater recharge is a key issue when investigating sustainable management of groundwater resources (Meijerink, 2007). Challenges arise in recharge estimation due to temporal and spatial variations of recharge, determination of sources of recharge, and the impacts of urban development on groundwater recharge (Vries & Simmers, 2002). Vries & Simmers also explains that the only means to realistically determine recharge processes is by incorporating field measurements in the investigation. Recharge is generally defined as the downward flow of water reaching the water table, replenishing the groundwater reservoir (Vries & Simmers, 2002). However, not all water that infiltrates the surface reaches the groundwater table. Water may be lost through interflow to local depressions as low-conductivity zones hinder the downward movement (Vries & Simmers, 2002). Moreover, water may be extracted from the groundwater reservoir by evapotranspiration. Vries & Simmers (2002) explains a distinction should be made between the actual recharge and the potential amount of water available from the unsaturated zone for conceptual and modelling purposes. Due to the complexity and heterogeneity of hydrological settings and the nature of recharge processes, direct measurement of actual recharge is almost impossible (Gemitzi et al., 2017). Groundwater recharge is more commonly measured indirectly by measuring physical and chemical parameters involved in recharge processes (Szilagyi et al., 2011).

Various studies have attempted to estimate recharge using hydrologic modeling, water balances, field measurements such as environmental isotopes and borehole data, remote sensing and GIS techniques. Choosing an appropriate method depends on available data and local parameters such as hydrological, hydrogeological and climatic conditions. This section looks at seven papers that estimated recharge using the previously mentioned techniques, namely Gemitzi et al. (2017); Rooyen et al. (2020); Anornu et al. (2009); Forkuor et al. (2013); Das & Pal (2020); Wakode et al. (2018); Meijerink (2007).

2.3.1 Hydrologic modeling

Hydrologic modeling is a useful tool to indirectly measure groundwater recharge and is best applied in basins where continuous long-term measurements of groundwater levels or streamflow measurements exist (Gemitzi et al., 2017). In countries where datasets are scarce or the quality

of data is poor, the application of such a method is limited (Wakode et al., 2018; Rooyen et al., 2020). The study by Gemitzi et al. (2017) attempts to provide a simple empirical equation for monthly recharge by simulating recharge using the Soil and Water Assessment tool, SWAT, and comparing this to effective precipitation. SWAT is a continuous time model that operates on a daily step on a basin scale, grouping subbasins based on climate, hydrological response units (HRUs), ponds/wetlands, groundwater, and the main channel draining the subbasin (Neitsch et al., 2009). The HRUs are distinguished by areas with similar land cover, soil, and land management characteristics that are used to represent spatial heterogeneity within the watershed (Neitsch et al., 2009). Gemitzi et al. (2017) defined recharge as the total amount of water entering the groundwater system and calculated recharge rates in SWAT over a 10 year time period. The model was then validated by comparing SWAT modeled monthly actual evapotranspiration to actual evapotranspiration retrieved from the MODIS satellite. Applying such a model in Kumasi is challenging due to the data requirements, such as streamflow and aquifer storage volumes. If enough datasets are available, then integrated surface-groundwater modelling is recommended as one of the more accurate approaches to estimate groundwater recharge and discharge (Chung et al., 2016).

2.3.2 Environmental isotopes

Using environmental isotopes as an indicator for groundwater recharge has been done in Gemitzi et al. (2017); Rooyen et al. (2020); Anornu et al. (2009). Anornu et al. (2009) used a chloride mass-balance, determining the tracer concentration in precipitation and in the groundwater. (Rooyen et al., 2020) estimated how actively groundwater was being recharged by measuring the activity of tritium in the groundwater and using potential evaporation to indicate the proportion of rainfall that remains to feed surface water or recharge groundwater reserves. Tritium has a relatively short half life so it can be used to differentiate between older, not actively recharged groundwater and shallow, actively recharged groundwater (Rooyen et al., 2020). Similar to the previous study, Gemitzi et al. (2017) used the concentration of oxygen and hydrogen isotopes in precipitation, boreholes, and spring water to estimate recharge rates and check the applicability of the developed formula. This method gives a fair approximation of the long-term average recharge value, and is relatively inexpensive and easy to apply (Chung et al., 2016).

2.3.3 Water balance

Understanding of the water balance is critical to do any sort of recharge estimation, as this forms the basis of understanding the processes that affect recharge. The water balance method explicitly makes use of the fluxes affecting groundwater and investigates those specifically. This method was applied in Anornu et al. (2009) and Wakode et al. (2018), the latter using a more complex approach. The simplified water balance is given as in the Equation 1 below, where GWR represents recharge, P is precipitation, Q is runoff, and ET_a is actual evapotranspiration (Anornu et al., 2009; Wakode et al., 2018). Wakode et al. (2018) investigated the impact of urbanisation on groundwater recharge and therefore implemented an urban groundwater recharge component, finding that the urban area brings water from external areas to meet the water demand which contributes to recharge through pipe leaks. This component was found to be larger than the natural recharge component, indicating urbanisation can also lead to an increase in groundwater recharge. This method can be well-applied in regions where precipitation is the governing source of recharge such as in humid areas like Kumasi, where deep percolation is controlled by the precipitation surplus, soil infiltration capacity, and subsurface transport capacity (i.e. permeability) (Vries & Simmers, 2002).

$$GWR = P - Q - ET_a \tag{1}$$

2.3.4 Precipitation relationships

One of the more direct methods of estimating groundwater recharge is the water-table fluctuation (WTF) method. In locations where rainfall infiltration is the principal source of groundwater

recharge, changes in water table level are related to precipitation patterns Das & Pal (2020). In the paper by Das & Pal (2020), recharge was estimated by the increase in water level, multiplied by the specific yield of the water bearing formation and the area of the assessment unit. Chakrabortty et al. (2018) used a similar approach but did not consider the specific yield, directly relating the recharge to the peak water rise between the dry and rainy season. Chung et al. (2016) explains it is best applied over a short time period in regions with shallow water tables. However, this method requires groundwater level measurements from wells in the area making it unfeasible in regions where there is lack of such datasets, such as in Kumasi.

Various studies have attempted to define the relationship between recharge and effective precipitation, but their uses are confined to specific areas. Anornu et al. (2009) developed a relationship based on the chloride balance method and water balance method in the Ejisu-Juaben district east of Kumasi, where the groundwater recharge was estimated as 7-9% of annual precipitation. Martin & Giesen (2005) combined rainfall and recharge studies in West Africa, creating an empirical relationship based on the different lithologies in Volta basin (see Equation 2 and 3). Other empirical relationships have been established, such as in Gemitzi et al. (2017), however these are less applicable to the study region. The challenge of using an empirical relationship is that it does not take factors such as land use or land cover into account. However, they can be used as an indication of natural recharge volumes without considering urbanisation effects.

$$\text{Sandstone rocks (Voltaian supergroup): } GWR = 0.01316P - 22.141 \tag{2}$$

$$\text{Weathered rocks (Precambrian supergroup): } GWR = 0.082P\check{}31.212 \tag{3}$$

2.3.5 Weighted approaches for groundwater sustainability

Many studies have attempted to model the vulnerability of groundwater to pollution (Bierkens & Wada, 2019). One of the most common applied methods is using the DRASTIC index, where weights are assigned to seven factors affecting groundwater vulnerability, namely: depth to water, net recharge, aquifer media, soil media, slopes, hydraulic conductivity and impact on vadose zone (Ewusi et al., 2016; Bierkens & Wada, 2019; Freitas et al., 2019; UNESCO, 2007). A weighted overlay is then created using GIS resulting in a final map of vulnerability. Such an approach allows for an analysis of each influencing factor in relation to its contribution to pollution before determining the final combined effect of the parameters. This analysis has been carried out in Kumasi by Ewusi et al. (2016). A map was created of Kumasi delineating areas that are vulnerable to pollution.

Rooyen et al. (2020) created a variation of the DRASTIC approach to not only include quality but also quantity controls to determine groundwater vulnerability. Five new model layers were introduced: 1) available water budget (surface temperature and precipitation), 2) recharge indicators (tritium distribution in groundwater, potential evaporation), 4) physical attribuites (slope, aquifer type), 5) aquifer chemical characteristics and 5) human groundwater dependence. Assigning weights to all parameters, the spatial distribution of vulnerability was derived. In Rooyen et al. (2020) each input parameter for the model layers is assessed with respect to its effect on vulnerability, which is then reclassified to a specified vulnerability unit from low to high. Weights are assigned to each layer depending on its contribution to vulnerability, and finally a weighted overlay is done using GIS tools combining all the vulnerability parameters to produce a vulnerability map.

Das & Pal (2020) used a similar weighted approach to determine aquifers vulnerability to over-exploitation. The methods used focused on assessing groundwater recharge using measurements and groundwater abstraction using field investigations. Seven parameters were input into the model: geomorphology, geology, elevation, slope, soil texture, land use or land cover, and groundwater recharge. These factors influence the availability of groundwater hence determining the vulnerability of the aquifers to over-exploitation. Many of these parameters can be estimated using existing geological and soil maps, digital elevation models, and other remote sensing tools. However, recharge is a required input parameter which remains a challenge when implementing such an assessment for groundwater sustainability.

2.4 Water balance components

2.4.1 Methods to estimate evapotranspiration

Evaporation can be estimated quite accurately using experimental methods such as the Bowen ratio technique, eddy correlation techniques and lysimeters Allen et al. (2002). There is a limitation to such techniques as they can only provide point values of evapotranspiration (ET), failing to provide ET on a regional scale. ET is temporally and spatially variable due to its dependence on precipitation, soil hydraulic characteristics, and vegetation types that also vary in space and time (Allen et al., 2002). Two common ways of estimating evaporation indirectly are the energy balance method and the soil water balance method (Allen et al., 1998). The first method makes use of the principle of energy conservation, as evapotranspiration is governed by energy exchanges at the vegetation surface (Allen et al., 1998). The energy balance equation for an evaporating surface is given by Allen et al. (1998) and shown in Equation 4. The parameters are latent heat flux (λET), net radiation flux at surface (R_n), soil heat flux (G) and sensible heat flux (H), all in units of W/m^2. Advection processes are ignored and therefore this equation should be used for large areas with homogeneous vegetation. Allen et al. (1998) explains that the net radiation and soil heat fluxes can be estimated from climatic parameters whereas the estimation of sensible heat is more complicated as it requires measurements of surface temperature gradients. Some examples of energy balance models are the Surface Energy Balance Algorithms for Land (SEBAL), Simplified Surface Energy Balance Index, and surface temperature-vegetation index triangle method (Lee & Kim, 2016). The soil water balance method requires measurements of the incoming and outgoing fluxes into the crop root zone (Allen et al., 1998). These fluxes are shown in Equation 5. The fluxes are described by Allen et al. (1998): irrigation (I) and precipitation (P) bring water into the root zone, but some of this water may be lost as runoff (RO) and deep percolation (DP) to recharge groundwater. From the shallow water table, capillary rise (CP) may bring water to the root zone or travel horizontally as subsurface flow (SF). Finally, the change in soil water content (δSW) represents the amount of water available for evapotranspiration.

$$\lambda ET = R_n - G - H \tag{4}$$

$$ET = I + P - RO - DP + CR \pm \Delta SF \pm \Delta SW \tag{5}$$

ET can also be calculated from weather data using empirical or semi-empirical equations to assess crop or reference crop ET (Allen et al., 1998). The standard method of calculating reference ET is by using the Penman-Monteith equation, which requires radiation, air temperature, humidity and wind speed data (Allen et al., 1998). If these values are known from station data, then such methods for ET can be used. Moreover, remote sensing data can be used to provide the spatial distribution of regional evapotranspiration due to the continuous information supply over land surfaces (Mu et al., 2013). The use of remote sensing for global ET measurements has proved to be convenient due to the spatial and temporal coverage (Falalakis & Gemitzi, 2020).

2.4.2 Runoff estimates

Runoff is a highly nonlinear processes influenced by many physical factors, some dependent one another with different dynamics making it a complex process to understand (Fan et al., 2013). Examples of simulation models that have been applied to predict urban runoff include the Sacramento model, Tank model, HBV model, and the Soil Conservation Service Curve Number (SCS-CN) (Fan et al., 2013). In ungauged or poorly gauged watersheds, the SCS-CN provides a simple but well-established method for runoff estimations (Soulis, 2021).

3 Study area

3.1 Location and population

Kumasi is the second largest city of Ghana, located in the south-central Ashanti region (Amoateng et al., 2018a). Accommodating nearly two-thirds of region's the population, Kumasi covers an area of 254 km^2 (Cobbinah & Amoako, 2012). The population census of 2010 by Ghana Statistical Service (2013b) determined the city was experiencing a growth rate of 5.5% and had a population of 2,035,064. With this growth rate, it is expected that the population is currently over 3 million. Population growth in Kumasi can be attributed to a combination of geographic, demographic, economic and social factors (Abass et al., 2020). Cobbinah & Amoako (2012) explains the centrality of Kumasi has made it a national traversing point, fueling the growth of industries and commercial activities and leading to high migration rates from within and outside the country. Figure 3.1 shows the traversing roads and largest communities within Kumasi.

Kumasi used to be known as the 'Garden City of West Africa' due to its abundant greenery (Ghana Statistical Service, 2013a). The city contained scenic landscapes such as rivers, wetlands, riparian zones, open spaces and parks (Amoateng et al., 2018b). However, due to urban expansion, physical and agricultural developments have taken place in important natural areas such as wetlands, flood plains, and rivers (Abass et al., 2020; Amoateng et al., 2018b). Cobbinah & Amoako (2012) estimated that 80% of the land in Kumasi was developed and that this development is expected to increase. The pressure from the city's expansions has caused alterations in the natural hydrologic conditions, causing frequent flood disasters especially during the rainy season (Amoateng et al., 2018b).

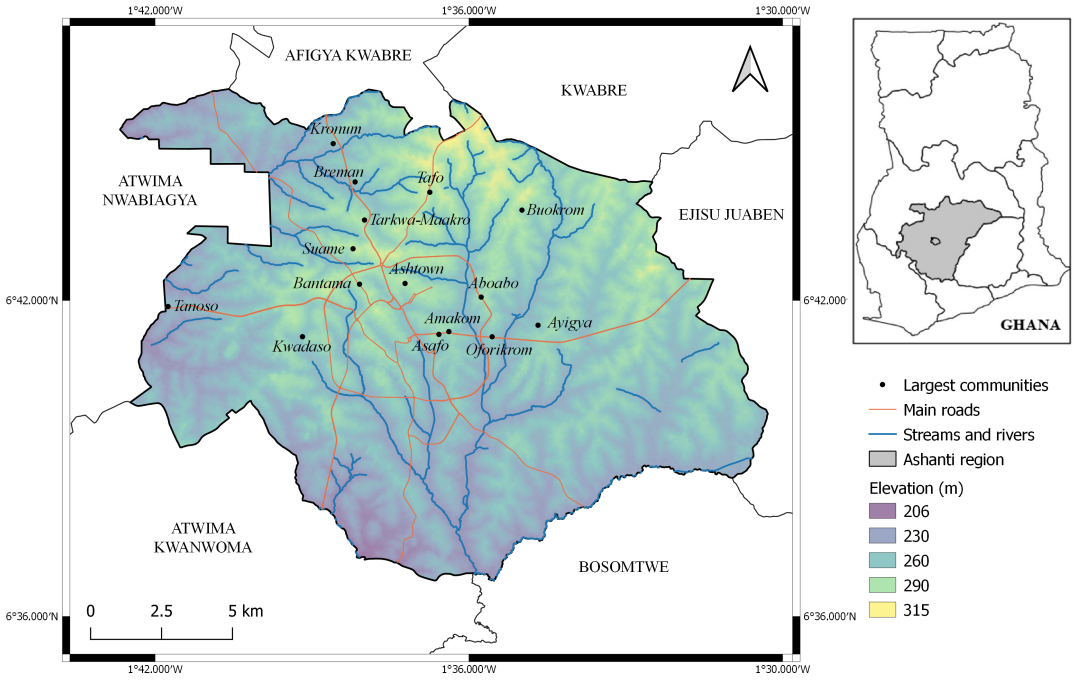

Figure 3.1: Map of Kumasi showing location within Ghana, traversing roads, major streams and rivers, and largest communities within the city. Information retrieved from Ghana Statistical Service (2013a) and underlying SRTM elevation map.

3.2 State of water resources

Drinking water in Kumasi is supplied from the Barekese and Owabi reservoir located 16km and 10km from the city respectively (Koranteng, 2017). These are shown in Figure 3.2 along with the rivers and water pipeline network in an around Kumasi. The treated water from the headworks is monitored and stored in ground and elevated reservoirs in Suame and from there, approximately 580km of pipelines distribute water through the Kumasi water supply system (Kuma et al., 2010). The water level at both headworks has been slowly declining and degradation has occured due to anthropogenic activities along the catchment area (Koranteng, 2017). Deforestation around the reservoirs has resulted in reduced inflow and increased evaporation (Koranteng, 2017). This is especially notable in the Barekese reservoir as yields have decreased due to human pressures such as encroachment, farming, and logging leading to high quantities of sediment entering the dam (Maoulidi, 2010). The rivers, streams and hand-dug wells in Kumasi have also faced patterns of pollution due to chemical and human waste contamination close to the water sources (McGregor et al., 2011).

The most common drinking water sources for households in Kumasi are pipe-borne (74.1%), borehole/pumps (12.6%) and protected wells (6.4%). A complete overview of water sources is given in Table A.6. The pattern for domestic water use is similar to the drinking water sources. (Ghana Statistical Service, 2013a). From the distribution of pipelines within the city it can be seen that the water pipeline density reduces radially, indicating there is less piped water access further from the center. In the population census of 2010, surveys indicated that 19% and 24% of households used groundwater for drinking and domestic purposes respectively (Ghana Statistical Service, 2013a).

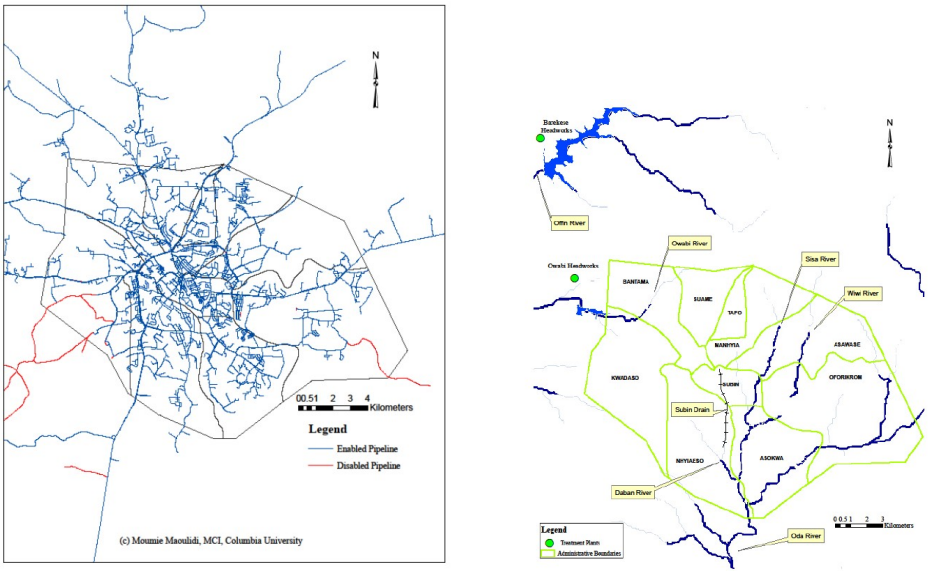

(a) Distribution of water pipelines in Kumasi in 2010.

(b) Surface water map showing treatment plants and headwork locations.

Figure 3.2: Water supply system in Kumasi showing a)pipeline distribution and b) location of head. Maps retrieved from Maoulidi (2010).

A declining trend has been noted in the piped water access of residents in the large metropolitan areas of Ghana. In 2000, it was estimated that 83% of Kumasi residents had access to piped water, but this decreased to 75.1% by 2010 (World Bank, 2015). This decline can be attributed to factors such as system losses, insufficient maintenance, and the inability of water companies to meet the demand in the rapid urbanising context of the growing metropolitan areas. According to Kuma et al. (2010), there has been a decrease of water produced by the Kumasi Water Supply System from the headworks. This will lead to an increased strain on the availability of water for Kumasi's residents in the long-term, which may be solved by looking into alternative resources

such as groundwater (Kuma et al., 2010).

In order to meet the missing water demand, groundwater has been used as a cheap and efficient alternative (Ewusi et al., 2016). This trend is seen in many growing African cities where groundwater is available, as utility wells can be built fast and cheap in the developing outer districts (Graaf et al., 2017). Similar to the surface water sources, groundwater in Kumasi is vulnerable to pollution due to anthropogenic activities (Ewusi et al., 2016). Discharge of sewage into water bodies and agricultural leaching have been connected to the deterioration of groundwater quality (Yeleliere et al., 2018). Ewusi et al. (2016) conducted a vulnerability assessment of Kumasi's groundwater resources, concluding that areas susceptible to contamination are related to areas where there is a high draining capability of the sand, namely in locations underlain by granite. Overall, the state of groundwater resources is determined by anthropogenic factors as well as natural factors affecting groundwater availability and flow.

3.3 Land use and land cover

A handful of studies have been conducted in Kumasi to assess the land use/land cover transitions through means of remote sensing (Abass et al. (2018); Koranteng (2017); Amoateng et al. (2018a)) and through empirical data collection (Cobbinah & Amoako (2012); Amoateng et al. (2018a)). Overall, there has been a transition from non-urban to urban land use due to rapid urbanisation (McGregor et al., 2011). Abass et al. (2018) determined that the urban/built-up area in Kumasi increased from 27.2% in 1986 to 79.4% in 2016, while vegetation cover decreased from 69.2% to 17.7% in the same time period. Amoateng et al. (2018a) investigated the changes in rivers and floodplains, concluding that the number of rivers in the city fell from 63 in 1985 to 34 in 2013. The the rivers have not only been reducing in quantity, they have also reduced in size as the water body size decreased from 23 meters in 1985 to 13 meters in 2013. This decline has been attributed to encroachment by squatters who illegally occupy riparian areas and land filling for the purpose of creating new sites for construction (Amoateng et al., 2018a).

Agglomerated, the industrial, commercial and educational land use consists of 26.7% of the total area, where the majority of the land use is residential (44%) and only 18.7% of the land remains undeveloped (Ghana Statistical Service, 2013a). Agriculture remains important in and around Kumasi as staple crops are extensively farmed to augment the food supply and support the financial needs of those involved (Afriyie et al., 2020). The arable lands in Kumasi are known to grow a variation of crops including plantain, yam, maize and cassava. Close to a tenth of households engage in agricultural activities mainly consisting of crop farming (Ghana Statistical Service, 2013a). However, there has been a decline in agricultural land use and farmers have reduced fallow periods and intensified agriculture near streams and rivers by increasing the use of irrigation (McGregor et al., 2011). The story at the outskirts is different, as a net expansion of agriculture and settlements has been experienced at the expense of forest cover (Koranteng, 2017). Koranteng (2017) explains this loss is concerning as deforestation is a large issue in Ghana as a whole, where 220km^2 of forest is lost a year.

Rapid urbanisation has led to increased housing demand, but the supply of housing is lagging behind the effective demand causing people to resort to live in slums or areas of poor housing conditions (World Bank, 2015). In Kumasi, the most common housing types are compound houses with households occupying single rooms, followed by separate houses, flats and semi-detached houses Ghana Statistical Service (2013a). A small percentage (6.5%) of households live in makeshift dwellings units (Ghana Statistical Service, 2013a). Roofs are generally characterised by corrugated metal sheets, where 90.8% of settlements are covered with this material (Ghana Statistical Service, 2013a).

3.4 Climate

Kumasi lies in Ghana's moist, semi-humid climate zone experiencing two rainfall seasons annually (Amoateng et al., 2018b). The major season occurs between March to July and the minor season between August/September to October, with an annual mean of 1386 mm recorded between

1980 and 2012 (Ewusi et al., 2016). The peaks of these seasons are in June and October, which can be seen in Figure 3.3. Average annual precipitation in Ghana ranges between 71 0mm and 203 0mm, with the south-west experiencing highest precipitation amounts Kabo-Bah et al. (2016). Mean annual minimum and maximum temperatures in Kumasi are respectively 21.5°C and 30.7°C and humidity is around 84% (Abass et al., 2020; Ghana Statistical Service, 2013a). Erni et al. (2011) conducted a study investigating actual evapotranspiration from different surfaces using the Penman-Monteith method, concluding that annual evapotranspiration in Kumasi was 680 mm.

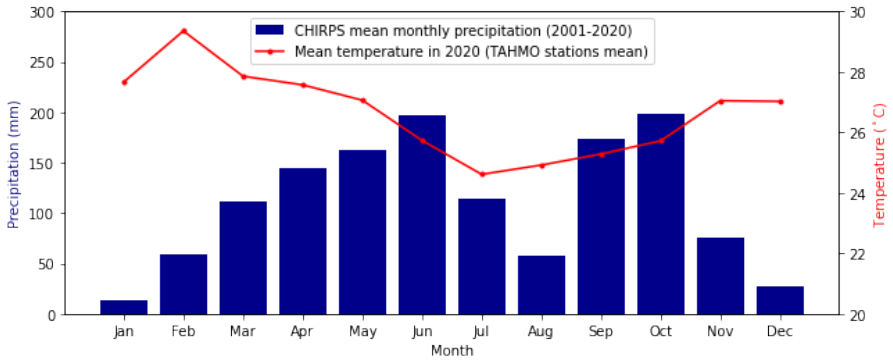

Figure 3.3: Mean monthly precipitation from CHIRPS for the period of 2001-2020 over Kumasi and mean monthly temperature from TAHMO stations TA00279, TA00393, TA00617 in 2020.

3.5 Hydrogeology

The availability of groundwater depends on geologic conditions (Gaye & Tindimugaya, 2019). Porosity describes whether the rock has pores or fractures that can store water or air, and if these pores are connected the rock is said to be permeable. Permeability develops through geological processes such as fracturing, weathering, and folding. Underlying Kumasi are the Birimian metasedimentary units and granitic batholiths (Ewusi et al., 2016). The Birimian formation is highly folded, fractured, and foliated, consistsing of shales and phyllites. Due to the intense fracturing, the unit has a high yielding potential due to its secondary porosity (Ewusi et al., 2016; Anornu et al., 2009). Figure 3.4 shows three dominant geologic formations in Ghana that are grouped by their aquifer productivity. Kumasi lies above the Basement complex, characterised by crystalline basement aquifers with deeply weathered and fractured aquifer properties (O'Dochartaigh et al., 2019). The rocks in this complex have little to no primary porosity (Kortatsi, 1994). The development of secondary porosity in the basement complex explains the occurrence of groundwater (Yeleliere et al., 2018).

Two main types of aquifers exist in the Basement complex: the weathered zone aquifer occurring at the base of thick weathered layer from the surface to 100m deep and the fractured zone aquifer, occurring at some depth beneath the weathered zone (Kortatsi, 1994). Groundwater occurs mostly under semi-confined or leaky conditions due to the weathered sandy/clay overburden (Kortatsi, 1994). Aquifer productivity estimates from O'Dochartaigh et al. (2019) were done by synthesising borehole yield data available for aquifers in Africa and using this to distinguish approximate ranges of yields. The Basement aquifer has a generally low to moderate productivity, but yields can occasionally be as high as 600L/min (Gaye & Tindimugaya, 2019). In the neighbouring district of Ejisu-Juaben, borehole yields between 10-180L/min were found in the Birimian and grantitic units, with wells having an average probability of yielding between 70-80% (Anornu et al., 2009). Aquifer depths in the Basement complex range between 10 m to 60 m (Yeleliere et al., 2018; Gumma & Pavelic, 2013). Kortatsi (1994) explains groundwater recharge in Ghana is dominated by direct infiltration from precipitation through fractures and fault zones and through sandy portions of the weathered zone. During the rainy season, recharge can also occur through seepage from ephemeral stream channels (Kortatsi, 1994). Per decade, Ghana experiences a total recharge of 970 mm ranging between 340-2800 mm depending highly on the climatic zone (MacDonald et

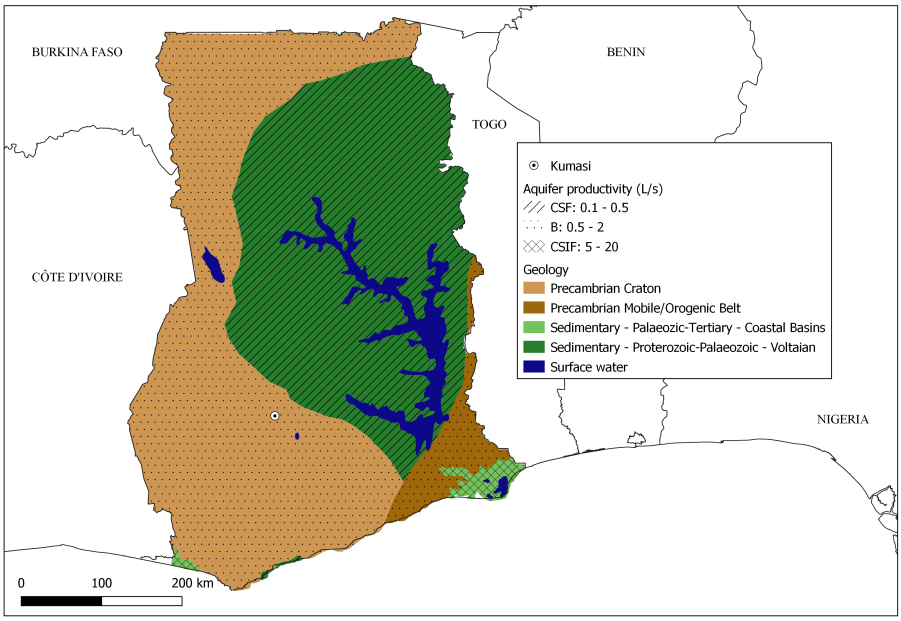

Figure 3.4: Map showing the geological units and approximated aquifer productivity for Ghana. CSIF: Consolidated Sedimentary Aquifer with mixed Intergranular and Fracture Flow, CSF: Consolidated Sedimentary Aquifer dominated by Fracture Flow, B: Basement aquifer. Created with data from O'Dochartaigh et al. (2019).

al., 2021). The estimated groundwater storage in the whole of Ghana is 1400km^3 (MacDonald et al., 2021).

3.6 Drainage

Drainage network densities can give a lot of information on groundwater recharge and movement by providing hydrological pathways (Gumma & Pavelic, 2013). The topography in Kumasi is undulating and ranges between 250-300 meters (Ghana Statistical Service, 2013a). Five major streams run through the depressions in the metropolis, namely the Subin, Wiwi, Sisa, Aboabo and Daban (Ghana Statistical Service, 2013a). The network of rivers and streams traverse the city in a general north to south direction following the ridges and valleys (Amoateng et al., 2018a). From the north west of the city, streams and runoff drain into the Owabi river (Ewusi et al., 2016). These water bodies are main sources of drinking water for residents of Kumasi and in the region making them critical for the socioeconomic well-being of the population (Ghana Statistical Service, 2013a).

3.7 Soil

The soils in Kumasi belong to the Forest Ochrosol soil group characterised by its dark greyish-brown colour, composed of sandy loam and and silty loam textures (Amoateng et al., 2018b; Adjei-Gyapong & Asiamah, 2002). This soil belongs to the latosol family, a group of high weathered soils with a high clay fraction (Adjei-Gyapong & Asiamah, 2002). These soils are generally well drained but have a low chemical fertility and organic matter content, rendering them susceptible to erosion (McGregor et al., 2011). Within the Forest Ochrosol group, six different soil associations can be defined, shown in Table 3.1. The soil associations were retrieved from Amoateng et al. (2018b) and the properties were determined by assessing the soil map of Kumasi from Panagos et al. (2011). Due to the high clay accumulation, the soils have low permeability leading to high runoff yields.

Table 3.1: Soil associations found in Kumasi and their corresponding properties

Soil compound association	Soil composition	Drainage characteristics
Bekwai-Akomadan-Oda	Silty clays, over abundant concentration of ironpan	Well drained
Bekwai-Oda	Bewkwai series: silty clay loams and clays Oda series: poorly drained, deep non-gravelly, alluvial silty clays and silty clay loams	Bewkwai series: well drained Oda series: poorly drained
Bomso-Offin	Sandy to gritty clay loams, abundant contents of large flakes of muscovite and white mica	Well drained
Bomso-Suko	Sandy clay loams, free from concretions, gravels and stones	Well drained
Kumasi-Offin	Alluvial sands	Poorly drained
Nhyanao-Yinkong	Rocky soils	Excessively drained

4 Data

In this section an overview of all datasets used are given. Table 4.1 shows the remote sensing products used for land use classifications and the water balance components of precipitation, evapotranspiration and runoff. Table 4.2 shows the values used for groundwater consumption estimates.

4.1 Satellite datasets

CHIRPS precipitation:
The Climate Hazards Infrared Precipitation with Stations (CHIRPS) dataset combines 0.05°resolution satellite imagery with in-situ data from stations and is available from 1981 providing a quasi-global daily rainfall dataset (Google Earth Engine, 2020). Long-term monthly precipitation means were used to create the in-situ datasets from a collection of FAO and Global Historical Climate Network (GHCN) stations (Funk et al., 2015). Moreover, CHIRPS also uses monthly-long term mean fields from five satellite products, namely Tropical Rainfall Measuring Mission (TRMM), CMORPH, monthly mean geostationary infrared precipitation estimates and land surface temperature estimates (Funk et al., 2015). Funk et al. (2015) explains in-situ data is used to calibrate the Cold Cloud Duration (CCD) rainfall estimates for specific regions to give a best estimate. The combination of these two datasets makes CHIRPS a reliable dataset covering daily precipitation estimates in areas where station data is not readily available.

MODIS evapotranspiration:
MODIS (MODerate Resolution Imaging Spectroradiometers) products provide information on vegetation dynamics and surface energy variations. One of the datasets derived from the MODIS products is evapotranspiration. The following description of the ET algorithm is summarised in this section from NASA's Algorithm Theoretical Basis Document (Mu et al., 2013). The measurement instrument is aboard NASA's Terra and Aqua satellites launched in 1999 and 2002 respectively with a repeat cycle of 16 days. The ET product provides terrestrial ecosystem ET on an 8-day (MOD16A2) and annual (MOD16A3) basis with a resolution of 500m. The original algorithm combined daily meteorological inputs and 8-day MODIS data using the Penman-Monteith equation as a basis for the calculation of daily ET.

Table 4.1: Overview of satellite datasets used for groundwater recharge estimations.

Product	***Availability***	***Provider***	***Resolution***
Landsat 7 ETM + sensor (Surface Reflectance – Tier 1)	January 1999 - Present	USGS	30m
Landsat 5 ETM sensor (Surface Reflectance – Tier 1)	March 1984 - May 2012	USGS	30m
Landsat 8 OLI/TIRS sensor	April 2013 - Present	USGS	30m
Sentinel-2 MSI (MultiSpectral Instrument)	2017-03-28 – Present	European Union /ESA/Copernicus	10m for visible and NIR
MODIS Evapotranspiration/ Latent Heat Flux	January 2001 – present	NASA	500 m 8-day composite
CHIRPS precipitation	January 1981 – present	USCB/CHG	0.05 arc degrees

4.2 Extra datasets

Open-access meteorological data is available from the network of Trans-African Hydro-Meteorological Observatory (TAHMO) stations across Africa. In Kumasi four TAHMO weather stations exist that have been measuring precipitation, relative humidity, surface air temperature and soil moisture, the oldest record going back to 2017. In this study, precipitation and temperature data from TAHMO is used to validate preciptation and evapotranspiration results. In Kumasi four TAHMO stations exist, their locations are shown in Figure A.9. The most complete temperature dataset for Kumasi was for the year 2020 from three of the four stations, namely TA00279 (Kumasi airport), TA00393 (Kumasi SHS), and TA00617 (KNUST Farm). For precipitation in 2020, datasets are incomplete for TA00039 and TA00617.

Table 4.2: Overview of non-satellite data and their sources.

Groundwater consumption data		
Variable	**Value**	**Source**
Population 2010 (P_{2010})	2,035,064	Ghana Statistical Service (2013a)
Population growth rate in 2010 (GR) (%)	5.5	Ghana Statistical Service (2013a)
Population 2020	3,476,183	$P_{2020} = P_{2010}(1 + GR/100)^{period(years)}$
Total water consumption (m^3/person/d)	0.094	Kuma et al. (2010)
Domestic groundwater consumption (%)	23.8	Summarised from Table A.6, data from Ghana Statistical Service (2013a)
Area kumasi	241 km^2	Extent of Kumasi outline from shapefile
Other datasets		
Kumasi shapefile	Download: *Shapefiles of all Districts in Ghana (170 districts)* (2019)	
TAHMO temperature	Accessed through TAHMO data portal, available stations in Kumasi shown in Figure A.9	
TAHMO precipitation	Accessed through TAHMO data portal, available stations in Kumasi shown in Figure A.9	

5 Methodology

5.1 Sustainable groundwater use

Sustainable groundwater use is assessed using the definition by Bierkens & Wada (2019): *Prolonged (multi-annual) withdrawal of groundwater from an aquifer in quantities not exceeding the average annual replenishment.*

By estimating long-term average groundwater recharge and groundwater abstraction volumes in Kumasi, the sustainability definition can be applied to define the state of the groundwater resources. Figure 5.1 shows an overview of the methodology used in this study. The domestic abstraction component of sustainability is carried out using data from Kuma et al. (2010) and Ghana Statistical Service (2013b) containing survey results on population, percentage of households reliant on groundwater consumption, and per capita water demand as shown in Table 4.2 and Table A.6. Non-domestic consumption is estimated from survey results conducted in Kumasi for this study between July and August at 52 different locations. The groundwater recharge component of sustainability is estimated using the water balance in Equation 1, requiring estimates on precipitation, runoff, and evapotranspiration. Precipitation datasets are readily available in Google Earth Engine, and runoff and evapotranspiration estimates are derived from remote-sensing products. Detailed descriptions of the methods used to determine each component are given in the following sections.

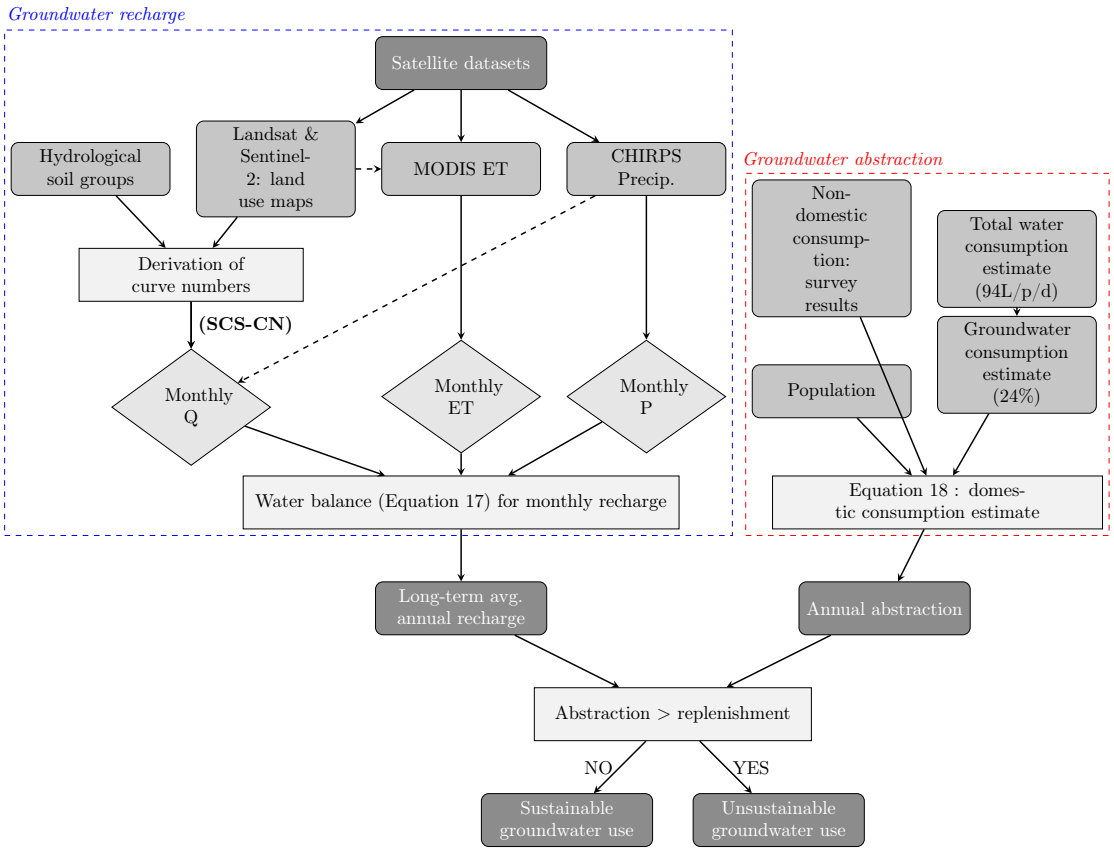

Figure 5.1: Simplified overview of the methodology used to assess sustainable groundwater use in Kumasi. Q: runoff, P: precipitation, ET: evapotranspiration, SCS-CN: Soil Conservation Service Curve-Number.

5.2 Land cover classification

Land cover directly affects surface water infiltration due to alterations in infiltration capacity, leading to the importance of determining the land cover for groundwater recharge. Groundwater recharge is therefore dependent on surface permeability. Urbanisation in Kumasi has led to a reduction in permeable surfaces, resulting in reduced infiltration areas. The first step is to determine the land use/land cover classes that are relevant for the hydrological significance of the study and the second step is to perform the classification in Google Earth Engine (GEE). In this case the aim is to distinguish land classes that have different groundwater recharge characteristics while also considering the land classes defined in USDA (1986) used to estimate the Curve Number.

5.2.1 Land cover classes

The first step in carrying out the classification is to determine which land cover classes are necessary to distinguish. The USDA land covers are shown in Table 5.1. For infiltration, the most important factor to distinguish is whether the surface is pervious or impervious. However, even impervious surfaces may have some infiltration potential. Examples include to the formation of cracks in pavement or use of semipervious building materials. In previous land cover maps created over Kumasi (described in section 3.3), distinctions have only been made between built-up, vegetated, and water bodies. Abass et al. (2018) also classified farmed areas in Kumasi. Considering the USDA curve numbers, infiltration properties of pervious surfaces and differences in vegetation, the land cover classes in Table 5.1 are chosen to create land cover maps.

Table 5.1: Land cover classes chosen for LULC classification in Kumasi. Curve numbers are given for the different HSG's and LULC classses from USDA (1986)

Land cover	***Corresponding SCS-CN cover***	***Hydrologic soil group***			
		A	***B***	***C***	***D***
Urban (impervious)	Paved lots, parking, driveways	98	98	98	98
Urban (semipervious)	Streets: paved; open ditches	83	89	92	93
	Streets: dirt	72	82	87	89
	Streets: gravel	76	85	89	91
Bare land	Open space, grass cover <50%	68	79	86	89
	Fallow: bare soil	77	86	91	94
Dense vegetation	Woods (no grass combination), assume good condition (i.e. woods protected from grazing, litter and brush adequately cover soil)	30	55	70	77
Sparse vegetation	Open spaces, grass cover >75%	39	61	74	80
	Pasture, grasslands (fair condition: 50-75% ground cover and not heavily grazed)	49	69	79	84
	Meadow (continuous grass, protected from grazing)	30	58	71	78
	Brush (fair condition: 50-75% ground cover)	35	56	70	77
	Woods with grass combination (fair condition: 50% woods, 50% grass)	43	65	76	82

5.2.2 Supervised classification in Google Earth Engine

A supervised classification is an automatic land cover classification based on a set of ground truth samples (Meijerink, 2007). The advantage of using a supervised method for a specific purpose such as estimation of runoff is that land classes can be defined by the user. In an unsupervised classification the classifications are done by grouping pixels with similar spectral values, resulting in less variation in classes but no identification of the type of object obtained (Meijerink, 2007). The land use maps in this study are created following the GEE methodology in *Guides: Supervised Classification* (2021) on how to conduct a supervised classification. There are four main steps, starting with collection of training data, initiating a classifier, training the classifier and classifying

the image, and estimating the classification error with independent validation data.

1. Collect sample data:
Sample data is used to carry out the classification and is created by selecting areas that are known to have a certain land cover. In this study ground truth is determined by looking at high-resolution imagery from Google Earth and Sentinel-2 imagery in GEE, where land classes can be well-distinguished. Sample data was created in GEE by drawing polygons over the Sentinel-2 composite for 2020 using the polygon tool that can be imported into the running script and saved as a "feature collection". Features were assembled per class represented by numeric values from 0 to 5 that are used to train the classifier at a further stage.

A sufficient number of pixels per cluster should be selected, which is often done by applying the rule of thumb 30 x n (n being the number of spectral bands) (Meijerink, 2007). However, previous studies have not indicated an optimal number of training sets (Li et al., 2014). The total number of samples is also dependent on the area of the region being classified and the number of classes. For example, Abass et al. (2018) used 256 training samples to carry out the land cover classification of Kumasi, but only distinguished three different classes. Tang & Di (2019) created 200 samples per class, with 6 different land cover classes in the an area around Delhi, India of 34,144km^2. For land cover change over the whole continent of Africa, Midekisa et al. (2017) used 5664 training samples and 1420 for validation, where 7 different classes were distinguished. In this study, a total of 106 polygons were collected consisting of 100,422 pixels, where 70% of the polygons were used for training data and the remainder for validation purposes. The effect of changing sample size was investigated, with a detailed explanation of this methodology given in the following section 5.2.3.

A classification requires a base surface reflectance (SR) image to be classified from earth observation satellite products. Earth observation data used for the 2020 classification is from Sentinel-2 Multi Spectral Instrument, Level-2A, and classifications in years before this are carried out over Landsat SR products. Sentinel-2 products have a resolution of 10m compared to the 30m resolution from Landsat, allowing for a more detailed land cover classification. The 2020 composite was made with the Sentinel-2 images available between 2020-01-01 and 2021-01-01 by taking the median value from the images after applying a cloud mask in GEE. The masking procedure is provided by GEE developers, where the Sentinel-2 QA60 cloud mask band is selected to mask both cirrus and opaque clouds. Such a mask creates no-data gaps for areas that are covered with clouds. When the images are temporally aggregated, the no-data values are replaced by median cloud-free pixels from other images within the time frame. The same method can be applied to Landsat SR products, as cloud masking algorithms are provided by GEE. Carrasco et al. (2019) explains that temporal aggregates work better when there are enough images with cloud-free pixels within the time frame. For the older Landsat products, especially Landsat 7, this issue is seen as the aggregates contain cloud-contaminated data due to insufficient images with cloud-free values for one year. Landsat 7 was launched in 1999 but since June 2003 the sensor has delivered data with data gaps due to a Scan Line Corrector failure USGS (2021). This, along with lack of cloud-free data over Kumasi, has caused a gap of usable images for classification between 1986 and end 2000s. The time scale for aggregation can be increased up to two years if no cloud-free composite can be found for a shorter time period. For this study, a timeline of one year was sufficient and aggregation over a longer time scale reduced image quality due to pollution from light clouds not removed by the algorithm. Increasing the time scale to a range over two years is also not recommended as land cover changes may be more notable over a longer time frame. The best surface reflectance composites for the time period between 1986 to 2020 over Kumasi are shown in Table 5.2.

2. Initiate the classifier:
The next step is to choose a classifier and train it. Classification algorithms available from GEE are CART, Random Forest, Naive Bayes and SVM. For this study the Random Forest (RF) classifier is used due to its common application in land cover classifications; RF is a common algorithm used for forest cover mapping, wetland mapping, cropland mapping, and land cover mapping (Midekisa et al., 2017). It is an ensemble machine learning algorithm meaning it combines the decision of

a set of classifiers by voting to classify the unknown pixel (Pal, 2005). The RF algorithm starts creating trees by selecting random training samples and random features. Each tree casts a vote to classify the input and the class with the maximum amount of votes is chosen as the feature's classification (Pal, 2005; Xie et al., 2019). The only parameter that needs to be set to carry out the classification is the number of trees. In the study conducted by Pal (2005), the classification accuracy is assessed for a varying number of trees. The accuracy fluctuates between 88% and 88.4% from 100 to 12000 trees, with the highest accuracy achieved using 100 trees. Carrying out the classification with a large amount of trees comes at the cost of computational time. For this study, 10 trees are used initially to conduct the classification as this is the value used in the GEE classification guide. Various studies using RF showed variations in the number of trees chosen, for example Midekisa et al. (2017) used 200 to classify the whole of Sub-Saharan Africa, Carrasco et al. (2019) used 100 trees to classify Wales using 13 classes, and Tassi & Vizzari (2020) used 50 trees to classify and area of 154km^2 with 7 classes. The effect of using more trees is investigated by conducting an accuracy assessment.

3. Train the classifier and classify the image:
Training the classifier requires defining the number and order of the bands in the image. Image classifications are dependent on the reflectance properties of the surface. The classifications are conducted over the SR products of satellites. For the GEE classification, specific bands need to be selected to train the classifier. Every satellite SR product contains at least basic six bands, namely blue, red, green, near infrared and two shortwave infrared bands. Sentinel-2 contains more detailed bands in the visible red spectrum called the red-edge bands. These, along with the six basic bands, are often used for land cover classifications as seen in (Carrasco et al., 2019). The effect of using different bands for the classification was investigated by conducting an accuracy assessment using the basis bands and full bands for Sentinel-2. A detailed analysis of the effect of band selection is given in section 5.2.4. The image is then classified using the selected bands and training data.

4. Accuracy assessment:
Lastly, the accuracy assessment is done by generating a confusion matrix to evaluate the accuracy across classes and overall accuracy. This method is used in Abass et al. (2018); Midekisa et al. (2017); Xie et al. (2019); Pal (2005). Of the total samples collected, 70% are used for training purposes and 30% for for validation purposes. As explained in the GEE guide (*Guides: Supervised Classification* (2021)), the first step is to get resubstitution accuracy from the training data by creating a confusion matrix. The same can be applied to the validation data. Calling an error matrix the classified image will generate a confusion matrix representing the accuracy per class. Once the classification has been made, it can be applied to different composites and trained over different satellite images. In this study the changes in land use over time are of interest, therefore a few different composites from different years were selected to see the changes in land use over the years, as shown in Table 5.2.

Table 5.2: Overview of composites used for classification.

Composite	***Product***	***Resolution (m)***	***Composite date range***
1986	Landsat 5	30	1986-01-01 to 1986-01-20
2013	Landsat 8	30	2013-01-01 to 2014-01-01
2020	Landsat 8	30	2020-01-01 to 2021-01-01
2020	Sentinel-2	10	2020-01-01 to 2021-01-01

5.2.3 Effect of sample size

Moreover, the sensitivity of the algorithm to the training sample size of this study was tested by conducting the classification with different sizes as seen in Li et al. (2014). Four subsets were created using the feature collection of training samples, starting with 100% of the training samples, followed by 80%, 60%, and 40%, subsequently conducting an accuracy assessment on each of the subsets to determine whether the sample size is sufficient.

The effect of sample size is investigated by creating subsets of the samples collected, namely with with 100%, then 80%, 60%, and 40% of the data. This is done by creating an extra column in the total samples that generates random values between 0 and 1. To get 80% of the samples only, select all random values below 0.8. This then gives a new sample set containing only 80% of samples. The same is done for the other percentages. By carrying out a validation on each classification created using only subsets of the total samples, the errors and classification maps are compared to determine the effect.

5.2.4 Effect of band wavelengths

Surface reflectance products from sensors aboard satellites are designed in a way that when radiation bounces back from the Earth's surface, the radiation is split into different spectral bands (Meijerink, 2007). For each satellite this categorisation may differ slightly, which is the case for the Landsat and Sentinel-2 surface reflectance products. Each surface reflectance product has at least six bands in common, namely blue, green and red in the visible light spectrum and near infrared (NIR), shortwave infrared 1 (SWIR 1) and shortwave infrared 2 (SWIR 2) in the infrared spectrum. The wavelengths corresponding to each of these bands for the different satellites is show in Table A.2. Figure 5.2 shows the range of each wavelength for the different products, and it can be seen that although the naming for the bands may be similar, the ranges slightly differ. This is important for land use classifications as the classification is created based on bands from the composite image from a specific satellite. If the same classification is applied to another surface reflectance product with slightly different wavelength ranges for corresponding bands, the classification will perform differently.

In this project, the classification is created using Sentinel-2 as the underlying classification image. Firstly, the classification is made using all Sentinel-2 visible bands (2-7) and NIR, SWIR1, SWIR2 (8,11,12). However, red-edge bands 6 and 7 do not exist for the Landsat products, which go further back in time. To apply the same classification to historical images to see land use trends, the same bands are selected in order for the classification to work on Landsat images. Therefore, the bands shown in Figure 5.2 are be selected. The exact ranges of the wavelengths for each band are shown in Table A.2. To see the effect this has on classification, a validation assessment is performed on both classifications.

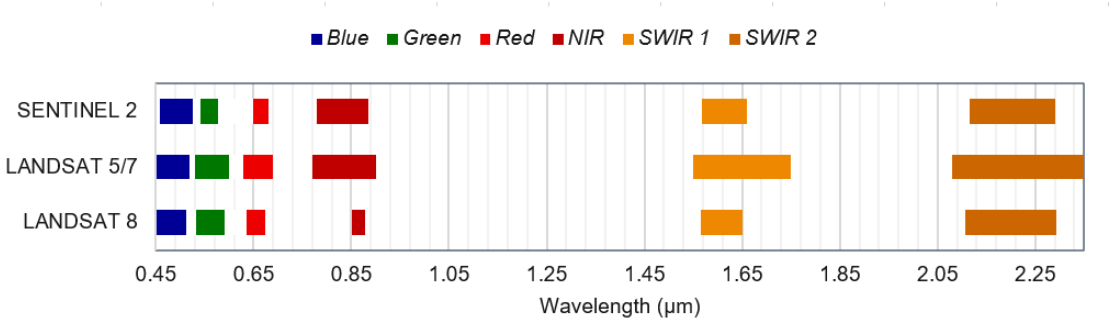

Figure 5.2: Spectral ranges for surface reflectance products of Landsat 5, 7, 8, and Sentinel-2 Level A.

These small differences in band categorisation are important for land use classification as the classification is carried out using selected bands only. If some wavelengths are left out that are important for certain classes, misclassification may occur more frequently. Therefore, it is important to understand the different reflectance properties of selected classes, namely of the ones shown in Table 5.1. Meijerink (2007) explains the spectral signatures of water and soils are affected by viewing conditions, roughness, moisture, and mineral content to name a few. The following explanation on spectral signatures is retrieved from Meijerink (2007). Water's reflectance properties depend on whether the water is clear, has high suspended matter (murky/muddy), highly vegetated under or above the water surface. Wavelengths of about 0.5-0.6 μm in the blue/green

spectrum can penetrate water to about 10 meters. Red is partly absorbed and wavelengths beyond NIR are fully absorbed, therefore shallow water bodies are best detected using the infrared bands. For soils, reflectance spectra generally show a rise from 0.40 to 1.75μm, with scattering and absorption governed by mineral and organic matter and surface roughness. Soil moisture has a great influence on the reflectance, as a more humid soil will generally have a lower reflectance.

5.3 CHIRPS for precipitation

CHIRPS provides readily-usable precipitation data that can easily be directly implemented into the GEE water balance. To investigate the performance of CHIRPS over Kumasi, 5-day and monthly CHIRPS precipitation for 2020 is compared to 2020 TAHMO rain-gauge data. Comparing the two datasets is complex due to the differences in satellite-based precipitation data and rain-gauge precipitation. Rain gauges make point measurements while CHIRPS observes precipitation over a large area. Bowman (2005) explains satellite precipitation can average out high precipitation events while rain gauges observe short-term events, leading to higher precipitation sums. Meijerink (2007) explains correlation coefficients between satellite-based and rain-gauge based precipitation estimates generally range between 0.5-0.7 depending on the region and methods used. Therefore, correlation between the two datasets is determined using Pearson's r correlation coefficient for the precipitation events of 2020.

5.4 Evaporation

5.4.1 MODIS for evapotranspiration

The Penman-Monteith equation used to in the MODIS algorithm is shown below in Equation 6, where s= slope of the curve relating saturated vapor pressure (e_{sat}) to temperature, A' = available energy partitioned between sensible heat and latent heat fluxes on land, $e_{sat} - e$ = air vapor pressure deficit, C_p = specific heat capacity of air, r_a = aerodynamic resistance, and r_s = surface resistance. The algorithm has been further improved to account for night-time ET (Falalakis & Gemitzi, 2020). Total daily ET in the MOD16 algorithm is the sum of wet canopy surface evaporation, dry canopy surface transpiration and soil surface evaporation. The pixel values from MOD16 are the sum of ET in the 8-day period, hence referred to as an 8-day composite. Due to the dependence of the calculations on vegetation indices such as LAI, evaporation from urban areas ET cannot be estimated using the MOD16 algorithm.

$$\lambda E = \frac{s \times A' + \rho \times C_p \times (e_{sat} - e)/r_a}{s + \gamma \times (1 + r_s/r_a)} \tag{6}$$

The MODIS remotely sensed data used in ET calculations are land cover, albedo, leaf-area index (LAI), and fraction of absorbed photosynthetically active radiation (FPAR). Each variable has global coverage with a 1km^2 spatial resolution and an 8-day temporal resolution. The land cover classification consists of 17 different land cover types. Due to the coarse resolution, accurate land cover is difficult to obtain in areas with complex vegetation, but the product allows for consistent monitoring of global land cover. Albedo is also an 8-day composite product, represented as an average of the underlying 500m albedo quantities that are produced from anisotropy models and is used to determine net incoming radiation to the surface. LAI/FPAR is an 8-day composite product where the maximum value across 8 days is chosen as the output pixel. In the algorithm, FPAR is used to determine the vegetated cover fraction, finally used in the soil heat flux calculations. LAI is used to determine aerodynamic and wet canopy resistance. The MOD16 algorithm assumes that LAI and FPAR do not vary in an 8-day period. Moreover, daily meteorological data at a global coverage is provided by the NASA's Global Modeling and Assimilation Office (GMAO), with spatial resolutions of 1°x1.25°(GMAO) and 0.5°x0.6°(MERRA GMAO). Data includes average and minimum air temperature, incident PAR, and specific humidity, which is derived using a global circulation model incorporating satellite and ground-observations.

Two main complications arise when using the MOD16 algorithm to estimate ET, these are the issues of no-data urban ET and cloud-cover. Firstly, an urban dataset on ET is not provided due

to MOD16 requiring LAI inputs that are not available for urbanised areas. LAI/FPAR is only available for areas that are non-urban, as classified by the MODIS land cover product. Moreover, the dataset is not always reliable as it requires albedo and FPAR/LAI inputs that are governed by cloud-cover. ET calculations are made over cloud-free pixels producing inconsistent datasets over an area when cloud cover is high. This issue has been seen in studies such as (Jia et al., 2012), where remotely sensed ET was validated over the Hai River Basin in China. Spatial and temporal gaps in ET were filled by generating a continuous ET series using surface resistance from clear sky days. On cloudy days the LAI and meteorological elements from clear sky days was used for ET estimates. Such a method is not applicable to this study as the remotely sensed evapotranspiration is directly extracted from MODIS. Instead, a modified ET estimate is made following the methodology in Figure 5.3. The general method uses the land cover classification, where average ET estimates per land cover class are made by finding the average ET on each land cover pixel on the extent of the whole classification image. The ET estimates are then updated by applying the average ET onto each land cover pixel. Cloud cover is highest during the rainy season, where it is assumed that ET is close to potential ET due to more available water for ET. In the dry season the average ET is retrieved from the actual ET product from MODIS, whereas in the wet season this is from potential ET. Finally, the monthly ET used in the water balance is found by applying a weighted sum to each ET pixel within the months for the time period of 2001-2020.

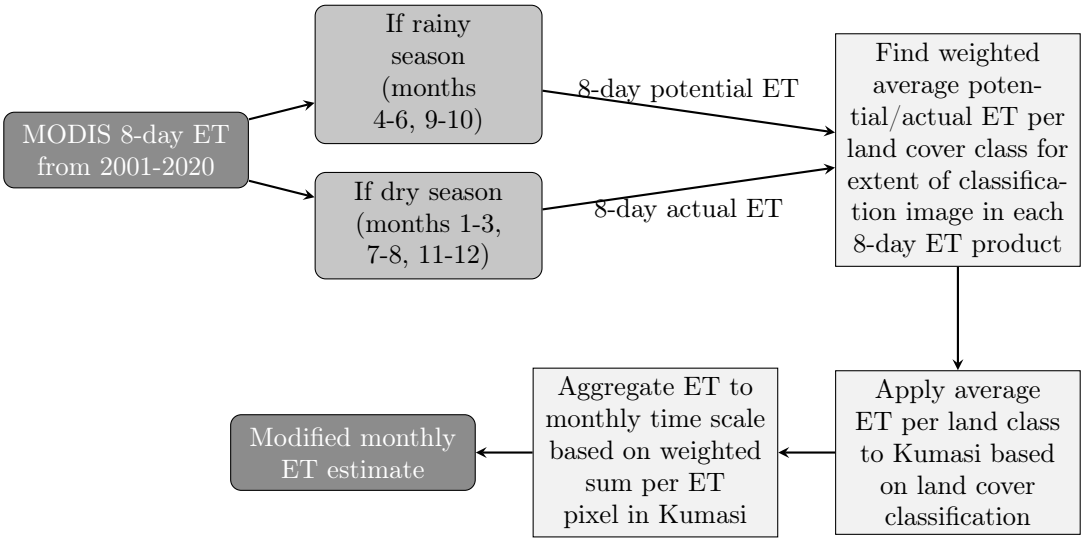

Figure 5.3: Methodology for modified evapotranspiration estimates in Google Earth Engine.

5.4.2 Hargreaves methodology for evapotranspiration

One of the main challenges in this study is the lack of access to available meteorological data necessary to validate MOD16 ET. In cases when climatic data is missing, the Hargreaves method proposed by Allen et al. (1998) can be used to estimate potential evaporation. Potential evaporation indicates the upper limit of evaporation, which can be used to confirm the potential ET results from MODIS. Therefore, the Hargreaves method (described in section 5.4.2) is used to cross-check MODIS ET results over Kumasi.

Methods to calculate evapotranspiration require meteorological and physical parameters that can be measured directly in weather stations or by use of an empirical relationship proposed by FAO (Allen et al., 1998). Allen et al. (1998) proposed alternatives for when data on solar radiation, relative humidity or wind speed data is missing, namely the Hargreaves ET_o equation shown in Equation 7. ET_o is the potential evapotranspiration, T is temperature, and R_a is the extraterrestrial radiation. One disadvantage of using this method is that ET results do not incorporate general climatic components of wind speeds or relative humidity which influence ET making them

less accurate than methods that do. Allen et al. (1998) explains that Equation 7 tends to underpredict under high wind conditions and overpredict under high relative humidity conditions.

$$ET_o = 0.0023(T_{mean} + 17.8)(T_{max} - T_{min})^{0.5} R_a \tag{7}$$

TAHMO temperature data was used to calculate Hargreaves ET. Each station provides mean, minimum and maximum daily temperature records which can then be input into Equation 7. The difference between the measured average daily temperatures for different weather stations can be seen in Figure 5.4.

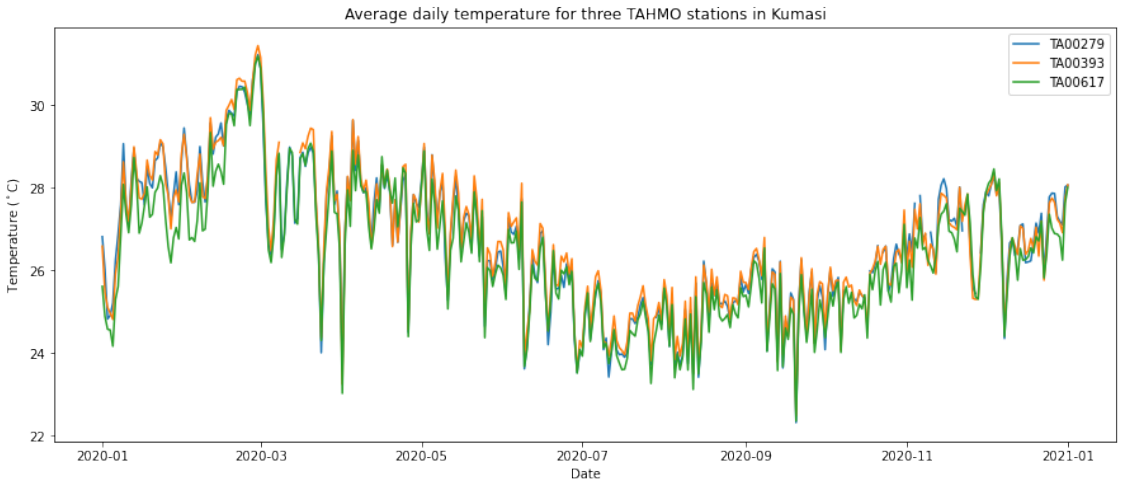

Figure 5.4: Average daily temperature in Kumasi from TAHMO weather stations.

Extraterrestial radation, R_a is the local intensity of the incoming solar radiation at the top of the atmosphere. This intensity is governed by the angle between the direction of the sun rays and the normal to surface of the atmosphere, which changes throughout the day and during different seasons. For daily time periods Allen et al. (1998) gives Equation 8 to calculate R_a [MJ/m^2/d], where G_{sc} is the solar constant (0.0820 MJ/m^2/min), d_r is the inverse relative distance Earth-Sun, ω_s is the sunset hour angle [rad], ϕ is latitude [rad], and δ is solar decimation [rad]. The inverse relative distance Earth-Sun, d_r, is calculated from Equation 9 and δ, is calculated using Equation 10, where J is the number of the day in the year. Sunset hour angle, ω_s, is given by Equation 11.

$$R_a = \frac{24(60)}{\pi} G_{sc} d_r [\omega_s sin(\phi) sin(\delta) + cos(\phi) cos(\delta) sin(\omega_s)] \tag{8}$$

$$d_r = 1 + 0.033 cos \frac{2\pi}{365} J \tag{9}$$

$$\delta = 0.409 sin(\frac{2\pi}{365} J - 1.39) \tag{10}$$

$$\omega_s = arccos[-tan(\phi) tan(\delta)] \tag{11}$$

5.5 Runoff using SCS-CN

The SCS-CN method has been applied in Wakode et al. (2018), Sisay et al. (2017) and Domfeh et al. (2015) to estimate runoff. This method considers the distribution of soil type and land cover, and can be applied to estimate runoff in small urban catchments (Wakode et al., 2018). It is easily applicable due to the minimal input data required (Yao et al., 2018). The SCS-CN runoff equation is given in Equation 12 where Q is runoff depth, P is accumulated rainfall depth, I_a is the initial abstraction of water, and S is the potential maximum retention all in millimeters. All

of the following equations and information was summarised from the USDA manual on how to use the SCS-CN method, unless stated otherwise.

$$Q = \frac{(P - I_a)^2}{(P - I_a) + S} \tag{12}$$

I_a includes all losses before runoff begins and is influenced by soil and cover parameters and can be related to S. The losses include of interception, initial infiltration, surface depression storage, and evapotranspiration. Studying many small agricultural watersheds the empirical relation in Equation 13 was found. Substituting this relation in Equation 12, Equation 14 is achieved. Finally, S can be calculated with the Curve Number (CN) using Equation 15.

$$I_a = 0.2S \tag{13}$$

$$Q = \frac{(P - 0.2S)^2}{P + 0.8S} \tag{14}$$

$$S = 25.4(\frac{1000}{CN} - 10) \tag{15}$$

The CN is determined by hydrologic soil group (HSG), cover type, treatment, hydrologic condition, and antecedent moisture condition (AMC). Urban areas are not completely covered by impervious surfaces and therefore soil remains an important factor when estimating runoff. The soil groups are divided into four hydrological soil groups according to their minimum infiltration rates. Land cover also influences runoff and therefore distinctions should be made between different cover types. Treatment modifies land cover and refers to the management of cultivated agricultural lands. The hydrologic condition of the area indicates the land use/land cover effects and describes the soil runoff potential for the specific HSG. Factors such as vegetation density, year-round cover, and surface roughness can be considered when determining condition, however this is mostly important for agricultural lands and not urban areas. Lastly, the AMC indicates the runoff potential before a storm event, accounting for the variation in CN for storm events.

Table 5.3 shows the factors required to determine the Curve Number. The HSG's can be found using the criteria from USDA (1986) to group the soil groups in the study area, as shown in Table 5.5. The antecedent moisture conditions are classified into three different classes. AMC I: soils in basin are practically dry, AMC II: average condition, AMC III: soils are practically saturated from antecedent rainfalls. The soil moisture conditions can be estimated from the 5-day antecendent precipitation, as shown in Table 5.4.

Table 5.3: Overview of factors used to estimate the curve number, their relevance for runoff estimations and how the factors can be determined.

Factor	Relevance for runoff	Method
Land use/land cover	Represents surface conditions in drainage basin and effect of cover on runoff generation.	Land cover classification
Hydrological soil groups	Different soils influence runoff potential due to their infiltration potential.	Derived from soil properties
AMC	Thoroughly wetted soils will lower infiltration rates and dry soils yield high infiltration rates.	5-day antecedent precipitation
Treatment/practice relating to hydrological condition	Applied to agricultural land uses including mechanical agricultural practices. For urban areas this effect can be considered small in relation to other factors.	Not applicable

Table 5.4: Antecedent soil moisture conditions (AMC) derived from 5-day precipitation sum. Values retrieved from Mishra & Singh (2013)

AMC	Antecedent 5-day precipitation (mm)	
	Dormant season	*Growing season*
I	Less than 13	Less than 36
II	13 to 28	36 to 53
III	More than 28	More than 53

In the SCS-CN method, another important factor is the condition of the urban impervious area. Percentage of impervious area and the connectivity of the area to the drainage system should be considered when determining an urban CN. A connected impervious area is described as one where runoff directly flows into the drainage system or if runoff occurs as concentrated shallow flow that first goes over a pervious area before arriving in the drainage system. In this study it is assumed that the urban area is connected directly to a drainage system. When estimating the CN for an urban area with a certain percentage of non-urban cover, it is assumed that the non-urban area is in good hydrologic condition and the impervious areas have a CN of 98 directly connected to the drainage system. The hydrologic condition applies to agricultural catchments and therefore is only a determining factor in vegetated land use. Here it is assumed that vegetated areas are always in good condition, indicating that the area is lightly grazed and there is more than 75% plant cover in the area.

Finally, the direct runoff can be estimated using Equation 14 once the CN is known. However, the curve number is not constant per HSG as the AMC varies depending on the relative soil moisture. This can be solved by either using the normal AMCs (seen in Domfeh et al. (2015)), differentiating between dry and rainy seasons (seen in Wakode et al. (2018)), or using antecedent 5-day precipitation to determine which curve number to use. In this study, the curve number is selected depending on the 5-day antecedent precipitation as seen in Table 5.4. For example, if 5-day antecedent precipitation is higher than 13mm, then the CN corresponding to AMCI is selected to compute runoff. Look-up tables from USDA (1986) are used to determine curve numbers for AMCII (normal conditions) based on land use properties, and then converted to AMCI and AMCIII by conversion tables given in Mishra & Singh (2013). HSGs are determined using available soil maps for Kumasi (shown in Figure A.1) and comparing these to the soil properties given by USDA (1986) in Table 5.5. Equations 14 and 15 are applied on each land use class pixel in Earth Engine to compute the curve number and retention giving a spatial distribution of runoff.

Table 5.5: Properties of the hydrological soil groups defined by USDA (1986).

HSG	Soil textures	Soil properties
A	Sandy, loamy sand, sandy loam	Low runoff potential, high infiltration rates when thoroughly wetted and high rate of water transmission. Deep, well to excessively drained sand or gravel.
B	Moderately fine to fine texture, e.g. silt loam or loam	Moderate infiltration rates when thoroughly wetted, moderately deep to deep, well drained soils.
C	Moderately fine to fine texture, e.g. sandy clay loam.	Low infiltration rates, consist of soils with layer impeding downward movement of water and soils. Low rate of water transmission.
D	Clay loam, silty clay loam, sandy clay, silty clay, clay	High runoff potential, low infiltration rate when thoroughly wet. Water movement through soil is very restricted.

General limitations of this method include that various dynamic are not considered, such as rainfall intensity and duration (Mishra & Singh, 2013). Soulis (2021) explains slope and initial soil moisture conditions can also affect runoff generation, factors which are not implemented into the SCS-CN method. The accuracy of the method is heavily influenced by the selection of the proper curve number which requires a good understanding of surface characteristics (USDA, 1986). Moreover, the initial abstraction remains an uncertain factor in the method, Krajewski et

al. (2020) recommends local verification of the abstraction ratio. These processes are not included as a balance is made between creating the best possible runoff prediction without sacrificing the simplicity of the method. However, combining SCS-CN and earth observation is a valuable tool to understand the evolution of runoff responses under heavy urbanisation (Psomiadis et al., 2020).

5.6 Groundwater recharge

Groundwater recharge estimations were done using the water balance principle and carried out in Google Earth Engine. This required components of precipitation, evapotranspiration, and runoff to be input into Earth Engine. In Table 4.1 the availability of the satellite products used is given, where the largest overlap of forcing data is shown to be between January 2001 to the present. Therefore, this was the time range chosen to compute long-term average natural groundwater recharge. Natural recharge was estimated on a monthly basis by combining monthly precipitation, evapotranspiration and runoff by using Equation 1. In studies that used the water balance approach (e.g. Szilagyi et al. (2011) and Kortatsi (1994)), net groundwater flow and groundwater storage changes are assumed to be negligible when averaging over a longer time period (over 10 years), which is also assumed in this study. For shorter time periods the water balance equation is shown in Equation 16, where P is precipitation, Q is runoff, ET is evapotranspiration, GWR is the average annual recharge/discharge, Δ S_S and Δ S_G are the change in surface water storage and the change in groundwater storage respectively. Averaging over several years Δ $S_S \approx$ Δ $S_G \approx 0$, reducing the water balance to Equation 17 as seen in Section 2.3.

$$P = Q + ET + GWR + \Delta S_S + \Delta S_G \tag{16}$$

$$P = Q + E + GWR \longleftrightarrow GWR = P - Q - ET \tag{17}$$

Recharge was modelled spatially in Earth Engine following the methodology shown in Figure 5.5. The satellite datasets used for meteorological inputs were CHIRPS for precipitation and MODIS for evapotranspiration. In Earth Engine, the forcing data between 2001 and 2020 was selected and monthly sums for the forcing data were calculated. For the MODIS ET dataset, the low resolution resulted in areas of Kumasi where no ET was calculated as the area was majorly urban. However, in the 30m resolution land classification, clear vegetated patches were present where no MODIS ET pixels existed. In reality these areas would exhibit high ET values due to the vegetation. Therefore, the average ET values per month were calculated per land class, and these averages were masked over areas with no ET based on their land cover classification.

Monthly runoff was calculated using the SCS-CN method using the created land use classification for 2020. This method was initially applied for 2020, creating one image per month that contained 5 bands: precipitation (mm), runoff (mm), evapotranspiration (mm), recharge (mm) and classification. The recharge was calculated per land cover pixel using effective precipitation (P - Q) as inputs to the groundwater system and evapotranspiration as a flux removing water from the groundwater system. Due to annual variations in precipitation and evapotranspiration, the long-term average groundwater recharge was firstly calculated between 2001-2020 using the 2020 land cover classification. The sensitivity of the estimations to land classification was then determined by using the same long-term average and applying the model to historical land classifications.

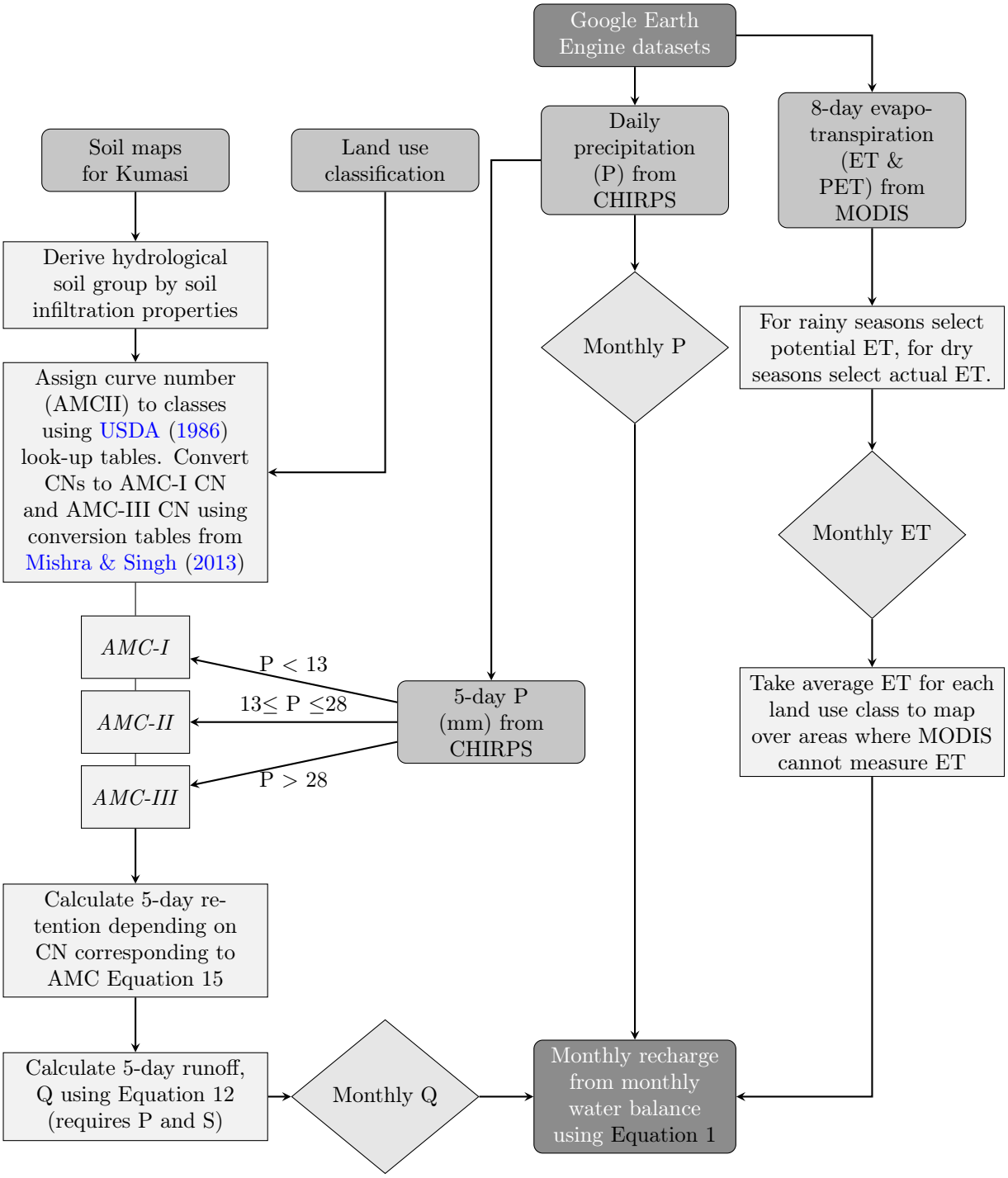

Figure 5.5: Flow chart for groundwater recharge estimation using the water balance approach in GEE.

5.7 Groundwater consumption

5.7.1 Domestic groundwater consumption

Domestic groundwater consumption requires data on groundwater consumption per capita, total water consumption per capita, and total population. Consumption for 2020 is estimates using Equation 18, where $C_{GW,domestic}$ is total groundwater consumption per month [Mm^3/month], P is the population in the investigated year, $C_{tot,daily}$ is total water consumption per capita [Mm^3/cap/d], N_{month} is the days in the corresponding month, and $GW\ use$ is the percentage of the population dependent on groundwater. The main assumption is that the percentage of households reliant on each source is translatable to the per capita reliance on each source.

$$C_{GW,domestic} = P \times C_{tot,daily} \times N_{month} \times \text{GW use} \tag{18}$$

Daily per capita water consumption ($C_{tot,daily}$) is dependent on socio-economic factors: low income residents were estimated to consume 0.025-0.035m^3/day compared to the 0.060-0.075m^3/d of middle-income residents and 0.120m^3/d of high-income residents (Maoulidi, 2010). Kuma et al. (2010) states average daily consumption for inhabitants of Kumasi is estimated to be at 0.094m^3/d. This data comes from surveys conducted in four major suburbs of the city.

An overview of the sources of water is given in Table A.6 where it can be seen that piped water is the predominant water source, which comes from the Barekese and Owabi reservoirs. The percentage of households dependent on groundwater is calculated by summing up the percentage of households relying on boreholes/pumps/tube wells, protected wells and unprotected wells as shown in Table A.6. For drinking purposes it is 19.2% and for domestic purposes it is 23.8%. Assuming that domestic water consumption is much greater than drinking water, the value of 23.8% is used as the percentage of groundwater sourced supply ($GW\ use$).

5.8 Survey for non-domestic groundwater consumption

A survey was carried out by AAMUSTED in Kumasi from June to August 2021 to determine the component of non-domestic groundwater consumption. At each survey point data was collected on whether the source has dried up before, usage period in years, purpose of abstracted groundwater, any water quality issues, and water used per day. The final estimate of total non-domestic groundwater consumption (C) per facility (F) can be estimated using Equation 19, requiring estimates on groundwater consumption per facility and how many of each facility exist in Kumasi. Here, $C_{non-domestic,F}$ is non-domestic water consumption per facility in Mm^3/d, n_F is the estimated number of the facility in Kumasi, C_{survey} is the average water use for the facility from survey results in Mm^3/d, and groundwater dependence is the estimated average dependence of the facility on groundwater in percentage. The annual total of non-domestic groundwater consumption for 2021 is then estimated by summing up the consumption per facility and multiplying this by the days in the year. In this study, 2021 consumption is assumed to be the same as 2020 consumption.

$$C_{non-domestic,F} = n_F \times C_{survey} \times \text{GW dependence per facility} \tag{19}$$

6 Results

6.1 Land cover classification

6.1.1 Spectral signatures

Overlap of different classes is assessed with the spectral signatures of the collected samples. The Google Earth Engine code can be found in Appendix B. Spectral signatures are found by accumulating all sampled polygons for each class into one GEE Feature Collection with 6 distinct properties corresponding to the unionised polygons per land cover class. Reflectance properties are stored in the surface reflectance product for each band on Earth Engine. The samples are collected over the Sentinel-2 SR composite of 2020, which contains different bands used to determine the signatures. By renaming each band with its corresponding central wavelength, a chart can be made in GEE showing the average reflectance properties of all the polygons for each class. This chart is shown in Figure 6.1, representing the unique signatures of each land cover class from the sample data.

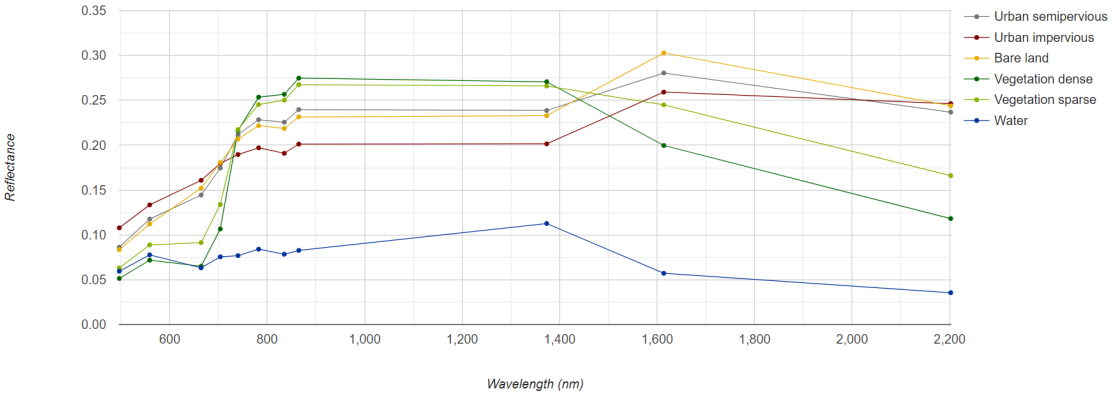

Figure 6.1: Spectral signatures of collected samples for classification. Wavelengths are based on the Sentinel-2 bands used for the initial classification.

Starting with the vegetation classes, it can be seen in Figure 6.1 that there is an overlap in the reflectance properties for wavelengths between 700nm and 1400nm. Distinction between the two classes is therefore determined by reflectance in the red ($\sim 680nm$) and shortwave infrared bands ($1900nm$-$2200nm$). When looking at bare land there is a large overlap of this class with the urban semipervious class, with reflectance properties only differing in the SWIR1 band. Semipervious urban samples were selected as a combination of vegetated and urban areas, explaining the large overlap. Especially in urban agglomerations, vegetation that does exist consists of small gardens, sparsely-vegetated areas or bare land leading to an overlap in reflectance properties. Moreover, impervious urban areas have unique signatures in in the visible spectrum and NIR, showing generally lower reflectance in the wavelengths than the other classes (excluding water). In the SWIR2 band, the urban and bare land classes become indistinguishable, making the visible and NIR bands important for impervious urban classification. Lastly, water shows the most unique signature with very low reflectance properties, the largest overlap being seen with vegetation in the visible red, green, blue (RGB) bands.

These spectral signatures are important to understand misclassification issues and can be used to improve initial classifications. To apply the same classification trained on Sentinel-2 to the Landsat products only red, blue, green, NIR, SWIR1, and SWIR2 bands are selected as these are the overlapping bands. Looking solely at the reflectance properties in the visible bands (RGB), it is difficult to distinguish dense vegetation from water and bare land from semipervious urban. For the dense vegetation/water distinction, the infrared bands become important. For the bare land/semipervious urban distinction only SWIR1 shows a difference in reflectance properties.

Initial samples were re-evaluated to produce more unique spectral signatures.

6.1.2 Improvements in classification

The samples trained on the Sentinel-2 composite for 2020 cannot be directly applied to the Landsat 8 composite for the same year due to the differences in resolution. Samples initially selected were too detailed and contained high resolution pixels that could not be seen in the Landsat 8 composite. Some examples are shown in Figure 6.2, where it can be seen that individual urban pixels cannot be seen using the 30m Landsat resolution. Moreover, streams in Kumasi are very narrow and can only sometimes be spotted using Sentinel-2 (such as in Figure 6.2.b). Initially these samples were selected but had to be removed when applying the same classification to the Landsat 8 composite due to inaccuracies. The samples were therefore re-evaluated by removing some that captured small details while adding new ones that represented the land classes better.

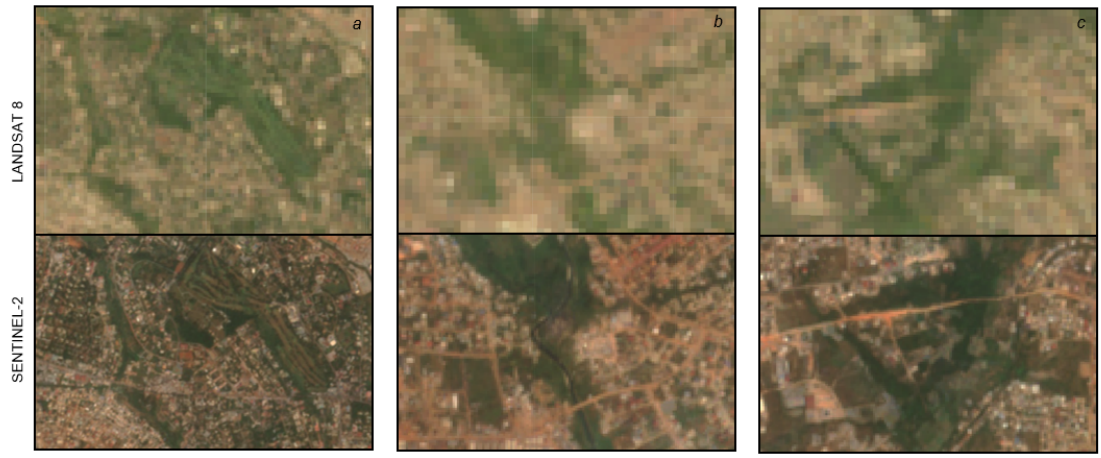

Figure 6.2: Differences in resolution between Sentinel-2 and Landsat 8. a) Agglomeration of urban pixels in L8, whereas S2 shows details that are not captured. b) Stream can be delineated with S2, but this is not captured in L8. c) Bare-land pixels are clearly seen in S2 but not in L8.

Moreover, the effect of changing the sample size is evaluated using the initial samples. Results are shown in Table 6.1, where it can be seen that the accuracy decreases slightly with a smaller sample size. The classes that are mostly affected are impervious and semipervious urban and sparse vegetation, where generally the loss of urban semipervious area is attributed to a gain in impervious area. This confirms that the sample size chosen is sufficient and not too large, as the accuracy is best when using the full sample size. The updated sample size is 100,422 with a total of 106 polygons.

Table 6.1: Effect of changing the sample size on classification. Sample size shown as number of pixels and class areas are rounded to the nearest squared kilometer.

Percentage of samples	***100%***	***80%***	***60%***	***40%***
Sample size	82182	65974	48976	32788
Training size	57484	46121	34639	22898
Training accuracy	0.980	0.978	0.974	0.970
Class	***Area (km^2)***			
Urban semipervious	130	132	129	128
Urban impervious	45	43	46	43
Bare land	4	4	4	5
Dense vegetation	9	9	9	9
Sparse vegetation	54	54	54	56
Water	0	0	0	0

6.1.3 Final classifications

Three different classifications for 2020 are compared, one trained on the Sentinel-2 2020 composite using the full bands, the other using the common bands and the last using Landsat 8. Using the common bands, classifications for the historical Landsat images from 2013 and 1986 are also carried out. An overview of the results of all classifications over Kumasi is shown in Table A.3. Table 6.2 shows the final results of the 1986, 2013 and 2020 classifications that were are in the water balance calculations. The 2003 composite is not included in the final investigation due to light cloud pollution over the whole image. It can be seen that the 2020 classification results agree well with each other and have a high accuracy. The areas that are mostly misclassified are bare land and sparse vegetation, which may be due to their overlap in spectral signatures. In the 1986 classification outside of the urban boundary, dense vegetation is misclassified as water in some cases due to common reflectance properties in the visible bands. The Sentinel-2 2020 classification using the full selection of visible and infrared band has a validation accuracy of 90% compared to the 80% accuracy of the Landsat classifications. Therefore, the 2020 full band classification is selected to carry out the recharge estimations for 2020. Figure 6.3 and Figure 6.5 show the 2020 and 1986 classifications, with small pixels sieved out for visualisation ease. The raw classifications used for calculations are shown in Figure A.2, Figure A.3 and Figure A.4. From 1986 to 2020 there has been a total loss of 63km^2 of vegetated land attributed to the growth of urban areas.

Table 6.2: Areas (rounded to the nearest km^2) and percentage cover per land class in Kumasi for the final classifications of 1986, 2013, and 2020. The percent point change in land cover area is given as the difference in percentage cover for the corresponding years.

Land cover	**1986**		**2013**		**2020**		***Percentage point change***		
	km^2	%	km^2	%	km^2	%	*1986 - 2013*	*2013-2020*	*1986-2020*
Urban semipervious	38	16	113	47	166	69	*31*	22	53
Urban impervious	4	2	4	2	28	12	*0*	10	10
Bare land	3	1	2	1	3	1	*0*	0	0
Dense vegetation	118	49	40	17	7	3	*-32*	-14	-46
Sparse vegetation	79	33	83	34	37	15	*2*	-19	-17
Water	0	0	0	0	0	0	*0*	0	0

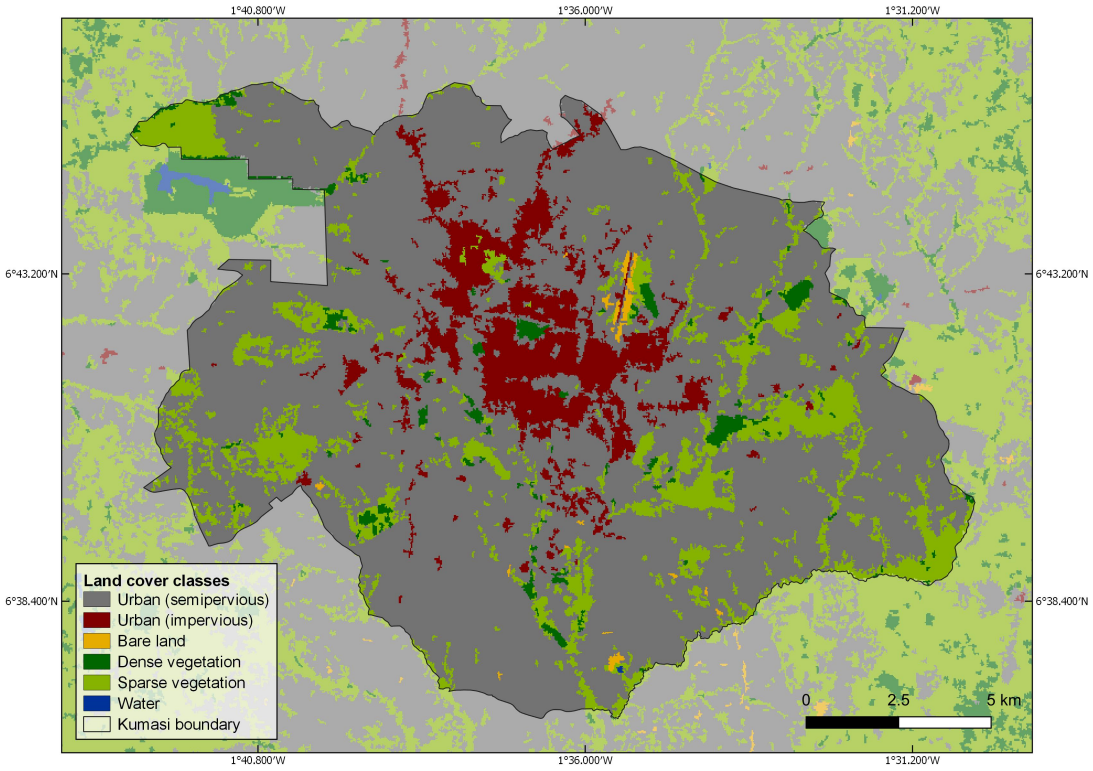

Figure 6.3: Land cover map for Kumasi in 2020 using Sentinel-2 composite.

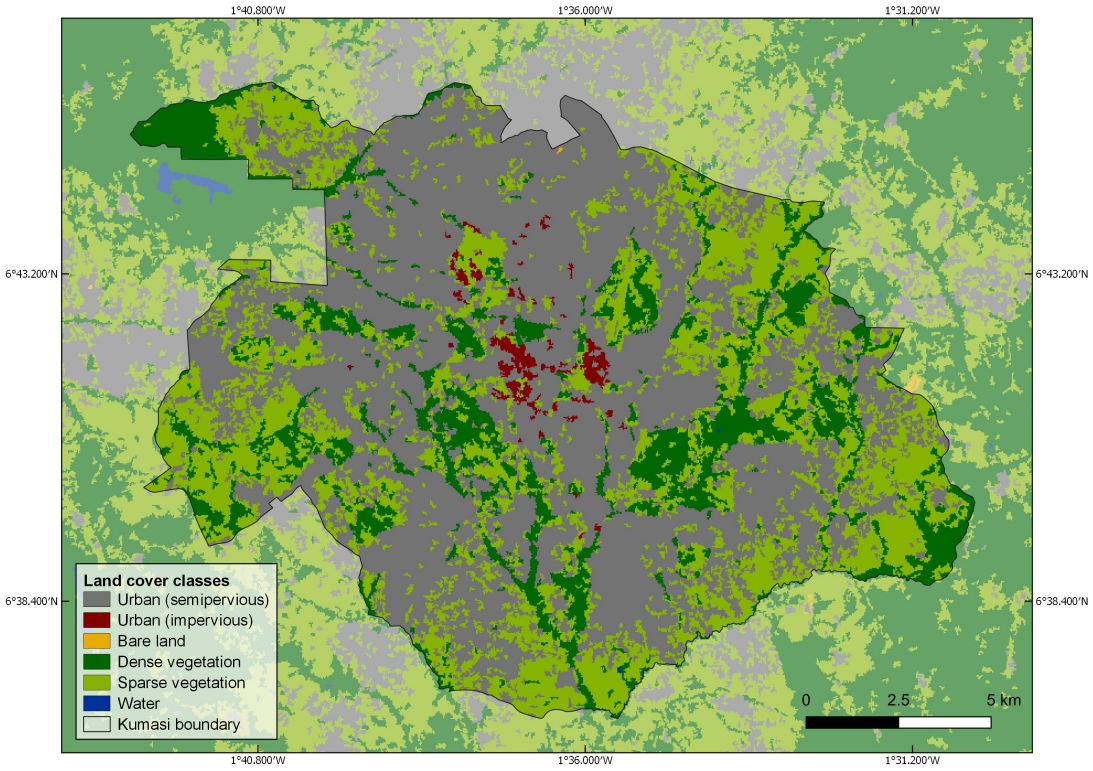

Figure 6.4: Land cover map for Kumasi in 2013 using Landsat 5 composite.

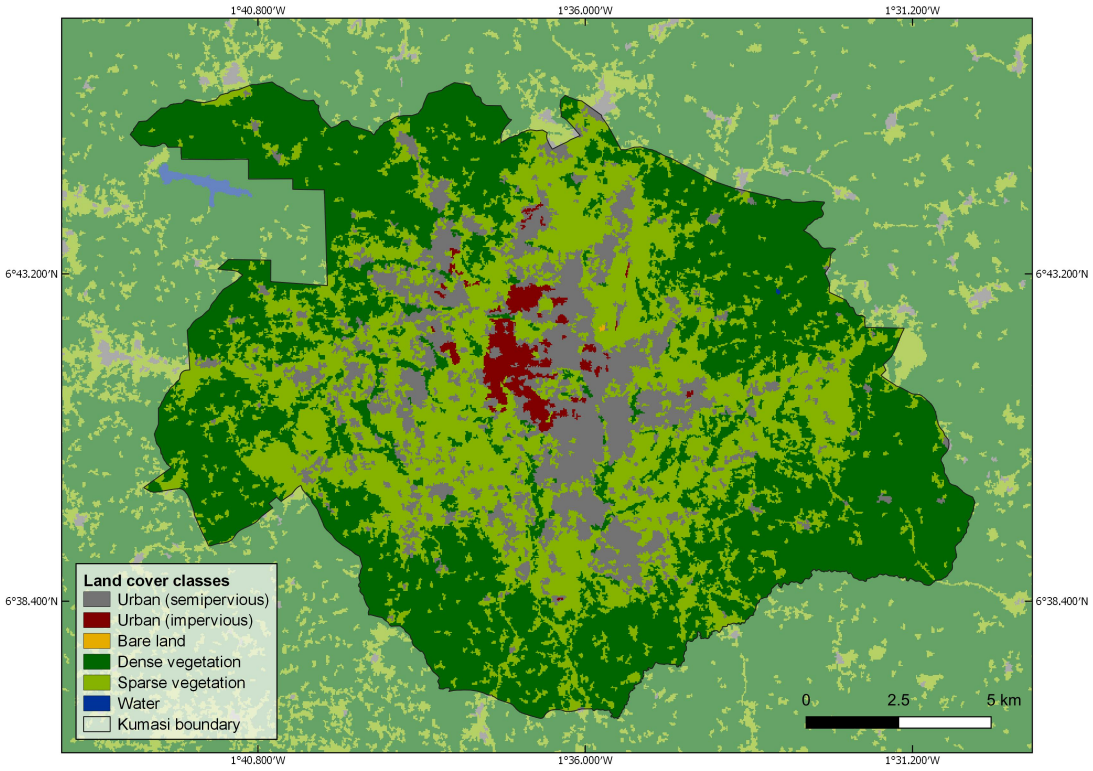

Figure 6.5: Land cover map for Kumasi in 1986 using Landsat 5 composite.

6.2 Runoff using SCS-Curve Number method

6.2.1 Hydrological soil groups

Based on the soil properties shown in Table 5.5, the HSG of known soils is derived. For Kumasi, a combination of the soil map by Ewusi et al. (2016) and the more detailed soil map from the European Soil Data Center (Figure A.1) is used to determine soil properties. Table 6.3 gives an overview of the soil characteristics for the different soil associations in Kumasi and the corresponding hydrological groups associated to each soil type. The spatial distribution of the HSGs is made in QGIS by digitising the map by Ewusi et al. (2016), creating a vector layer with polygons representing the different soil groups. This layer is then rasterised using the processing tools available in QGIS. The created raster file is imported into GEE as an asset to carry out the curve number estimation. The spatial distribution of the HSGs is shown in Figure 6.6.

Table 6.3: Soil characteristics in Kumasi. Comparison of soil maps from Amoateng et al. (2018b) and Panagos et al. (2011) in combination with the HSG characteristics from USDA (1986).

Soil compound association	Soil composition	Drainage characteristics	HSG
Bekwai-Akomadan-Oda	Silty clays, over abundant concentration of ironpan	Well drained	A
Bekwai-Oda	Bekwai series: silty clay loams and clays (largest part), Oda series: poorly drained, deep non-gravelly, silty clays	Mostly well-drained	A
Bomso-Offin	Sandy/gritty clay loams,large flakes of muscovite to white mica derived	Moderately well drained	B
Bomso-Suko	Sandy clay loams, free from concretions, gravels and stones	Well drained	A
Kumasi-Offin	Alluvial sands	Poorly drained	D
Nhyanao-Yinkong	Rocky soils	Excessively drained	A

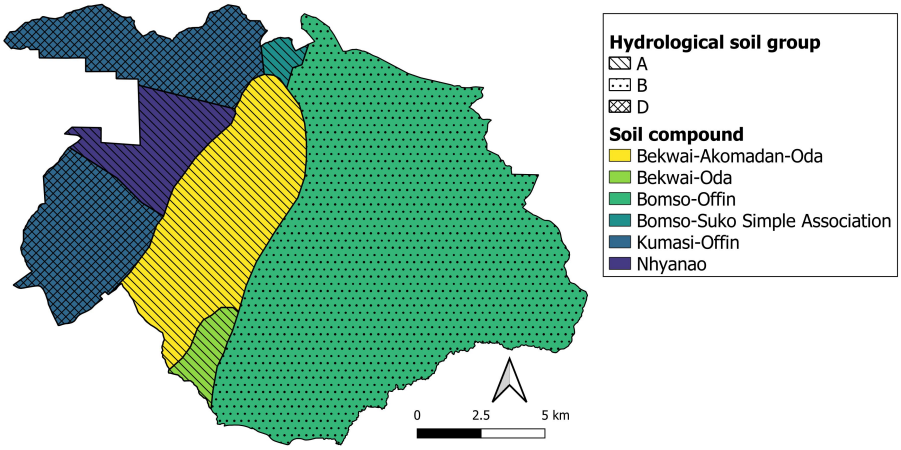

Figure 6.6: Hydrological soil groups and soil compounds of Kumasi.

6.2.2 Curve Numbers

Curve numbers per land cover class are selected by firstly assuming normal soil moisture conditions and subsequently analysing the defined land cover classes using look-up tables given by USDA (1986). A detailed overview of the land classes and their corresponding properties from USDA is given in Table A.4. These results are summarised in Table 6.4, where the ranges of curve numbers are also given. The sensitivity of recharge to these curve numbers are tested in Section 7.2. The best estimates correspond to the curve numbers used for the recharge computations. Note the curve number for water is always equal to 0.

Table 6.4: Curve number ranges and initial abstraction ratio for runoff computation.

Variables		**Best estimates**			**Min**			**Max**		
		Hydrological soil groups								
AMC	*Land cover*	**A**	**B**	**D**	**A**	**B**	**D**	**A**	**B**	**D**
II: average conditions	*0*	89	92	95	86	91	94	92	94	96
	1	98	98	98	98	98	98	98	98	98
	2	68	79	89	68	79	89	68	79	89
	3	30	55	77	30	55	77	30	55	77
	4	37	60	79	30	56	77	43	65	82
I: soil not wet at all	*0*	76	81	87	72	80	85	81	85	89
	1	94	94	94	94	94	94	94	94	94
	2	48	62	76	48	62	76	48	62	76
	3	15	35	59	15	35	59	15	35	59
	4	20	40	62	15	36	59	25	45	66
III: almost completely wet situation of the soil	*0*	96	97	98	94	97	98	97	98	99
	1	99	99	99	99	99	99	99	99	99
	2	84	91	96	84	91	96	84	91	96
	3	50	74	89	50	74	96	50	74	96
	4	57	78	91	50	74	96	63	82	92
Initial abstraction		0.2			0			0.3		

6.2.3 Runoff

Runoff in Kumasi is computed for each 5-day period from January 2001 to December 2020 using 5-day precipitation from CHIRPS and Equations 13 to 15. A 5-day period instead of a daily period is chosen due to the high computational time in Earth Engine. The 5-day runoff results are aggregated onto a monthly scale to be used for the monthly water balance. Average annual runoff between 2001-2020 is shown below in Figure 6.7. Long-term average runoff for Kumasi is 686 mm/y. Table 6.5 shows the variation of runoff per land use class. The effect of land cover on runoff can be seen as areas with the highest runoff correspond to those classified as urban impervious areas. On the western side of Kumasi where soil infiltration capacity is less, runoff is significantly higher than in areas with a different soil but similar land cover. Areas with low runoff are related to vegetated areas, such as in the flood plains and parks. In urban agglomerations the soil cover remains important for runoff generation as it can be seen that urban areas with soil group A have lower runoff generation than some vegetated areas in group D. Monthly variations follow a similar monthly pattern to precipitation due to the dependence of runoff on precipitation. Runoff is lowest during the dry season and highest in the months of the rainy season with peaks in June and October.

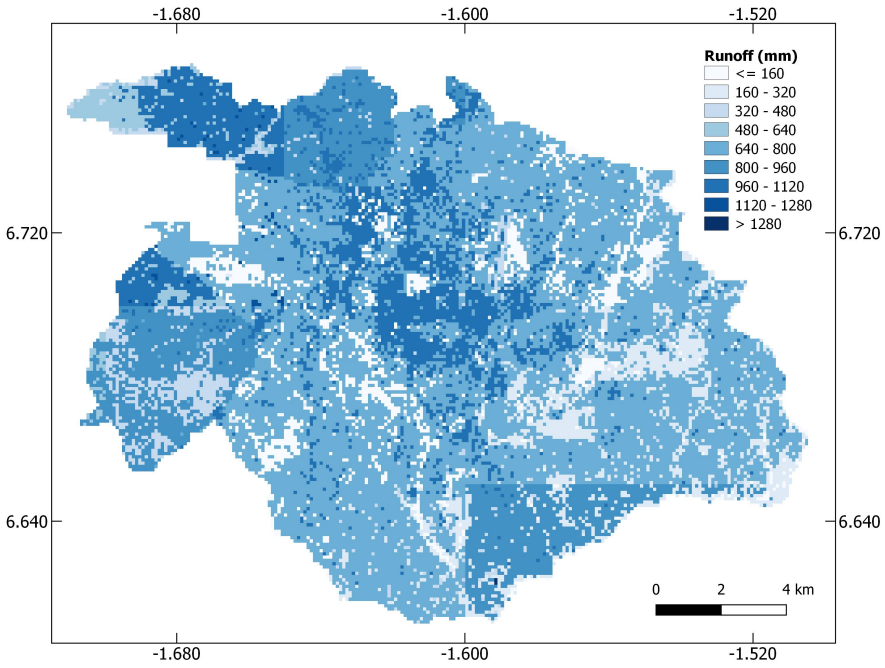

Figure 6.7: Average annual runoff in Kumasi for period of 2001-2020 using 2020 land cover classification.

Table 6.5: Runoff per land cover class using 2020 land cover map and long-term forcing (2001-2020)

Land cover	Runoff (mm)		
Semipervious urban	773	±	85
Impervious urban	1023	±	26
Bare land	427	±	114
Dense vegetation	142	±	138
Sparse vegetation	222	±	158
Water	1369	±	12
Sum	**686**		

6.3 Evapotranspiration results

Using the MODIS actual evapotranspiration dataset allows for a temporal and spatial assessment of the water balance as groundwater recharge can be calculated per pixel. This is the major benefit when using satellite products, however many challenges also exist when using such products. In this study, initial evapotranspiration estimates over Kumasi failed to reproduce the expected values of evapotranspiration (e.g. 680mm/y from Kortatsi (1994)). Three main issues were discovered: 1) low resolution of MOD16 ET masks the effect of smaller vegetated patches within Kumasi, 2) urban evaporation is unavailable due to the reliance of the MOD16 algorithm of LAI/FPAR, and 3) cloud cover affects spatial data availability, leading to underestimates of actual ET during the rainy season.

6.3.1 Resolution differences

Land cover maps used in this study have a resolution of 30m based on Sentinel-2 and Landsat products, whereas MODIS ET has a lower resolution of 500m. Due to this low resolution, ET data is unavailable for vegetated patches smaller than 500x500m within the urban area. This leads to an underestimate of ET in Kumasi as no data exists for evapotranspiration from vegetated and bare areas that contribute to the total ET of the area. For vegetated areas outside the urbanised region, evapotranspiration data does exist. The total potential and actual evapotranspiration for Kumasi in 2020 from MODIS is given in Figure 6.8. The no-data areas in the center of the region correspond to the areas identified as urban by MODIS, where no LAI/FPAR data exists. This no-data area comprises of approximately 38% of Kumasi's total surface area. The work-around used to retrieve values for the vegetated pixels within Kumasi consists of finding the average actual evapotranspiration per land cover class and applying this to areas where no evapotranspiration data exists. For consistency, the average ET values are then overlain on the land cover classification over the whole of Kumasi. The area chosen to derive the average evapotranspiration per land cover class is the extent of the classification image, which differs depending on the satellite product (see Table 6.6 for areas).

However, including actual evapotranspiration per land cover class still leads to an underestimate of monthly evapotranspiration. This underestimate is attributed to cloud cover during the rainy season, which is discussed in the following section 6.3.2. When applying the average evapotranspiration per land cover class onto the 2020 classification using monthly MODIS data from 2001-2020, mean annual actual and potential evapotranspiration is respectively 443mm and 891mm. The spatial annual variations and monthly variations can be seen in Figure A.5. Comparing the 398mm/y to the expected 680mm/y, this is an underestimate. During the rainy seasons MODIS actual and potential ET is underestimated due to the inability of the algorithm to produce results under high cloud-cover. To combat this, the potential ET during the rainy seasons is used to estimate the averages per land cover class. In Kumasi, the major rainfall season occurs between March to July and the minor season between August/September to October. In the long-term average monthly rainfall between 2001-2020, precipitation was over 120mm/month for the months of April to June and September and October. Although March still experiences high rainfall volumes, it was not included as a rainy season as it is the onset of the rainy season, therefore surfaces are assumed to be less saturated and ET rates are assumed to be closer to actual ET rather than potential ET. The accuracy of the ET estimates is therefore governed by the accuracy of the MODIS ET and the land cover classification.

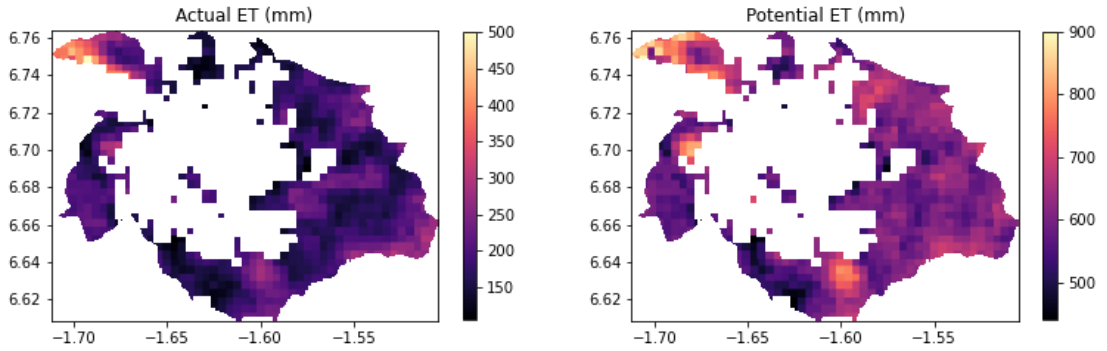

Figure 6.8: Average evapotranspiration from MODIS over Kumasi.

The final ET used in the water balance is therefore based off the average monthly actual evapotranspiration during the dry season and average monthly potential evapotranspiration during the wet season. The average ET for different land cover classes was calculated per month using a weighted sum of all 8-day evapotranspiration data from the corresponding month. The average annual evapotranspiration over Kumasi using this method is shown in Figure 6.9, referred to as "modified ET". Comparing this image to the 2020 land cover classification in Figure 6.3, similar spatial land cover patterns can be seen. Table 6.6 shows impervious urban areas have the lowest evapotranspiration, followed by semipervious urban and bare land. The highest evapotranspiration values are seen in the densely vegetated areas followed by sparsely vegetated areas.

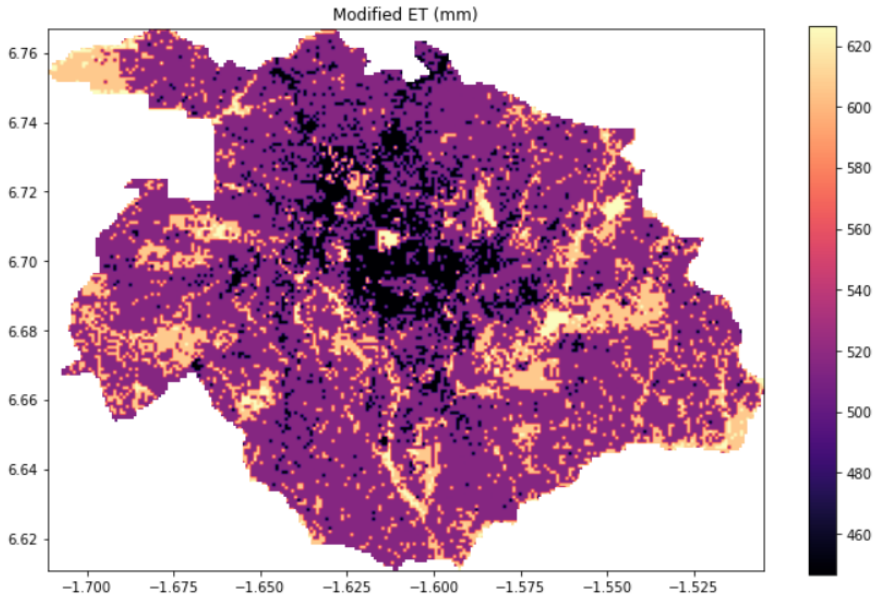

Figure 6.9: Annual mean evapotranspiration over Kumasi between 2001-2020. Improved estimate using average ET values over land cover classification of 2020.

Table 6.6: Annual mean evapotranspiration in Kumasi per land cover class for the period 2001-2020.

Classification	**2020**	**2013**	**1986**
Area (km^2)	*10765*	*4876*	*4876*
Urban (semipervious)	516	402	481
Urban (impervious)	447	372	408
Bare land	515	398	426
Dense vegetation	627	583	569
Sparse vegetation	606	472	509
Water	617	606	640
Annual sum	527	456	531

6.3.2 Effect of cloud cover

Cloud cover affects the MODIS ET dataset as LAI/FPAR and albedo data is required in the MOD16 evapotranspiration calculation algorithm. These datasets are only available for cloud-free pixels they are based on surface reflectance properties. In cases where there is no cloud free data throughout an entire year over a pixel, MODIS assigns fill values of ET/LE/PET/PLE (Mu et al., 2013). Figure 6.10 shows the percentage of cloud free data over Kumasi in 2020. Generally, the dry season (light grey) experiences less cloud cover hence providing more complete ET datasets over Kumasi. When looking at a larger area to retrieve average ET values per land class, there is generally more cloud free data available. However, nearing the end of the first dry season and on the onset of the second rainy season there is little cloud free data available independent of the selected area.

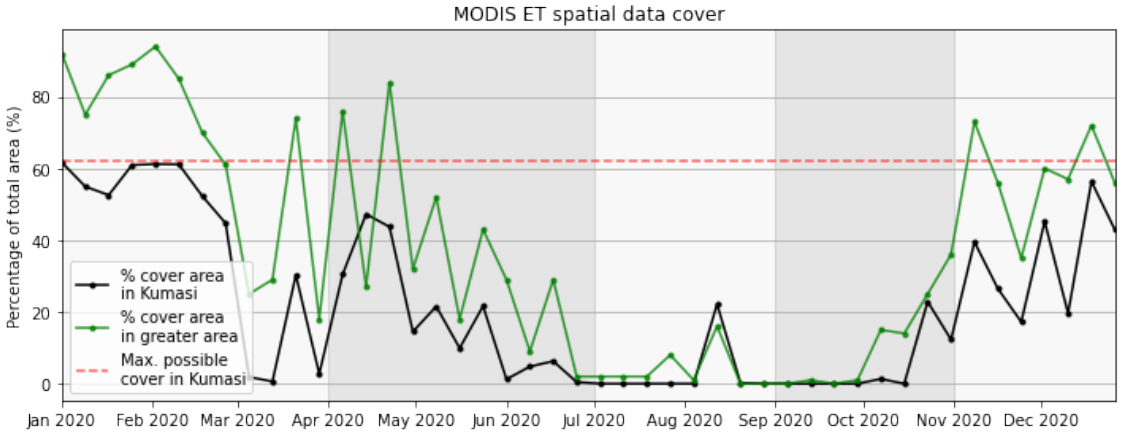

Figure 6.10: Percentage of total area in Kumasi covered by MODIS ET pixels throughout 2020. Red indicates the upper limit of pixel cover due to the no-data urban regions, dark grey indicates the rainy season and light grey indicates the dry season.

Scaling down individual MODIS ET products to a monthly period instead of an 8-day period increases the cloud free data over the area. Due to the low cloud free data cover, a weighted sum of ET per pixel was done over the whole classification area. Retrieving average ET values per land class was also conducted with a weighted average, with areas containing more complete ET data weighing more. For the classifications of 2013 and 1986, not all land cover classes contained cloud free pixels for monthly ET. This is due to two reasons: the classification area was significantly smaller resulting in some land cover classes and less urban pixels for these years led to a lower probability of cloud free pixels over the urban land cover classes.

6.3.3 Comparison to Hargreaves evapotranspiration

The Hargreaves evapotranspiration gives an indication of the upper limit of potential evapotranspiration. It does not include factors such as surface roughness, humidity, and wind speed, which are important for increasing the accuracy of evapotranspiration estimates (Allen et al., 1998). However, such a method is useful when access to meteorological data is limited, such as in this study. Comparing Hargreaves potential ET to MODIS potential ET in Figure 6.11 it can be seen that the greatest differences between MODIS and Hargreaves occur during the months of March and May/June to September. For the months where more data is available (see Figure 6.10) MODIS and Hargreaves correspond better than when less data is available. Moreover, the modified ET is generally lower than MODIS actual ET values. This can be explained by the dependence on land cover for the modified ET estimates: due to low percentage of green cover in Kumasi, the majority of ET results comprise of urban ET which is substantially lower than ET of vegetated areas.

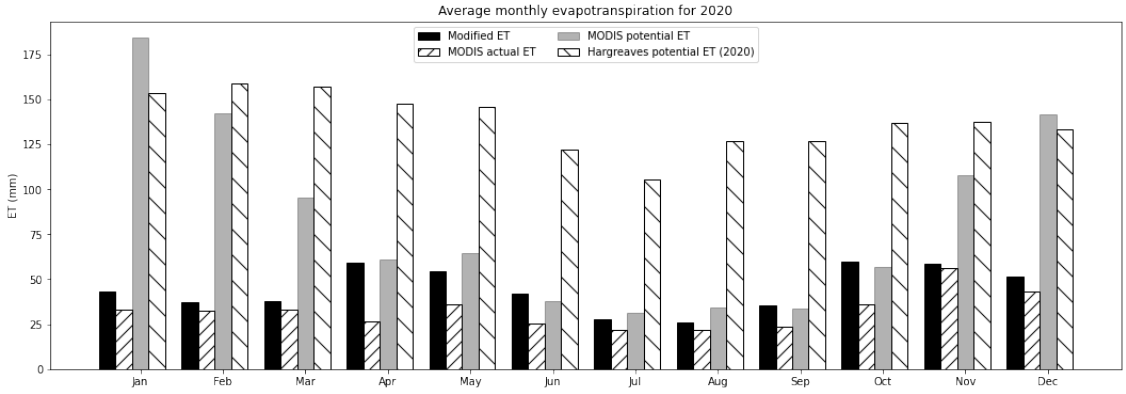

Figure 6.11: Comparison of 2020 evapotranspiration data from MODIS (actual ET dataset and potential ET dataset), updated ET estimates using ET and PET averages per land cover class, and Hargreaves potential ET (only available for 2020). Extent of 2020 classification used as region for monthly sum for MODIS PET and ET: 10,765km^2.

6.4 Groundwater recharge

6.4.1 Long-term average

Groundwater recharge per pixel for each month between 2001-2020 is calculated using a monthly water balance including the components of precipitation, runoff, and evapotranspiration presented in the previous sections. Results are presented in Figure 6.12 showing the mean annual and monthly variations of recharge between 2001-2020. Figure 6.14a shows the average annual recharge in Kumasi, with smaller pixels filtered out (detailed recharge map can be found in Figure A.6).Figure 6.14a shows impervious urban areas experience “negative" recharge, indicating evapotranspiration and runoff components are greater than precipitation leading to drainage. Small vegetated patches within Kumasi are important regions for groundwater recharge as these are locations with the highest infiltration capacities. Some western parts of the city also experience negative recharge, which correspond to the areas with urban cover where soils are poorly drained (hydrological soil group D). Average decadal groundwater recharge for the time period of 2001-2020 is 1291mm.

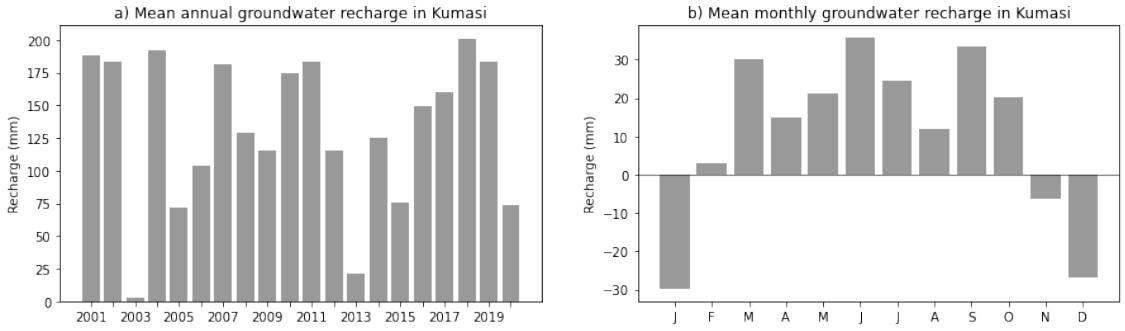

Figure 6.12: Final groundwater recharge results in Kumasi using the water balance approach showing a) annual variations and b) average monthly variations in groundwater recharge for the period of 2001-2020.

6.4.2 Past recharge

The effect of changing land use on groundwater recharge patterns in Kumasi is shown in Figure 6.14. Some similarities and differences can be seen when comparing the 2020 recharge map in 6.14a to the 2013 and 1986 map in 6.14b and 6.14c respectively. Firstly, areas of negative groundwater recharge in all three maps correspond to impervious urban areas. The coverage of these areas are much lower in the 2013 and 1986 land cover classifications resulting in less areas with negative groundwater recharge. For the maps of 1986 and 2013 there is more non-urban cover resulting in more areas with high recharge. When looking at the recharge per land cover class in Table 6.7, it is notable that from 1986 to 2013 the groundwater recharge for all land cover classes has decreased. The largest land cover change is seen in the urban semipervious class, which has grown by 53% since 1986 resulting in a 72% decrease in its contribution to groundwater recharge. Urban impervious areas do not contribute to groundwater recharge, instead being areas of discharge. This discharge has seen an increase over the years, which may be due to growth in the land class and increased evapotranspiration estimates over impervious urban areas since 1986. A possible explanation is the growth in the urban area does not translate to growth in urban area as seen by MODIS due to the 500 m resolution. Averaged urban ET therefore is overestimated due to the major part of the MODIS pixel being considered as vegetated. Moreover, the large loss of dense vegetation has not translated to a great reduction in recharge, as there has only been a reduction of 4% in recharge since 1986. Recharge from sparse vegetation has decreased a similar amount to recharge from bare land. Lastly, the decrease in recharge from water is not consistent as 2020 recharge was higher than in 2013 indicating the effect of water on recharge fluctuates between years.

Table 6.7: Annual average groundwater recharge in mm for 2020, 2013 and 1986 per land cover class using 2001-2020 monthly precipitation and evapotranspiration.

Land cover class	2020	2013	1986	Percentage change (1986 to 2020)
Urban (semipervious)	45.4	96.2	163.2	- 72
Urban (impervious)	-159.1	-123.9	-85.3	87
Bare land	382.1	499.7	514.4	- 26
Dense vegetation	566.1	581.5	588.0	- 4
Sparse vegetation	513.5	641.5	654.0	- 21
Water	-614.3	-640.2	-605.7	1
Sum	515	399	120	1

The effects of changing land cover on monthly variations in groundwater recharge are shown in Figure 6.13. The data is visualised using the same monthly forcing data for each land cover map, where the only changing variable is evapotranspiration as this is connected to land cover.

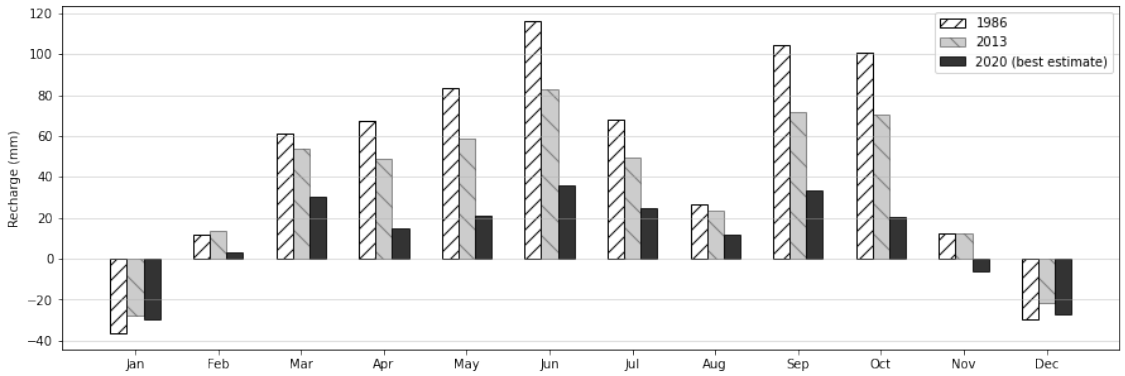

Figure 6.13: Average monthly groundwater recharge (mm) for the years of 1986, 2013, and 2020 using 2001-2020 monthly precipitation and evapotranspiration.

Figure 6.14 shows the differences in groundwater recharge patterns between the three investigated years. Patterns from 1986 show a larger recharge range with dry seasons experiencing more drainage than other years and wet seasons experiencing more recharge. This can be attributed to the large vegetated areas, which have higher evapotranspiration rates than urbanised areas resulting in more water being removed from the natural system. In the wet seasons, vegetation decreases runoff volumes increasing infiltration. For the month of November, no recharge occurs using the 2020 land cover map conversely to the maps of 1986 and 2013 where recharge does occur. Compared to 1986 maps, 2013 and 2020 recharge maps show a decline in monthly recharge and an increase in discharge during dry seasons. Annual totals are shown in Table 7.3, with groundwater recharge in 2020, 2013, and 1986 being 120mm, 399mm, and 515mm respectively.

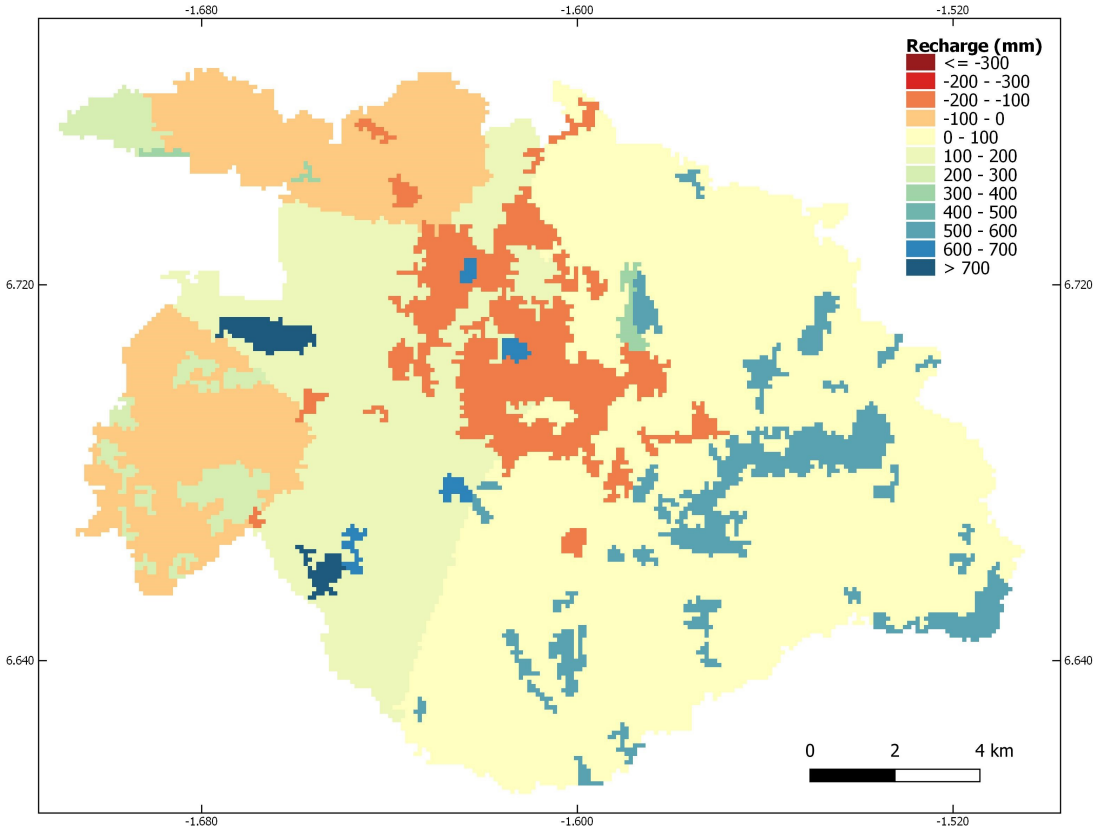

(a) 2020

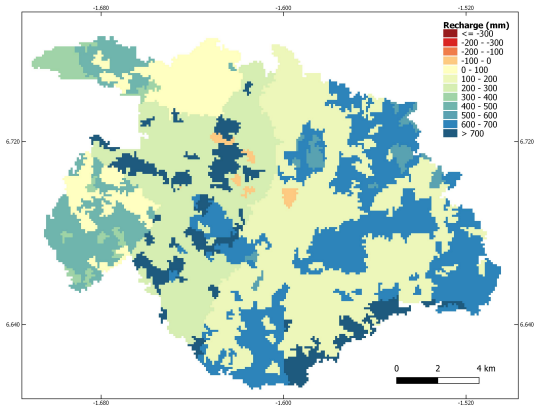

(b) 2013

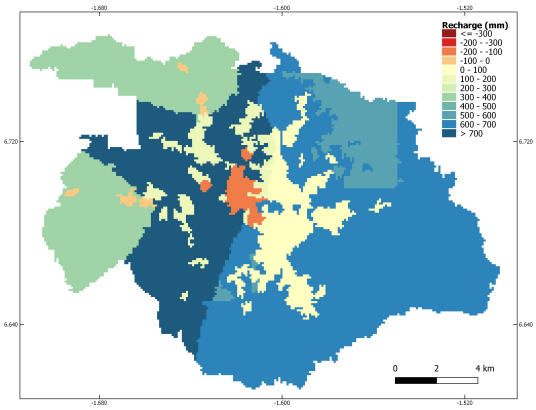

(c) 1986

Figure 6.14: Average annual groundwater recharge in Kumasi using forcing data from 2001-2020 and land cover maps of a) 2020, b) 2013 and c) 1986. Same legend applies to all.

6.5 Groundwater consumption

6.5.1 Domestic groundwater consumption

Data used to estimate domestic groundwater consumption is a daily per capita water consumption of 0.094m^3/d as stated by Kuma et al. (2010) and a domestic groundwater consumption reliance of 23.8% based off Table A.6. Historical estimates of consumption can be carried out using the population of Kumasi in previous years as population data is available since 1960 (population shown Table A.5). In 2010, the population of Kumasi was 2,035,064 (Ghana Statistical Service, 2013b) and was experiencing a growth rate of 5.5% (Ghana Statistical Service, 2013a). Assuming the same growth in the last 10 years, the population of Kumasi in 2020 is expected to be 3,476,183. Having this data, Equation 18 becomes Equation 20. Results for 2020 are shown in Table 6.8, where the total water consumption and total groundwater consumption are estimated to be 119.3Mm^3 and 28.4Mm^3 respectively.

$$C_{GW,domestic} = P \times 0.094 m^3/d \times N_{month} \times 23.8\% \tag{20}$$

Table 6.8: Estimated monthly groundwater (GW) consumption for the population of Kumasi per month in 2020. Population of 3,476,183, water demand of 0.094m^3/d and groundwater consumption of 23.8%.

Month	**Jan**	**Feb**	**Mar**	**Apr**	**May**	**Jun**	**Jul**	**Aug**	**Sep**	**Oct**	**Nov**	**Dec**	***SUM***
N_{month}	*31*	*28*	*31*	*30*	*31*	*30*	*31*	*31*	*30*	*31*	*30*	*31*	
Consumption total (Mm^3)	10.1	9.1	10.1	9.8	10.1	9.8	10.1	10.1	9.8	10.1	9.8	10.1	***119.3***
Consumption GW (Mm^3)	2.4	2.2	2.4	2.3	2.4	2.3	2.4	2.4	2.3	2.4	2.3	2.4	***28.4***

6.5.2 Non-domestic groundwater consumption

Data was collected at 52 different locations in Kumasi (distribution shown in Figure A.10). Full survey results and estimates of the number of facilities in Kumasi and their dependency on groundwater are given in Table A.7. Non-domestic groundwater consumption based on survey results are shown in Table 6.9, where estimates on how many of each type of facility exists in Kumasi (n) are retrieved from literature and assumptions based on local expertise from AAMUSTED. Total average water use per facility was calculated using Equation 19. Results indicate the most consumptive facilities are sachet water, followed by hotels, toilet facilities, and car wash stations. General survey results indicate only 3 out of 52 facilities experienced drying of the groundwater source and an additional 4 facilities reported low yields during the dry season. No clear correlation can be seen between low yields and groundwater use. However, there is a bias in estimated total groundwater use for sachet water, laundry, private hospital, and school facilities as only one survey point is available for each of these facilities. Having sufficient survey points for each facility is important to gain an accurate assessment of how much groundwater is being used. Moreover, data from private industries has not been included in this survey due to the difficulty in retrieving water use information from these sectors. Based on the results, total average annual non-domestic groundwater use from the surveyed facilities is 2.7Mm^3, ranging between 1.4-4.0Mm^3.

Table 6.9: Survey results on water use per day alongside estimates on the number of each facility in Kumasi. n: estimated number of each facility in Kumasi based on the given sources.

Facility	**Average water use from survey (L/d)**		**n**	**% using boreholes**	**Source**	**Total average water use per facility (m^3/d)**	
Hotel	7000	(1500-12,500)	242	95	242 search results for number of hotels in Kumasi	1609	(345-2874)
Car wash	9000	(2000-16,000)	120	95	Monney et al. (2020)	1026	(228-1824)
Sachet water	10000	-	200	90	Awuah et al. (2014): Kumasi has over 190 different sachet water brands and this continues to grow.	1800	-
Toilet facility	5750	(1500-10,000)	400	60	WSUP (2016): More than 400 public toilet owners and operators.	1380	(360-2400)
Laundry	6000	-	15	50	Assumption	45	-
Private Hospital	6000	-	30	100	Local knowledge	180	-
Restaurant	5350	(2400-10,000)	150	50	Local knowledge	401	(180-750)
School	5000	-	200	50	Ghana MOE (2018)	500	-
Hostel	2312.5	(1000-3000)	220	90	Local knowledge	458	(198-594)
Public tap	2000	-	30	50	Assumption	30	-
Daily total (m^3)						7429	3866-10,997
Annual total (Mm^3)						2.7	1.4-4.0

7 Sensitivity analysis

In this section the sensitivity of recharge to the different water balance components is assessed. Firstly, the dynamics between land cover and the water balance components is used to determine how recharge is affected by changing land use. This has not been applied to CHIRPS precipitation as the dataset has been directly implemented into the GEE model. The accuracy of the ET estimates are governed by the accuracy of MODIS ET, the land cover classification, and the method used to derive ET per land use class. The sensitivity of recharge to the variables used in runoff computations is also tested to understand the uncertainties in estimates. Final results on sustainability are given in this section with the corresponding uncertainties in estimates.

7.1 Dynamics between water balance components

Evapotranspiration and runoff have opposite and disproportionate responses to land use changes. Vegetated areas have low runoff generation and high evapotranspiration rates, whereas paved areas experience high runoff generation and low evapotranspiration rates. This is best understood by looking at the rates of each water balance component (excluding precipitation, which is assumed to be independent of land use changes) for the different land use classes as shown in Table 7.1. The range in runoff based on land use is 161mm to 1366mm compared to 409mm to 621mm for evapotranspiration. The dynamics between the two components depend on which land use class is changing. Runoff generation for impervious urban is over 6 times greater than that of dense vegetation, whereas evapotranspiration from dense vegetation is only 1.4 times greater than impervious urban evapotranspiration. Although there is some uncertainty in the evapotranspiration estimates (discussed in section 8.2.3) it is clear that runoff generation has much greater variability and therefore is more sensitive to change in land use. The runoff component of the water balance under changing land use increases more than the evapotranspiration component, resulting in a non-linear recharge trend over time.

Table 7.1: Average runoff (Q), evapotranspiration (ET), and groundwater recharge (GWR) per land use class for 2020 results with standard deviation. All values in mm.

Land cover	**Average Q**	**Average ET** *(mm)*	**Average GWR**
0: Semipervious urban	773 ± 85	516 ± 130	45 ± 64
1: Impervious urban	1023 ± 26	447 ± 91	-159 ± 4
2: Bare land	427 ± 114	516 ± 130	382 ± 103
3: Dense vegetation	142 ± 138	627 ± 90	566 ± 116
4: Sparse vegetation	222 ± 158	606 ± 101	514 ± 141
5: Water	1369 ± 12	614 ± 126	-614 ± 0
Range (excluding water)	*142 - 1023*	*447 - 627*	*-159 - 566*
Sum	*686*	*526*	*120*

7.2 Runoff

The main uncertainty in the runoff estimates are the curve numbers that are used. These curve numbers represent the runoff characteristics of the land cover based on the land cover properties, soil moisture conditions and soil properties (hydrological soil groups). In Kumasi, three hydrological soil groups exist (A, B, D) therefore three different curve numbers were selected based on the soil and land cover properties. In non-urbanised areas, the soil characteristics play a dominant role in runoff generation. In the SCS-CN methodology, it is indicated that soil moisture is also an important factor for runoff generation (Mishra & Singh, 2013). Conversion tables are therefore given to convert from the normal antecedent soil moisture conditions (AMC II) to conditions with high antecedent precipitation (AMC III) and low antecedent precipitation (AMC I). Initially, it was assumed that using curve numbers from AMCII would be sufficient to compute runoff. However, in Kumasi the rainy season is very intense and precipitation can occur daily, which means the soils are heavily saturated and more runoff is generated. The AMC can be determined by looking at the 5-day antecedent precipitation. CHIRPS products are also available as a 5-day precipitation accumulation, which is the dataset that was used to estimate the AMC at a 5-day time period.

The retention for each 5-day time step is calculated using the curve number corresponding to the land cover and the AMC based on precipitation depth. Runoff is then also calculated at a 5-day time step using an initial abstraction ratio of 0.2, which is the standard when using the SCS-CN method. However, initial abstraction volumes may be higher or lower depending on the type of land cover, so this can be investigated by looking at the range of Ia, which is given by Mishra & Singh (2013) as 0-0.3. Initial abstraction is used to calculate retention using Equation 15, which includes initial losses of interception, surface storage, evaporation and infiltration. It includes only the short-term losses that do not contribute to runoff or infiltration, thus a higher initial abstraction reduces the runoff potential increasing infiltration potential and vice versa. As the initial abstraction ratio is unknown for Kumasi, the proposed 0.2 from Mishra & Singh (2013) and USDA (1986) is used. It is expected that the ratio boundaries are not realistic values for Kumasi, but they indicate the greatest possible range of recharge depending on climatic factors and initial losses. An initial abstraction of 0 indicates nearly no initial losses, hence more runoff generation and less infiltration. The upper boundary is be expected more common in vegetated catchments where interception losses are high.

In Table 6.4, the ranges in curve numbers can be seen for each land cover class. For the urban impervious (1), bare land (2) and dense vegetation (3) classes the curve numbers do not have a minimum or maximum as they directly correspond to curve numbers given by USDA (see Table A.4 for USDA cover description). The curve number for water is not included in this table as it is always given to be 100. For urban semipervious (0) and sparse vegetation (4) the curve numbers were estimated as an average of the possible corresponding land cover types. These classes are those that have the highest uncertainty when looking at computed runoff values. The selected curve number for a certain precipitation event depends on the precipitation depth, which

is incorporated into the GEE script.

7.3 Groundwater recharge

One of the main goals in this study is to investigate the effect of changing land use on groundwater recharge. Land cover maps have been made over Kumasi for 1986, 2003, 2013, and 2020. The 2003 land cover is removed from analysis as the image is polluted with light clouds that alter the surface reflectance properties, therefore providing a less accurate classification. The GEE model was applied to the different land cover maps to determine the relation between land cover and groundwater recharge.

Table 7.2 shows a summary of which variables are investigated. A total of 10 different variable combinations are investigated and compared to the best estimate for groundwater recharge, namely the results presented in previous sections. The effect of the curve numbers will is assessed by calculating recharge using at minimum and maximum CNs keeping the Ia, forcing, and land cover map constant. The effect of recharge will be investigated by looking at the minimum and maximum abstraction ratio keeping CN, forcing, and land cover constant. The effect of land cover is investigated by using the 1986 and 2013 classifications keeping the forcing constant. However, evapotranspiration estimates are tied to land cover classifications which alters the forcing data. The scenarios labelled as maximum runoff and minimum runoff correspond to low recharge and high recharge scenarios respectively.

Table 7.2: Combination of different variables implemented into recharge estimates.

Label		CN	Ia	Forcing	Land cover
0	Baseline	NORM	0.2	2001-2020	2020
1	CN min	MIN	0.2	2001-2020	2020
2	CN max	MAX	0.2	2001-2020	2020
3	I_a min	NORM	0	2001-2020	2020
4	I_a max	NORM	0.3	2001-2020	2020
3.1	Min I_a& CN	MIN	0	2001-2020	2020
3.2	Max runoff	MAX	0	2001-2020	2020
4.1	Min runoff	MIN	0.3	2001-2020	2020
4.2	Max I_a& CN	MAX	0.3	2001-2020	2020
5	LULC 1986	NORM	0.2	2001-2020	1986
5.1	Min runoff 1986	MIN	0.3	2001-2020	1986
5.2	Max runoff 1986	MAX	0	2001-2020	1986
6	LULC 2013	NORM	0.2	2001-2020	2013
6.1	Min runoff 2013	MIN	0.3	2001-2020	2013
6.2	Max runoff 2013	MAX	0	2001-2020	2013

The sensitivity analysis is done using the variables in Table 7.2, combining the different variables to see the range in monthly groundwater recharge and net annual recharge. The effect of these combinations on annual recharge per land class is also investigated. These scenarios can finally be used to estimate the sustainability aspect of groundwater use. Ranges in net annual recharge are then compared to the final annual abstraction estimates.

7.4 Sensitivity and uncertainty of groundwater recharge

To summarise, the uncertainty of computed groundwater recharge depends on the parameters chosen to calculate runoff and the land cover maps. Therefore, uncertainty in runoff is directly related to groundwater recharge uncertainty. The sensitivity of monthly recharge is assessed by looking at individual minimum and maximum values for the curve number and initial abstraction ratios (scenarios 1-4 in Table 7.2) and the uncertainty is assessed by combining the maximum and minimum possible recharge using a combination of the values (scenarios 3.2 and 4.1).

Figure A.8 shows the variation in monthly groundwater recharge when changing only one variable in the runoff calculations and keeping other inputs constant. Recharge is more sensitive to the initial abstraction ratio than to curve number inputs. However under negative recharge scenarios when evapotranspiration is greater than precipitation, results indicate that recharge is less sensitive to the input parameters. These coincide with the dry season months where runoff generation is lowest, therefore making evapotranspiration the larger flux in the water balance. The mean annual results for each component of the water balance per sensitivity scenario in Table 7.2 is shown in Table 7.3.

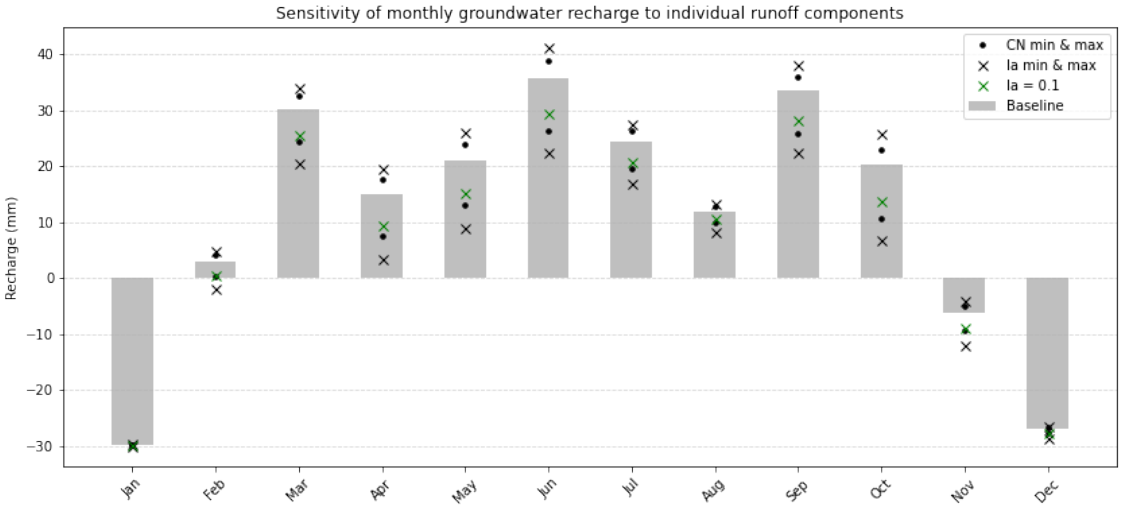

Figure 7.1: Sensitivity of groundwater recharge to initial abstraction and curve numbers using 2020 land cover and 2001-2020 meteorological forcing data.

Table 7.3: Mean annual results for components of water balance (mm) for 2020 sensitivity scenarios and scenarios 5 and 6 (1986 and 2013).

	0: Best estimate	**1**	**2**	**3**	**4**	**5**	**6**	**3.1**	**3.2**	**4.1**	**4.2**
P	1333	1333	1333	1333	1333	1321	1327	1333	1333	1333	1333
Q	686	663	752	781	648	275	472	760	839	624	718
GWR	120	144	54	25	159	515	399	46	-33	182	88
ET	527	527	527	527	527	531	456	527	527	527	527

Curve numbers represent the runoff potential in relation to land cover and soil properties, whereas the initial abstraction ratio controls the amount of water available for infiltration and runoff. Therefore, maximum runoff is generated in the scenario where curve numbers are highest (high runoff potential from land cover and soil components) and initial abstraction ratio is at its lowest (low initial losses). A combination of the minimum curve numbers and maximum initial abstraction ensures the lowest runoff potential. These scenarios are visualised along with the best estimate of groundwater recharge in terms of monthly groundwater recharge and groundwater recharge per land cover class Figure 7.2. A similar pattern can be seen as in the previous figure, where uncertainties are lowest during the dry season.

7.5 Groundwater sustainability

7.5.1 Recharge vs consumption

In the following sections, the minimum and maximum recharge scenarios are reconsidered to include case-specific boundaries. The maximum recharge scenario is that of minimum runoff, where the curve number is minimal and I_a ratio is 0.3. The minimum recharge scenario uses an I_a ratio of

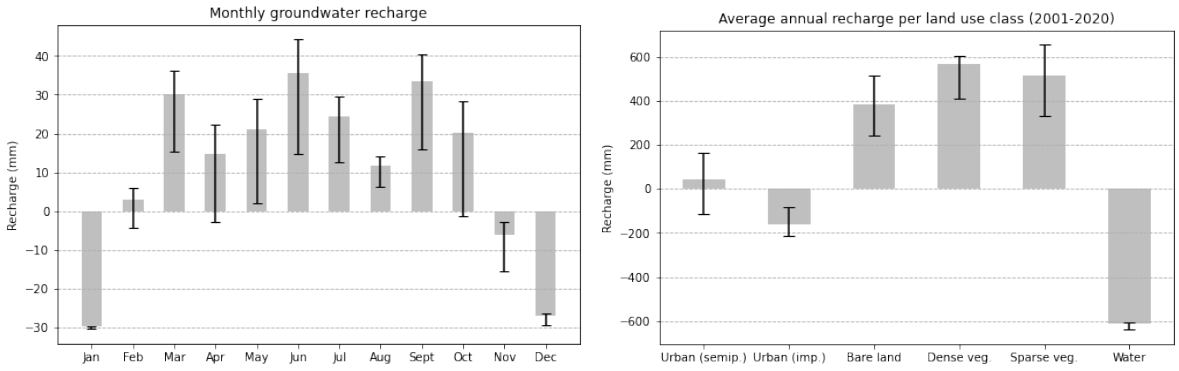

(a) (b)

Figure 7.2: Groundwater recharge uncertainty analysis using 2020 land cover for scenarios in Table 7.2. Blue bars represent the best estimate, with graphs visualising a) range in average monthly groundwater recharge and b) range groundwater recharge per land cover class. Scenario 5 and 6 not included in this analysis. Minimum and maximum recharge correspond to scenario 3.2 and 4.1.

0, which is unrealistic for Kumasi. This implies there are no initial losses from evapotranspiration, interception, initial infiltration, surface depression storage, and evapotranspiration. Therefore, an I_a ratio of 0.1 is chosen to carry out the minimum recharge scenario. In Wakode et al. (2018), I_a was altered depending on soil conditions, ranging between 0.1 and 0.3 in an urbanised catchment. Local estimations of I_a do not exist, therefore an I_a ratio of 0.1 and maximum curve number is hereafter assumed to be a realistic case for the minimum recharge scenario. The new updated ranges in recharge are shown in Table 7.4.

Table 7.4: Range of annual recharge for 1986, 2013, and 2020 (sensitivity scenarios 0,5, 6).

Year		**Recharge**	**Max**	**Min**	**Min (updated)**
Corresponding scenario		*Best estimate*	*Min runoff* $I_a = 0.3S$	*Max runoff* $I_a = 0$	*Max runoff with* $I_a = 0.1S$
1986	*mm*	515	530	339	404
	Mm^3	124.1	127.7	81.7	97.4
2013	*mm*	399	448	231	287
	Mm^3	96.2	108.0	55.7	69.2
2020	*mm*	120	182	-33	13
	Mm^3	28.9	43.9	-8.0	3.1

The volume of monthly groundwater recharge is calculated as the depth of recharge multiplied by the total area of Kumasi. The extent of the area of the recharge maps is 241km^2, which is the area of the shapefiles of Kumasi retrieved from *Shapefiles of all Districts in Ghana (170 districts)* (2019). Results of monthly groundwater consumption are shown in Figure 7.3. Figure 7.3a shows the monthly variations in recharge compared to monthly groundwater consumption values. Long-term average groundwater recharge calculated using the 2020 land cover map exceeds groundwater consumption from March to October. When the lower boundary of recharge is considered, recharge in April, May, August, and October falls below the monthly consumption. Cumulative recharge is plotted starting from March, as recharge in January and February is negative. This is shown in Figure 7.3b, where total groundwater recharge in 2020 is shown to equivalent to 17.8Mm^3 (73.8mm). Compared to the long-term average of 28.9Mm^3 (120mm) per year, 2020 experienced slightly lower cumulative groundwater recharge. Total groundwater (domestic and non-domestic results) is estimated to be 31.1Mm^3 for 2020. Groundwater abstraction therefore exceeds long-term average groundwater recharge.

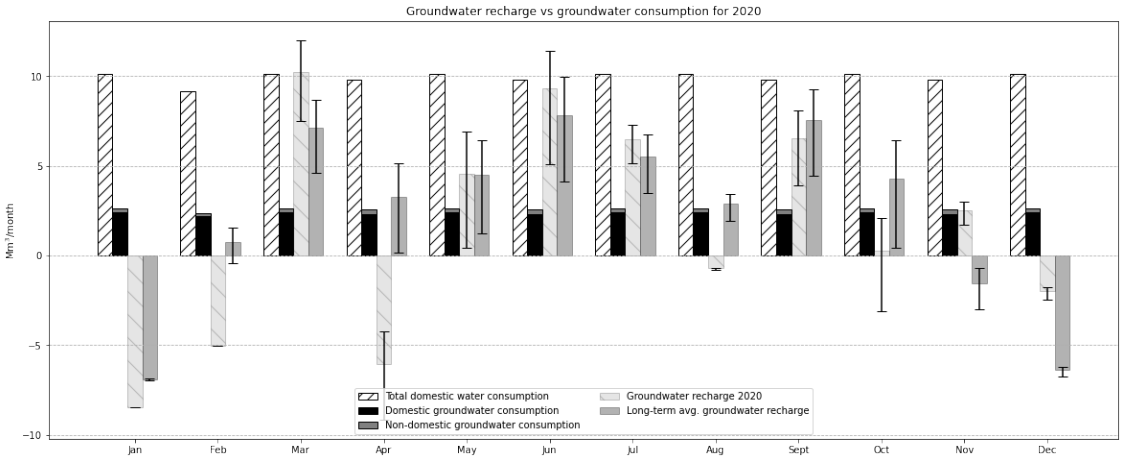

(a) Groundwater recharge versus groundwater consumption for 2020.

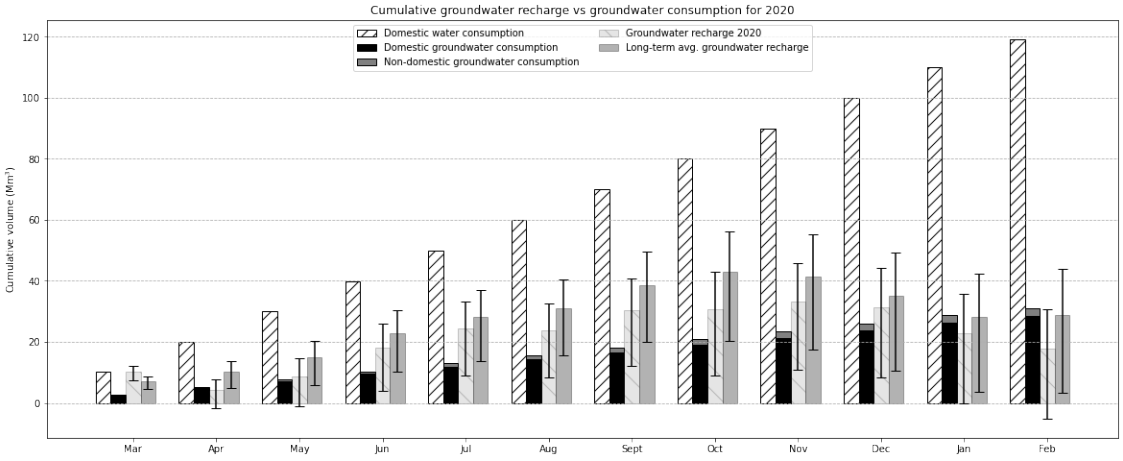

(b) Cumulative groundwater recharge for 2020 starting from March.

Figure 7.3: Groundwater recharge versus groundwater consumption in Kumasi for 2020. Mean monthly recharge is plotted to compare against 2020 recharge. Error bounds correspond to minimum and maximum runoff scenarios.

Exact groundwater recharge for 1986 cannot be estimated as the ET datasets are not available before 2001. Therefore, when recharge for different years is compared, the same long-term forcing data is used. Groundwater recharge for the years of 1986, 2013 and 2020 is shown against the growing groundwater consumption in Figure 7.4. The upper and lower boundaries for each year are calculated using the minimum and maximum runoff scenarios shown in Table 7.2 for the corresponding years. Dotted lines are used between the years, as it cannot be assumed that recharge trends between the years are purely linear. Instead the linear trend is used to visualise the declining groundwater recharge over the years. Groundwater consumption for the years before 2020 is calculated using Equation 18 for the population of the corresponding year. The population of Kumasi since 1960 is shown in Table A.5.

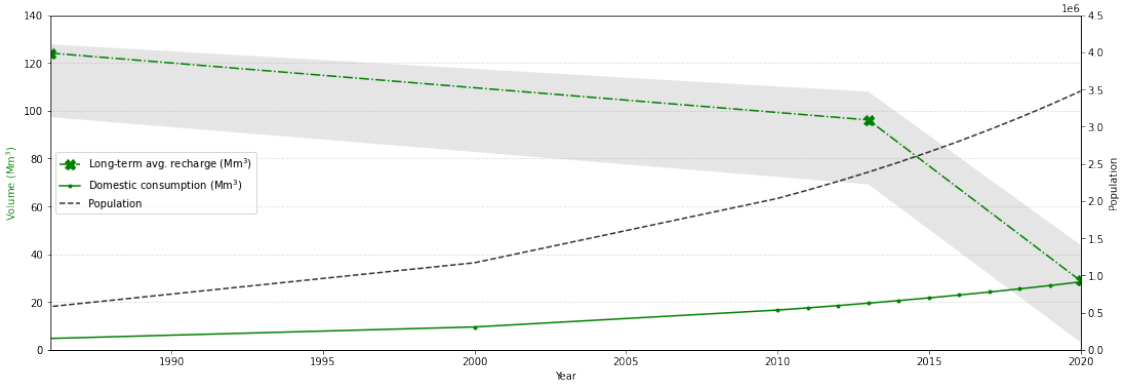

Figure 7.4: Groundwater recharge versus groundwater consumption based on yearly sums. Lines have been drawn through the available data points between the period of 1986 to 2020.

8 Discussion

8.1 Land use trends

Land use results from Section 6.1 give a visual representation of one of the effects of urbanisation in Kumasi. Results show that since 1986 Kumasi has experienced loss of 63% of its vegetated cover which is directly attributed to the growth of the urban areas. Initial changes in land use from 1986 to 2013 revolved around the conversion of vegetated land to urban semipervious. However, more recent land use changes show an increase of urban impervious land cover, while semipervious urban areas continue to grow and sparse and dense vegetation decline. The accuracy of land-cover maps is important for the final recharge accuracy, as the maps are used for runoff and evapotranspiration estimates. Between 1986 and 2020 only four cloud-free annual composite images were found, one of which has some light cloud cover pollution consequently being removed from analysis (2003 composite). Resultantly, land use change patterns are temporally coarse and do not give a good overview of changes in years between the classifications. Moreover, accuracy of the maps was hindered by a few factors, namely the overlap of some land classes, resolution differences between satellite products, selection of the correct classes to train data, and the classifier used. The consequences of this on groundwater estimates are discussed.

Pixels corresponding to the categorised land cover classes were selected manually over areas in Kumasi. Using Google Maps and the underlying surface reflectance images, polygons were created that seemingly fit under the six different land use categories due to their visual properties. This was done as accurately as possible by only delineating areas where there was a high certainty that the land cover was as selected. Grouping areas with low pixel quantities also made for better land use samples to train the classifier on. The effect of changing sample size on the accuracy of the classifiers was investigated with results shown in Table 6.1, where the accuracy was highest when using a the full sample size. Instead of increasing the sample size for an even greater accuracy, the sample size was left the same (largest size) as increasing it would take more computational time and create a larger bias due to more pixels being manually selected to fit specific classes.

The misclassification of land use classes affects runoff and evapotranspiration estimates, which in turn affect the accuracy of groundwater recharge. Overlaps between different land classes was assessed by looking at the spectral signatures shown in Figure 6.1. The greatest overlap of classes was seen between semipervious urban land with bare land, and there was an overlap of dense vegetation and water in older images. For the latter issue, the dense vegetation estimate was improved by adapting the training data to include some pixels outside Kumasi's boundary. Due to the largest part of the sample set only being within Kumasi, it can be expected that the land use classification outside of the urban boundary is not as accurate as within the city. This has

implications for evapotranspiration results as the classification outside of the urban boundaries is used for the average evapotranspiration estimates for land use class.

The accuracy of the 2020 classification was assessed in Earth Engine and the results show an accuracy of 90% for the classifier using the full Sentinel-2 bands (see overview Table A.3). Accuracy reduced to 82% when using Landsat compared to Sentinel-2 mostly attributed to the coarser resolution of the Landsat images as shown in Figure 6.2. Misclassifications can affect recharge results, especially if urban areas are misclassified as vegetated areas with high recharge potential or vice versa. Due to the unavoidable spectral overlap in certain wavelengths of classes such as water and dense vegetation or urban and bare land, an 82% accuracy is an agreeable result.

Implications of misclassification on recharge:
Errors that reduce the accuracy of the classification have been attributed to misclassifications between water and dense vegetation and semipervious urban and bare land. If vegetation is misclassified as water, ET and runoff are overestimated over the area and resultant groundwater recharge is underestimated. If semipervious urban is misclassified as bare land, the effect on ET is not significant due to the similarity in ET rates (see Table 7.1) but runoff will be underestimated resulting in an overestimate of recharge.

Accuracy can be improved by creating new sample data over each image, however this is time-consuming and for the purpose of this investigation the trained classifier was created to be applicable to all previous land cover images. For investigations using recent years, it is recommended to use higher resolution spectral reflectance images such as those from Sentinel-2 as this produces more accurate classifications. Using the full bands available for Senintel-2 also allows for better distinction between land use classes. Moreover, open access land cover products are available in Google Earth Engine but these have relatively coarse resolution (e.g. 100m from *Copernicus CORINE Land Cover* (2021) and 500 m *MODIS Land Cover Type/Dynamics* (2021)). Using ready-made land cover maps instead of creating new maps can also be done, as various desciptive land use classes exist. For example, MODIS land cover contains the class "urban and built-up lands" described as having at least 30% impervious area, which can then be assumed to have a CN of 98. Studies exist that used the SCS-CN over MODIS (Hong & Adler, 2008) and CORINE (Psomiadis et al., 2020) land cover maps. Hong & Adler (2008) created a global map of Curve Numbers based on land use and soil groups, using such a ready-made product allows for large-scale computations of runoff and application of the water balance. In this study a classification with 30 m resolution was created due to the importance of the smaller vegetated patches within Kumasi, which cannot be seen under coarse resolution. For large-scale applications of this water balance methodology, using ready-made maps is highly beneficial. Further improvements and developments of this study can include existing land cover maps to skip the step of creating a land use map for every year.

8.2 Groundwater recharge

8.2.1 Limitations of the simple water balance

Main assumptions
In this study, groundwater recharge is referred to in terms of direct potential groundwater recharge. After a precipitation event, water infiltrates the soil and a portion of this evaporates from the unsaturated zone. The rest is assumed to reach the groundwater table. This neglects the effect of surface flow, interflow, groundwater flow and subsurface storage. Over a period of >10 years, groundwater flow and storage changes are negligible (assumption carried in Szilagyi et al. (2011); Kortatsi (1994)). Interflow (outflow/inflow of water from unsaturaed zone to streams) is assumed to be negligible over the period of a year. This assumption is carried due to the non-perrenial nature of Kumasi's streams. This can indicate that drainage to streams occurs in the wet season (gaining streams), while streams recharge groundwater in the dry seasons (losing streams). Furthermore, surface water inflows and outflows are assumed to be equal over the study area. Recharge from interflow and groundwater flow can be assumed to be small in relation to recharge from direct infiltration, as studies indicate that recharge in the humid regions of Ghana is dom-

inated by direct infiltration from precipitation (Vries & Simmers, 2002; MacDonald et al., 2021; Kortatsi, 1994).

Recharge studies in Ghana
MacDonald et al. (2021) combined a series of studies and found the range of average decadal groundwater recharge in Ghana to be between 340-2800mm with the best estimate at 970mm. In this study, the average decadal groundwater recharge for Kumasi was estimated to be 1291mm, which falls between the range but is higher than the average. Comparing the recharge range to precipitation patterns over Ghana it is expected that the south-west of Ghana where highest precipitation amounts are experienced correspond to the areas of highest recharge. The lower end of the spectrum may be in the northern arid regions of the country. As Kumasi lies in the humid region of Ghana it follows that recharge will be on the upper end of the recharge range for the whole country. Looking at an annual scale, in Kumasi's neighbouring district Ejisu-Juaben, Anornu et al. (2009) used the chloride balance method estimating recharge to be 7-9% of annual precipitation. Applying this relation to Kumasi with an annual mean precipitation of 1333mm (Table 7.3), recharge should be between 93-120mm, which is comparable to the 120mm recharge result for the best estimate of recharge. Although no data exists for monthly variations, it is expected that as precipitation gives the water availability for recharge, patterns will follow those of monthly precipitation.

Having a storage component for groundwater recharge in Kumasi can be used to set a limit to recharge, especially during the rainy season. Once the soil fully saturated and the shallow groundwater storage is full, groundwater may flow directly to streams, rivers, and depressions in the area. This can indicate that current recharge estimations for the rainy months are overestimates. On the other hand, more recharge may occur in the dry months as streams can be feeding the groundwater system. In the study by Lapworth et al. (2013), shallow groundwater residence times in West Africa were estimated using environmental tracers. Results showed that for an area with maximum annual rainfall of 1300mm (such as Kumasi), residence times in the basement aquifer were 40 to 50 years. Due to the uncertainty in the subsurface storage, it cannot be said when the consequences of unsustainable groundwater use will take effect. If the storage component is large, then based on residence times depletion may occur in the far future. However, if storage is low as expected for humid, shallow aquifers (MacDonald et al., 2021) such as in Kumasi, then depletion may occur within the next 50 years.

Groundwater studies in urban areas
Moreover, in this study only natural components of the water balance are included which may lead to an underestimate of actual groundwater recharge. Factors such as pipe leakages, sewage leakages and irrigation can add to net recharge. Table 8.1 shows an overview of five different studies in different climatic zones and with different urbanisation characteristics. A water-balance approach was used in Wakode et al. (2018), Garcia-Fresca (2007) and Putra & Baier (2008). Afonso et al. (2019) estimated recharge using an Analytic Hierarchy Process (AHP) while Han et al. (2017) used at groundwater measurements. The urban components of groundwater recharge is generally significantly greater than or similar to the natural component. This varies depending on local water supply and urban drainage characteristics. Looking at the natural component from the different studies shows a variation from 31 mm/y to 233 mm/y year. Comparing natural recharge between studies is complex due to varying climate, urban land use, soil and hydrogeology that affect recharge estimates. These studies can be used as an indication of the order of magnitude of natural recharge in large cities and to better understand the urban component of recharge.

The urban component is especially important if water in the urban area is imported from external areas, bringing excess water into the urban water cycle. In Kumasi, the major water supply comes from the Owabi and Barekese reservoirs (Maoulidi, 2010) outside of the city boundaries. Moreover, the pipeline network shown in Figure 3.2 is old and experiences frequent leakages (World Bank, 2015). Therefore, it can be expected that the urban components of groundwater recharge are high. The effect of these urban components should be investigated if a more holistic approach of recharge estimations is to be made over Kumasi.

Table 8.1: Summary of urban and natural recharge from three urban recharge studies with similar urbanisation or climatic zones to Kumasi. P: annual precipitation, T: annual average temperature. T and P for study 1,3 and 5 from Climate Data (n.d.).

Study	Site characteristics	Groundwater recharge	
		Natural	Urban
Wakode et al. (2018): Hyderabad, India	Tropical savanna/semi- arid climate T =26°C, P= 745mm/y Population of 4,010,238	53 mm/y	568 mm/y
Afonso et al. (2019): Porto, Portugal	Temperate climate T=15°C, P = 1200 mm/y Population of 237,559, 81% urban cover	50 mm/y	-
Putra & Baier (2008): Yogyakarta, Indonesia	Hot and humid climate T = 25.1°C, P = 2681 mm/y Population of 1 million, rapid urbanisation	233 mm/y	201mm/y
Han et al. (2017): Beijing, China	Cold and temperate, P = 613 mm/y Rapidly urbanising, population >>10 million	0.14P (reduction of 150-190 mm/y)	-
Garcia-Fresca (2007): Austin, Texas, U.S.A	Arid climate T = 20.4°C, P = 924 mm	31 mm/y	63 mm/y

8.2.2 Sensitivity to runoff

Assumptions of SCS-CN and effect on recharge
General assumptions of SCS-CN method can have implications on the final recharge results. The general assumptions that will be assessed here are that urban areas are connected to a drainage system and that precipitation intensity and duration are negligible. The first assumption does not always hold for Kumasi, as Owusu-Ansah (2016) explains an open drain system was established in the 1980s that has not seen many improvements since then. The infrastructure has also not been put into place in all suburbs, where instead the water drains into streams. According to Owusu-Ansah (2016), the sewage system in Kumasi is unable to cope with the current and predicted demands. The consequence of this assumption is that with a larger unconnected area, the curve number becomes lower and generated runoff is lower leading to higher infiltration thus recharge. An improved curve number estimate can be made using the SCS-CN methodology if the percentage of unconnected impervious area is known, however this was not done during this study. Campion & Venzke (2013) states that flash floods occur often in Kumasi after heavy rainfall events, with flood-prone suburbs generally being those inhabited by urban poor and rural-urban immigrants. Assuming that these urban suburbs have less drainage infrastructure put in place, a probable consequence is that runoff generated is higher and that these areas experience higher recharge. Long-term surface inundation is also caused in these flood-prone suburbs by effluent stream floods due to a rise in the water table in peak rainy-season (Campion & Venzke, 2013), which can lead to higher recharge compared to areas where runoff is guided by drainage infrastructure. The second assumption of neglecting precipitation intensity and duration can have repercussions for recharge. Mishra & Singh (2013) explains intense precipitation are usually of short duration, therefore these events lead to low infiltration and high runoff as there is less time for retention on the land surface. The SCS-CN method does not account for intensity, which may lead to underestimates of runoff hence overestimates of recharge.

Hydrological soil groups
Sensitivity of recharge to hydrological soil groups is not tested in this study, but their effects on runoff generation and recharge are significant. Areas with lowest recharge potential due to soil correspond to group D, followed by B and A. In the 2020 recharge map (Figure 6.14a), this effect can clearly be seen. In semipervious areas of Kumasi, the shift of potential recharge from negative to positive is seen where recharge of -100mm to 0mm is experienced in western sections corresponding to HSG D and positive recharge areas (0mm - 200mm) correspond to HSG A and B. Even in sparsely vegetation sections with soil group D, recharge potential is lower than in areas

with other soils. In general due to the importance of soil for infiltration, it is recommended to have a more certain analysis of the soil groups and their drainage mechanisms. This can be done by collecting soil samples in the area and examining their properties.

Curve numbers
The curve numbers were selected by comparing land cover in Kumasi to land cover definitions from USDA (1986) as shown in Table A.4. For the classes of urban impervious, bare land, and dense vegetation there were no minimum or maximum ranges as they were chosen with high certainty seeing as no other class definition fell under the same category. This was not the case for semipervious urban and sparse vegetation. In this study the choice was made to select an average of the different curve numbers to use as the best estimate, while using the minimum and maximum ranges to conduct the sensitivity analysis. Therefore, the sensitivity of recharge to the curve number is governed by the semipervious urban and sparse vegetation class. Together these classes make up the largest area of Kumasi, explaining why the maximum curve number is the lower boundary for groundwater recharge.

Initial abstraction
I_a is a parameter that needs to be investigated locally in order to achieve the most accurate results. USDA (1986) stresses that using an I_a ratio of 0.2 in urban areas can imply significant initial losses that do not take place. The effect of the 0-0.3 range of I_a ratios proves the consequence of abstraction on recharge, where upper and lower recharge boundaries are governed by the range of I_a ratio (Figure 7.1). The assumption of an I_a ratio of 0.2 is derived from agricultural watersheds, however in the case of the urban watershed of Hyderabad in India, a range of 0.1-0.3 is given (Wakode et al., 2018) indicating that urban areas can also account for large initial losses.

Another consideration is that the time scale of this investigation is from 1986 to 2020, and land use changes have been significant enough that changes in initial abstraction have also occurred. The initial abstraction in 1986 is expected to have been higher due to larger vegetative cover, hence more interception, less effective precipitation and less runoff generation. As the components of precipitation and evapotranspiration remain constant and the runoff flux with a higher I_a ratio is lower than one with a standard ratio, recharge is consequently higher. For 1986 this indicates that recharge might be on the higher end of the range in Figure 7.1. The opposite can be said for 2020, where recharge may be closer to the lower boundaries than the higher bounds.

8.2.3 Challenges with evapotranspiration

Using MODIS for ET estimates includes various assumptions that affect the final recharge. Firstly, over Kumasi there is never more than ∼60% pixel cover as MODIS only creates ET estimates over vegetated areas. Due to the 500m resolution, no data exists for many vegetated patches within Kumasi leading to an underestimation of actual ET. In this study, this was combatted by finding the average ET per land cover class in the total extent over the classification image (total areas shown in Table 6.6) following the methodology shown in subsection 5.4. One issue that arises when using this procedure is that outside of Kumasi, small urban patches exist that MODIS consequently groups as vegetated cover with high ET. The MODIS ET pixel shown in Figure 8.1a will have a high ET, which when averaging per land class will give the urban pixel within the vegetated area this high ET. The opposite is seen in Figure 8.1b, where the vegetated cover will have 0 ET due to the major MODIS pixel being considered as urban. The effect of this is seen in the average ET per land use class in Table 6.6, where for 2020 impervious urban areas have an average annual ET of 447mm compared to 627mm for dense vegetation. Using this method to create a modified ET estimate, it is likely that urban evaporation is being overestimated while vegetated ET is being underestimated. Implications for recharge are that recharge from urban areas is being underestimated, resulting in less drainage than results current indicate, while recharge from vegetated areas is being overestimated. It can be expected that the net effect of this error is somewhat balanced out in the final water balance.

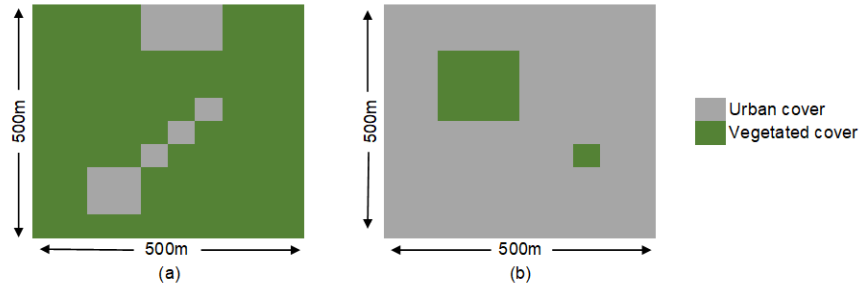

Figure 8.1: Example visualisation of one MODIS ET pixel over land cover classification. (a) shows majority vegetated cover with some urban pixels (expected case outside of Kumasi), whereas (b) shows the opposite (expected case within Kumasi).

Meteorological data is not readily available for Kumasi, hence ET estimates are compared to similar studies using GIS to comprehend the ET variation under different land cover types. Liu et al. (2010) used a surface energy-balance model (SEBAL) and Landsat 5 to estimate ET per land use class in a watershed in Oklahoma, U.S.. The study area consists of developed lands, agricultural areas, vegetated areas. Resulting ET ranged between 717 mm/y and 896 mm/y (excluding that of open water, which is 1019 mm/y). For the residential areas, ET was estimated to be 717.8 mm/y. Zarei et al. (2016) measured actual ET in the Mashhad catchment in northern Iran using a spatially distributed water balance model. The mean ET was between 128 mm/y (rangeland) and 207 mm/y (irrigation farming). Residential areas only made up around 1.5% of the total area, where estimated ET was 145 mm/y. Kundu et al. (2018) measured actual ET using SEBAL in the Narmanda Basin of Central India (12,290 km^2). Results showed that premonsoon levels ranged between 288 mm/y (wasteland) to 467 mm/y (forest). Actual ET over the urban area was estimated to be 294 mm/y. Results from these studies show a large range in urban ET, which is largely due to the different climatic zones. Exluding the open water ET, the range of ET for Liu et al. (2010), Zarei et al. (2016) and Kundu et al. (2018) are respectively 179 mm/y, 79 mm/y, and 179 mm/y. In this study, the ET range is 180 mm/y, varying between 447 mm/y and 627 mm/y. What can be said from this is that the ET ranges in this study are acceptable and realistic, however more meteorological data is needed to validate the ET results.

8.2.4 CHRIPS vs TAHMO

Comparing satellite-based precipitation to rain gauge measurements can be challenging. Firstly, rain gauges make point measurements while CHIRPS observes precipitation over a whole area. CHIRPS can therefore measure precipitation over an area while no precipitation is falling over a specific point. On the other hand, satellite precipitation data averages out localised high precipitation events by including regions that have lower precipitation rates (Bowman, 2005). Bowman (2005) also explains that gauges can observe short-term rain rates and therefore daily sums can be much higher than area-averaged rates from satellite data. The effect of this is seen in Figure 8.2 and is a factor that needs to be weighed when deciding to use satellite precipitation records over rain gauge precipitation. In the case of this study and the focus of implementing a remote-sensing based approach to calculate groundwater recharge, the choice was made to use CHIRPS for the precipitation as data is reliable, covers a long time range, and gives better spatial coverage over Kumasi compared to station data.

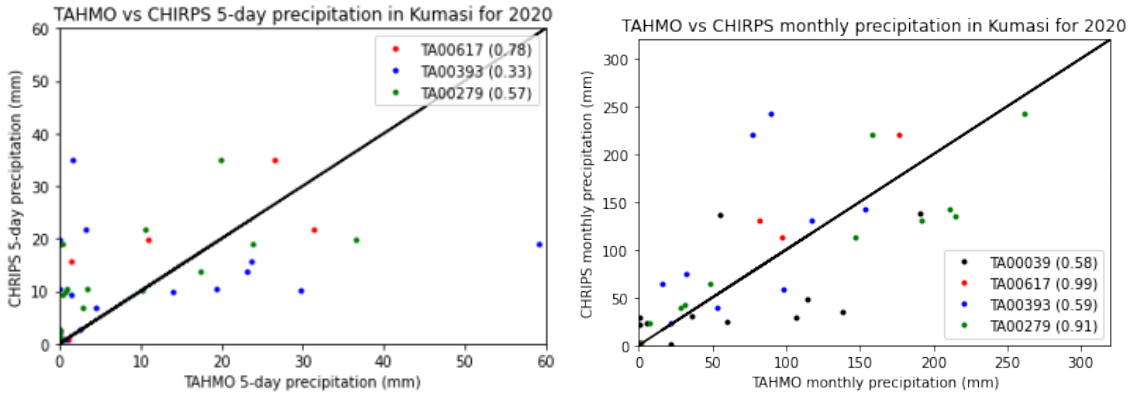

(a) (b)

Figure 8.2: Comparison of CHIRPS precipitation over the whole of Kumasi and the four TAHMO stations in Kumasi for 2020 using a) penta-daily records and b) monthly aggregates. Pearson's r correlation coefficient is shown in brackets for each station. Note: 2020 records are incomplete for TA00039 and TA00617.

8.3 Groundwater sustainability

Groundwater sustainability is assessed by comparing the results of groundwater abstraction to groundwater recharge. When abstraction is greater than recharge, then the rough assumption is that groundwater depletion is occurring (Bierkens & Wada (2019); Wada et al. (2010)). This is investigated in two ways: looking at the long-term average groundwater recharge and the specific annual recharge. The latter has only been done for 2020, therefore inter-annual comparisons are made using the long-term averages. Recall the definition of physically sustainable groundwater use by Bierkens & Wada (2019), defined as the prolonged(multi-annual) withdrawal of groundwater from an aquifer in quantities not exceeding the average annual replenishment. Prolonged (multi-)annual withdrawal indicates that even if pumping exceeds the long-term average recharge, groundwater can still be renewable if pumping stops as recovery may occur in some years to decades. However, if pumping continues then this can lead to depletion (Bierkens & Wada, 2019). The time scale of this change depends on groundwater residence times and storage volumes. If groundwater residence times in the shallow Basement aquifer are 40-50 years (Lapworth et al., 2013), then depletion may occur within that time scale if storage is not considered.

Starting with annual recharge, in Kumasi the average long-term annual replenishment is 28.9Mm^3 based on the land cover map 2020 (results in Figure 7.4). Looking at results since 2013, recharge was substantially higher at 69.2Mm^3. The decrease since then can be explained by changes in land cover, predominantly the conversion of semipervious urban to impervious urban, followed by a loss of sparse and dense vegetation. From 1986 to 2013, land cover changes consisted of shifts of vegetated land to semipervious urban areas (see Table 6.2). Although urban cover was extensive in 2013 (total cover of 49%), land cover changes until 2020 indicate urbanisation occurred mostly in the form of developments converting semipervious urban to impervious areas. In the land cover map of 2020, vegetated cover only consists of a remaining 18% of the total area. Changes in recharge between 2013 and 2020 are therefore attributed to the increase of impervious areas and the continuous loss of vegetated areas to semipervious areas. Kumasi's growth is being constrained by its boundaries as the developable land within its borders is limited (Cobbinah et al., 2020). Future urban developments expected to take place in semipervious regions will reduce the permeability of the urban area reducing recharge.

8.3.1 Groundwater abstraction

Survey results indicate that non-domestic groundwater consumption makes up around 8% of total groundwater consumption. Compared to the national estimate of 16% (Kortatsi, 1994), Kumasi is

on the lower-end of non-domestic groundwater consumption. The survey did not cover all major industries in Kumasi; groundwater use information from larger commercial industries, such as mineral water production companies, is difficult to obtain in surveys as such data is not always freely given. In Kumasi, the major industries are the Coca-Cola Company, two breweries, and an abattoir that consume around 0.2Mm^3/year (Erni et al., 2011). The estimate of 2.7Mm^3 is based off data from 52 survey locations around Kumasi. More points are required per facility in order to conduct a thorough investigation into non-domestic groundwater use.

Domestic groundwater use is based off total water consumption estimates and existing surveys carried out on water sources in Kumasi (see Table 4.2 for values used). Socio-economic factors have not been included in the study but can affect per capita domestic abstraction. In Kumasi piped water access decreases radially from the city and therefore it can be expected that suburbs on the outskirts are more reliant on groundwater than those in the center. Moreover, different income groups are expected to consume different volumes of water as stated by Maoulidi (2010). As the distribution of these income groups is not known for Kumasi, the average estimate by Kuma et al. (2010) of 94L/day is sufficient to estimate groundwater consumption while considering that there may be slight differences depending on socio-economic factors. Moreover, a growing reliance on alternative water sources such as groundwater is expected due to the failure of the public water supply system to meet demands (Cobbinah et al., 2020). Groundwater consumption may therefore grow towards total water consumption, which is shown in Figure7.3b for 2020.

8.4 Future of groundwater sustainability

As current groundwater use practices are nearing the edge of sustainability, it is important to investigate how the groundwater system will be affected by intensification of urbanisation, population growth, and possible effects of climate change. For this analysis, three main factors are considered: land use changes (particularly the further loss of green space and increase in impervious urban cover), increased population growth resulting in more domestic groundwater consumption, and the effect of increasingly intense precipitation events. Current available data falls short on giving reliable inter-annual estimates of groundwater recharge due to the lack of surface reflectance images from the satellite products. Drawing future trends from the past is therefore limited. This section aims to provide an initial pathway to future scenario investigations in Kumasi. Possible scenarios are sketched out and a preliminary investigation into the future of groundwater sustainability in Kumasi is conducted.

8.4.1 Intensification of urbanisation and land use changes

Land use maps from 1986 to 2013 indicate an increase of semipervious urban areas at the cost of dense vegetation. In the same period, groundwater recharge decreased from 124.1Mm^3 to 96.2Mm^3. However, from 2013 to 2020 great land use changes occurred, such as a 10% increase in impervious urban, a 22% increase in semipervious urban and a further loss of 33% of vegetated cover. From 2013 to 2020, recharge decreased by a factor 3, leaving recharge at 28.9Mm^3. Using results of percentage land cover in 2020 (Table 6.2) and average recharge per land cover class (Table 6.7), a rough estimate can be made to investigate the effect of changing land cover on urbanisation. The future recharge can be estimated by using a weighted average for recharge as shown in Equation 21, where i is a land cover class from 0 to 5, $\mathrm{GWR}_{2020,i}$ is the average recharge for the land use class in 2020 in mm, and $\mathrm{A}_{2050,i}$ is the predicted percentage cover of the land class for 2050.

$$\mathrm{GWR}_{2050} = \sum_{i=0}^{5} (\mathrm{GWR}_{2020,i} \times A_{2050,i}) \tag{21}$$

For future scenarios, three different possibilities are investigated: business as usual, urban intensification, and greening of Kumasi. Percentage cover of each class over Kumasi for these three scenarios are loosely chosen to investigate the resulting effects of different land use combinations

on groundwater recharge. The predicted areas are shown in Table 8.2 for each scenario. In the business as usual scenario, the general trend of an increase in impervious area as assumed alongside the loss of sparse vegetation. For the intensification scenario it is assumed that impervious areas increase while semipervious urban area decreases, and there is a continued loss of vegetated area. A more positive approach is taken for the greening scenario, where semipervious urban areas increase slightly due to a decreases in impervious urban areas while vegetated areas increase. Weighted average recharge for each scenario is shown in Table 8.2. An important observation is that the magnitude of change in groundwater recharge is dependent on which land class is growing or reducing. Changes in recharge are greater when there are changes in the area of impervious urban, water, and both vegetation classes due to their large individual contributions to net groundwater recharge (negative for impervious and water classes). This dynamic relationship explains why the change in groundwater recharge from 2013-2020 was greater than that between 1986-2013, as the former period experienced a great growth in the impervious urban classes whereas the latter experienced a growth in sermipervious urban.

Table 8.2: Average groundwater recharge over Kumasi for different land use scenarios in 2050. GWR: groundwater recharge.

i: Land cover	*2020 avg. GWR (mm)*	2020 land cover %	Scenarios 2050, land cover %		
			Bs. as usual	*Intensification*	*Greening*
0: Semipervious urban	*45.4*	68	68	34	70
1: Impervious urban	*-159.1*	11	21	60	7
2: Bare land	*382.1*	1	1	1	0
3: Dense vegetation	*566.1*	3	2	1	5
4: Sparse vegetation	*513.5*	17	8	4	18
5: Water	*-614.3*	0	0	0	0
Weighted average annual GWR		*120 mm (28.9 Mm^3)*	*54 mm (12.9Mm^3)*	*-50 mm (-12.1Mm^3)*	*141 mm (34.1Mm^3)*

Results in Table 8.2 show the effect that each scenario will have on groundwater recharge. With intensification, if the impervious urban area grows drastically to 60%, there will be no groundwater recharge in Kumasi. If urban growth is considered mostly in the impervious area, while parks are retained but sparse vegetation decreases, recharge is also expected to decrease but will still remain positive. In a greening scenario where green spaces are protected and urbanisation occurs in the form of growth in semipervious and not impervious urban area, groundwater recharge can be stimulated and even increased.

8.4.2 Increased population growth

Freshwater supply in Ghana is compromised by the exploitation of freshwater resources due to growing populations, pollution, and climate change. Industrial waste, illegal mining, farming, and household waste disposal have been a major sources of pollution as around 60% of water bodies in Ghana are polluted (Yeleliere et al., 2018). Pollution has been found to be less prevalent in groundwater (Yeleliere et al., 2018), so as populations grow and water supply becomes less reliable, it can be expected that groundwater use per capita will increase (Cisneros et al., 2014). It is also expected to increase due to the decrease in per capita water availability in Kumasi (World Bank, 2015). This brings two main changes in groundwater consumption: an growth in consumptive population and an increase in per capita groundwater consumption. Assuming a consistent population growth of 5.5% in Kumasi, the population in 2050 is projected to be 17,325,127. Using Equation 18 and inputting a per capita water demand of 0.094m^3/d and 23.8% groundwater consumption (same values as in Table 6.8), the 2050 consumption based on population increase is estimated to be 141Mm^3. This is close to a five-fold increase compared to the 2020 domestic groundwater consumption estimate. Table 8.3 shows how domestic groundwater consumption changes depending on population growth rate and domestic groundwater dependency. If the growth rate slows down to the regional average of 2.5% (Ghana Statistical Service, 2013b), then domestic groundwater consumption will only be 60Mm^3. If total domestic water consumption remains constant, the total

domestic groundwater consumption is linearly proportional to the growth/reduction in percentage of groundwater consumed domestically.

Table 8.3: Estimated domestic groundwater consumption for 2050 for different population growth rates and groundwater dependencies. GW: groundwater, water demand: 0.094Mm^3/cap/day.

Growth rate (%)	Population in 2050	Domestic GW consumption 2050		*Factor increase (2020-2050)*
5.5	17,325,128	23.8 %	141 Mm^3	*10*
		48 %	285 Mm^3	*5*
2.5	7,291,528	23.8 %	60 Mm^3	*2*
		48 %	120 Mm^3	*4*

If Kumasi's population growth continues at its current rate, domestic groundwater consumption by 2050 may become over 10 times greater than groundwater recharge when compared to the business as usual scenario. Since 2010, no survey has been found investigating sources of domestic and drinking water consumption in Kumasi. The last survey was done alongside the population census of 2010 (see Ghana Statistical Service (2013a)). Having such data can be used to understand changes in groundwater consumption and to have a better overview of the dependency of groundwater within the city. This can also be used to make more accurate predictions on how groundwater consumption will change in the future. Such a survey can also be used to make better population projections, which in turn also improved future groundwater consumption estimates. Another factor that can eventually be considered is the socio-economic effect contributing to water consumption. An increased socio-economic status can lead to higher per capita consumption rates, which may alter total water demand in Kumasi.

8.4.3 Climate change scenarios

The impacts of climate change on groundwater are difficult to assess due to the lack of long-term groundwater data and slow aquifer response to climatic fluctuations (Bovolo et al., 2009). Kundzewicz et al. (2007) explains assessments of groundwater recharge under climate change should include changes in precipitation and variability of inundation areas. It is also explained that groundwater levels are sensitive to temperatures increases, especially where the confining layer in thin or the aquifer is unconfined, which is assumed for the shallow aquifers of Kumasi. However, changes in the water cycle, such as in runoff and groundwater recharge, are not linearly related to climate change due to the interaction of multiple drivers, feedbacks and time scales Douville et al. (2021). This complicates the prediction of future groundwater recharge under climate change using the simple water balance. Notable is that total runoff is expected to increase more than groundwater recharge from the effects of climate change (Kundzewicz et al., 2007).

The sixth assessment report of the International Panel on Climate Change (IPCC (2021)) reported an observed increase in river in river flooding, increase in agricultural and ecological droughts, and a projected increase in meteorological droughts in seasonal timescales over West Africa. In Ghana specifically, there has been an observed slight increase of precipitation over the last 30 years (Ministry of Foreign Affairs, 2019). Ministry of Foreign Affairs (2019) explains there is a large uncertainty in rainfall change, as increases are predicted from July to December but decreases are predicted from March to June. Intensity of heavy rainfall events is expected to increase along with the proportion of total annual precipitation that falls during these events. Initially there is a predicted increase of precipitation in 2030, but by 2050 there is an expected precipitation change of -19 to -10mm. Cisneros et al. (2014) explains an increased precipitation intensity in humid areas may decrease groundwater recharge due to an exceedence of the infiltration capacity. Temperature over the same period is projected to increase by 2.1°C to 2.2°C. Groundwater recharge changes are variable, as Cisneros et al. (2014) presents four different projections under two different climate models, results ranging from no change in groundwater recharge to a >10% decrease in groundwater recharge.

Using the water balance methodology to recalculate runoff and evapotranspiration under a climate change scenario requires understanding of how individual precipitation events and monthly evapotranspiration will change in the future. For future runoff estimates, two variables are therefore required: changes in the magnitude of precipitation events and land use changes as retention requires CN estimates. Future evapotranspiration estimates under climate change are governed by temperature changes. It is expected that if temperatures rise evapotranspiration rates will also increase. The extent of its increase is not investigated due the variability between months. Changes in the magnitude of each water balance component under climate change is complex and requires more in-depth investigation into the monthly changes. Therefore, the current scope looks only at estimated changes in groundwater recharge. If a decrease of at least 10% is expected by 2050 (projected by two climate scenarios of Cisneros et al. (2014)), this decreases recharge to 26Mm^3 (103mm). This is much smaller than changes brought by urbanisation, as the rough estimate of recharge under the 2050 business as usual land use scenario is 12.9Mm^3.

Although climate change is expected to affect the groundwater system, the largest changes in groundwater level are attributed to influences of land use changes and groundwater abstractions (Cisneros et al., 2014). Dragoni & Sukhija (2008) explain the impacts of anthropogenic activities on water resources are much larger than changes from recent past climate change. Anthropogenic activities may also be driven by climate change, but the extent of this effect is unknown (Cisneros et al., 2014). The slow response time of aquifers prompts the need to properly manage groundwater as a resource as it can be used as a source to buffer the impacts of climate change on other freshwater sources.

8.5 Summary for policy makers

Results from this study indicate groundwater consumption in Kumasi has exceeded groundwater recharge, meaning current practices are unsustainable. Based on the initial analysis of future scenarios, the greatest challenge to sustainable groundwater use is population growth. Following the business as usual scenario, by 2050 climate and land-cover changes are expected to decrease recharge by a minimum of 10% and 55% respectively. Moreover, domestic groundwater consumption is expected to increase four-fold due to the increase in population (5.5% annual growth) and continued reliance on groundwater (23.8% domestic reliance). In the optimistic scenario in which groundwater consumption remains at current rates and population grows with the national average, consumption is still expected to double by 2050. The adverse trend of unsustainability can be reversed by promoting groundwater recharge and reducing groundwater consumption. As seen in Table 8.2, groundwater recharge can increase when green spaces are protected and development occurs in the form of growth of semipervious surfaces instead of impervious surfaces. The major recommendations for policy-makers to incentivise sustainable groundwater use are given below.

Promoting low-impact development (LID) provides an important means to manage groundwater recharge. The term refers to practices that preserve the natural process resulting in infiltration, evapotranspiration, and runoff (EPA, 2021). In Kumasi, the decrease in recharge over the last decade has been attributed to the growth of the impervious urban area and the overall loss of vegetation. In the case of future land developments in the urban area, LID includes growth of permeable surfaces instead of impermeable surfaces as this promotes natural infiltration of water. More specifically, this could include green infrastructure plans for roads and parking lots and using permeable surface building materials (EPA, 2021). Moreover, the re-development of impervious spaces to include more green patches and permeable surfaces will also promote natural infiltration processes. Lastly, the existing green spaces in Kumasi need to be protected as these are the most important areas for groundwater recharge.

Monitoring groundwater use is the first step in tracking groundwater abstractions in Kumsi. Results from this study are based on general estimates of total water consumption and groundwater dependency. Improving these estimations requires information on abstraction in Kumasi. No complete overview of the distribution of domestic and non-domestic boreholes and their pumping rates is available. Furthermore, there is a lack of information on hand-dug wells, which are expected to grow in the future due to the uncontrolled population growth and an inadequate

water-supply system. Conducting multi-annual surveys in the city, similar to the survey conducted into non-domestic consumption, can improve the estimation accuracy of temporal changes in groundwater consumption. Creating such a database requires cooperation between landowners, private companies and policy-makers.

Monitoring changes in the groundwater system is an effective method to gain insight into the groundwater system's reaction to groundwater developments and urbanisation. Changes in groundwater quantity as well as quality are important when examining aquifers. The uncertainty of model predictions dictate that monitoring is essential in confirming the effectiveness of implemented measures (Gleeson et al., 2012). Developing the capacity to monitor and manage urban groundwater use is challenging as it requires appropriate technology and financing (Adelana et al., 2008). Data from water-level monitoring networks can be used in hydrological models to estimate components of groundwater storage (Chung et al., 2016). Moreover, such a network can be employed to directly estimate short-term groundwater recharge in shallow aquifers through the water-table fluctuation method. Groundwater quality should also frequently be monitored to assess whether it is safe for consumption. Monitoring is vital for adaptive aquifer management as a hydrogeological understanding is required in order to make informed land- and groundwater-use policies.

9 Conclusion and recommendations

9.1 Conclusion

Groundwater in Kumasi has been used as an alternative water source due to its efficiency and low development cost. Urbanisation, specifically population growth, land use changes and increased groundwater demand, is putting the future availability of groundwater at risk. There is a concerning lack of assessments into the city's groundwater system and how it will be affected by future challenges. This study aims to conduct a preliminary assessment into the sustainability of current groundwater use in Kumasi by investigating groundwater recharge and groundwater abstraction. Hydrological datasets in Kumasi are not readily available and often incomplete, complicating detailed analyses into groundwater flows and storage volumes. To bridge the data gap, remote sensing data has proven to be invaluable in estimating potential groundwater recharge. The main finding are summarised below to answer the research question,

To what extent are the urbanisation trends in Kumasi sustainable for the availability of the groundwater resources?

Urbanisation trends
Major land developments have occurred in Kumasi to accommodate the growing population. In 1986, vegetated land covered 82% of Kumasi's surface area but due to rapid urbanisation this cover dropped to 18% in 2020. The loss has been attributed to the growth of the total urban area and intensification of urban developments. Initial trends (1986-2013) showed a 31 percentage point increase in the cover of semipervious urban surfaces, while impervious growth was negligible. However, more recent trends (2013-2020) indicate impervious cover increased from 2% to 12%. Although semipervious urban areas make up the largest part of land cover in Kumasi, it is expected that further developments will require the conversion of semipervious to impervious urban areas as the radial growth of the city has surpassed the city bounds.

Availability of groundwater (water-balance components)
Groundwater recharge is governed by precipitation, runoff, and evapotranspiration processes. Evapotranspiration estimates per land-cover class were derived from the 8-day MODIS evapotranspiration product using land-cover maps created for 1986, 2013, and 2020. Runoff was calculated using the SCS-CN method, through which it was determined that areas with the highest runoff correspond to those with the highest curve number based on land use and soil type. Soil type is

especially important for non-urban areas due to higher infiltration potential where soil can alter drainage capacities. For impervious urban areas soil is unimportant but under semipervious urban lands the soil type can still alter runoff potential. Long-term average annual runoff for Kumasi was estimated to be 686 mm, ranging between 142 mm to 1023 mm for different land-cover classes. The range in runoff is much larger than that of evapotranspiration as the long-term average annual evapotranspiration is 527 mm, varying between 447 mm and 627 mm. Therefore, runoff is more sensitive to land-cover changes than evapotranspiration.

Sustainability
Defining groundwater sustainability in Kumasi requires the components of groundwater recharge and groundwater abstraction. Results from the monthly water balance carried out in Google Earth Engine indicate a current annual long-term average groundwater recharge (forcing data from 2001-2020) of 120 mm, or 28.9Mm^3. Using long-term average recharge instead of annual recharge minimises the effect of inter-annual precipitation differences allowing for a better understanding of mean recharge. Based on the land-cover maps of 1986 and 2013, annual groundwater recharge was estimated to be 124.1Mm^3 and 96.2Mm^3 respectively. Groundwater recharge from 1986 to 2020 has therefore decreased by nearly 80%. Domestic groundwater use was estimated using water consumption, dependency on groundwater, and population data. Non-domestic groundwater abstraction was estimated from a survey conducted in Kumasi at 52 facilities between June and August 2021. Survey results for 2021 were assumed to be approximately equal to non-domestic consumption in 2020. Total groundwater consumption for 2020 was estimated to be 31.1Mm^3, with the domestic and non-domestic component being 28.4Mm^3 and 2.7Mm^3 respectively. Referring back to the definition of sustainable groundwater use by Bierkens & Wada (2019), long-term average annual groundwater recharge should be less than the (multi-)annual groundwater abstractions. Results indicate that this is not the case in Kumasi.

Current urbanisation trends in Kumasi are unsustainable for future availability of groundwater. Following a business as usual scenario, by 2050 land-cover changes are expected to decrease recharge by 55% while groundwater consumption may increase four-fold. Climate change is expected to exacerbate future unsustainability but the largest challenges lie in monitoring groundwater consumption and promoting low-impact development strategies.

9.2 Recommendations for further research

This study is a preliminary investigation into the components affecting natural groundwater recharge in Kumasi. Understanding the dynamics between anthropogenic processes of land-use changes and population growth alongside natural processes such as precipitation, runoff, and evapotranspiration gives a better insight into the sustainability of groundwater practices in Kumasi. Estimates of groundwater recharge and abstraction are of the same magnitude, prompting the need for further assessments to validate these results. Four recommendations are given for further investigations into the sustainability of groundwater in Kumasi.

1. Further studies in Kumasi to validate groundwater recharge results.
Due to the complexity of groundwater recharge estimations, it is recommended that various groundwater studies are carried out in Kumasi. The main challenges with recharge estimation are the nonlinear recharge response over time, data scarcity, and unique complexities of each component within the hydrological balance (Chung et al., 2016). Therefore, direct methods should be implemented to estimate recharge such as chloride mass-balance, which indicates groundwater residence times through the varying concentrations of chloride in precipitation and groundwater. Such a method is inexpensive and easy to apply, providing a fair approximation of the long-term recharge value (Chung et al., 2016). Moreover, implementing groundwater monitoring boreholes will improve the understanding of groundwater-system changes as a result of long-term urbanisation stresses. More data-intensive methods include implementation of hydrologic modelling, which requires long-term measurements of streamflow or groundwater levels. However, the application of such a method is only possible with sufficient data (Wakode et al., 2018; Rooyen et al., 2020).

2. Improvement of current methodology.
The methodology developed here uses remote sensing to bridge the data gap in groundwater recharge estimates. Using readily-available datasets to estimate the water-balance components requires some assumptions and simplifications. The accuracy of current recharge estimates can be improved if the components of evapotranspiration and runoff can be validated. There is a high certainty that urban evaporation is being overestimated while vegetated evapotranspiration is being underestimated. Evapotranspiration can be validated with an energy-balance models such as SEBAL (explained in section 2.4.1). Such methods require meteorological datasets that are difficult to obtain for Kumasi, especially over a long time period. Moreover, runoff estimates can be improved by applying a daily runoff estimate instead of a 5-day estimate. This was not carried out in this study due to the heavy computational load in Google Earth Engine. The major benefit of remote-sensing datasets is the spatio-temporal availability and accessibility of data, making it possible to conduct studies that would otherwise not be possible.

3. Continued surveys into domestic and non-domestic groundwater recharge.
Based on this study's results, the greatest challenge to sustainable groundwater usage is the abstraction component. If consumption continues at current rates, groundwater use is expected to increase fourfold by 2050. Groundwater abstraction results should be confirmed by up-to-date surveys on abstraction in Kumasi as the last population survey was done by the Ghana Statistical Service in 2010. If population growth reflects the rapid changes in land use cover, then it is expected that changes have occurred in respect to water consumption that need to be investigated. Results from the survey into non-domestic groundwater use was the tipping point to push groundwater consumption over groundwater recharge. This highlights the significance of such surveys for the understanding of groundwater consumption.

4. Detailed investigation into future scenarios.
The major challenges for future groundwater sustainability are the growing population and its continued reliance on groundwater in addition to the reduction of recharge in the future due to land cover changes. The good news is that consequences of unsustainable groundwater use can be mitigated with proper adaptive aquifer management. To better understand the future challenges it is recommended that detailed scenarios are investigated relating to best-case scenarios, business-as-usual scenarios, and worst case scenarios. This study only gives a glimpse into the future challenges based on rough assumptions of land use changes, population growth, groundwater reliance, and climate change scenarios. Shifting from "what-if" scenarios to well-developed future scenarios will allow for better decisions for policy makers.

Groundwater management remains complex due to the hidden nature of the resource, often making it non-attractive for policy and decision makers (Chung et al., 2016). It is therefore important to raise awareness for issues surrounding groundwater, which is what this study aims to do. Results show that groundwater abstraction in Kumasi has exceeded long-term average annual recharge. This is concerning for the future of the socio-economic well-being of Kumasi's residents as groundwater has provided water for agriculture, industry, and people. In the face of climate change and urbanisation, both ground- and surface-water sources are at risk. Groundwater can be used as an alleviation to the issues facing other water sources, but this is only possible with efficient management and the adoption of strategies that deal with future challenges.

References

Abass, K., Adanu, S., & Gyasi, R. (2018). Urban sprawl and land use/land-cover transition probabilities in peri-urban kumasi, ghana. *West African Journal of Applied Ecology*, *26*, 118–132.

Abass, K., Buor, D., Afriyie, K., Dumedah, G., Segbefi, A. Y., Guodaar, L., ... others (2020). Urban sprawl and green space depletion: Implications for flood incidence in Kumasi, Ghana. *International Journal of Disaster Risk Reduction*, *51*, 101915.

Adelana, S.-S. A. S., Abiye, T., Nkhuwa, D., Tindimugaya, C., & Oga, M. (2008). Urban groundwater management and protection in sub-saharan africa. In *Applied groundwater studies in africa* (pp. 241–270). CRC Press.

Adjei-Gyapong, T., & Asiamah, R. (2002). *The Interim Ghana Soil Classification System and its Relation with the World Reference Base for Soil Resources. Rapport sur les Ressources en Sols du Monde.* FAO.

Afonso, M. J., Freitas, L., & Chaminé, H. I. (2019). Groundwater recharge in urban areas (porto, nw portugal): the role of gis hydrogeology mapping. *Sustainable Water Resources Management*, *5*(1), 203–216.

Afriyie, K., Abass, K., & Adjei, P. O.-W. (2020). Urban sprawl and agricultural livelihood response in peri-urban ghana. *International Journal of Urban Sustainable Development*, *12*(2), 202–218.

Allen, R., Pereira, L. S., Raes, D., Smith, M., et al. (1998). Crop evapotranspiration-guidelines for computing crop water requirements-fao irrigation and drainage paper 56. *Fao, Rome*, *300*(9), D05109.

Allen, R., Tasumi, M., Trezza, R., Waters, R., & Bastiaanssen, W. (2002, August). *SEBAL: Advanced Training and Users Manual.* Univerity of Idaho: Department of Water Resources.

Amoateng, P., Finlayson, M., Howard, J., & Wilson, B. (2018a). Dwindling rivers and floodplains in Kumasi, Ghana: A socio-spatial analysis of the extent and trend. *Applied Geography*, *90*, 82–95. doi: 10.1016/j.apgeog.2017.11.007.

Amoateng, P., Finlayson, M., Howard, J., & Wilson, B. (2018b). A multi-faceted analysis of annual flood incidences in Kumasi, Ghana. *International Journal of Disaster Risk Reduction*, *27*, 105–117. doi: 10.1016/j.ijdrr.2017.09.04

Anornu, G. K., Kortatsi, B. K., & Saeed, Z. M. (2009). Evaluation of groundwater resources potential in the ejisu-juaben district of ghana. *African Journal of Environmental Science and Technology*, *3*(10), 332–340.

Awuah, E., Gyasi, S. F., Anipa, H. K., & Adjei, A. (2014). Microbial quality of sachet and bagged drinking water: A case study in kumasi, ghana. *Research Journal of Microbiology*, *9*(4), 199.

Bierkens, M. F. P., & Wada, Y. (2019). Non-renewable groundwater use and groundwater depletion: a review. *Environmental Research Letters*, *14*, 1–43. doi: 10.1088/1748-9326/ab1a5f

Bovolo, C. I., Parkin, G., & Sophocleous, M. (2009). Groundwater resources, climate and vulnerability. *Environmental Research Letters*, *4*(3), 035001.

Bowman, K. P. (2005). Comparison of trmm precipitation retrievals with rain gauge data from ocean buoys. *Journal of Climate*, *18*(1), 178–190.

Campion, B. B., & Venzke, J.-F. (2013). Rainfall variability, floods and adaptations of the urban poor to flooding in kumasi, ghana. *Natural hazards*, *65*(3), 1895–1911.

Carrasco, L., O'Neil, A. W., Morton, R. D., & Rowland, C. S. (2019). Evaluating combinations of temporally aggregated sentinel-1, sentinel-2 and landsat 8 for land cover mapping with google earth engine. *Remote Sensing*, *11*(3), 288.

Chakrabortty, R., Pal, S. C., Malik, S., & Das, B. (2018). Modeling and mapping of groundwater potentiality zones using AHP and GIS technique: a case study of Raniganj Block, Paschim Bardhaman, West Bengal. *Modeling Earth Systems and Environment*, *4*, 1085-–1110. doi: 10.1007/s40808-018-0471-8

Chung, I.-M., Sophocleous, M. A., Mitiku, D. B., & Kim, N. W. (2016). Estimating groundwater recharge in the humid and semi-arid african regions. *Geosciences Journal*, *20*(5), 731–744.

Cisneros, B. E. J., Oki, T., Arnell, N. W., Benito, G., Cogley, J. G., Döll, P., ... Mwakalila, S. S. (2014). Part a: Global and sectoral aspects. contribution of working group ii to the fifth assessment report of the intergovernmental panel on climate change. In *Freshwater resources* (p. 299-269). Cambridge, United Kingdom: Cambridge University Press. Retrieved from `https://www.ipcc.ch/site/assets/uploads/2018/02/WGIIAR5-Chap3_FINAL.pdf` (Accessed: 13-09-2021)

Climate Data. (n.d.). *Climate-Data.* Climate-Data.org.

Cobbinah, P. B., & Amoako, C. (2012). Urban Sprawl and the Loss of Peri-Urban Land in Kumasi, Ghana. *International Journal of Social and Human Sciences*, *6*, 387–397.

Cobbinah, P. B., Gaisie, E., Oppong-Yeboah, N. Y., & Anim, D. O. (2020). Kumasi: Towards a sustainable and resilient cityscape. *Cities*, *97*, 102567.

Copernicus corine land cover. (2021). `https://developers.google.com/earth-engine/datasets/catalog/COPERNICUS_CORINE_V20_100m#description`. Google Earth Engine. (Accessed: 2021-08-10)

Das, B., & Pal, S. C. (2020). Assessment of groundwater vulnerability to over-exploitation using MCDA, AHP, fuzzy logic and novel ensemble models: a case study of Goghat-I and II blocks of West Bengal, India. *Environmental Earth Sciences*, *79*(104), 1–16. doi: 10.1007/s12665-020-8843-6

Domfeh, M. K., Anyemedu, F. O. K., Anornu, G. K., Adjei, K. A., & Odai, S. N. (2015). Assessment of the water balance of the Barekese reservoir in Kumasi, Ghana. *Journal of Science and Technology*, *35*(3), 34–51. doi: 10.4314/just.v35i3.4

Douville, H., K. Raghavan, J. R., Allan, R. P., Arias, P. A., M. Barlow, R. C.-M., Cherchi, A., ... Zolina, O. (2021). Water cycle changes. In *The physical science basis. contribution of working group i to the sixth assessment report of the intergovernmental panel on climate change* (chap. 8). Cambridge University Press.

Dragoni, W., & Sukhija, B. S. (2008). Climate change and groundwater: a short review. *Geological Society, London, Special Publications*, *288*(1), 1–12.

EPA. (2021). *Urban runoff: Low impact development.* (Accessed: 20-09-2021)

Erni, M., Bader, H.-P., Drechsel, P., Scheidegger, R., Zurbrügg, C., & Kipfer, R. (2011). Urban water and nutrient flows in kumasi, ghana. *Urban Water Journal*, *8*(3), 135–153.

ESA. (2020). *Sentinel-2 MSI Technical Guide: MultiSpectral Instrument (MSI) Overview.* `https://sentinel.esa.int/web/sentinel/technical-guides/sentinel-2-msi/msi-instrument`. (Accessed: 26-05-2021)

Ewusi, A., Asante-Annor, A., Seidu, J., & Gyeabour, L. (2016). Groundwater Vulnerability Assessment using Drastic Index and GIS in Kumasi Metropolitan Assembly, Ghana. *Hydrogeology Journal*, *16*(1), 21–30.

Falalakis, G., & Gemitzi, A. (2020). A simple method for water balance estimation based on the empirical method and remotely sensed evapotranspiration estimates. *Journal of Hydroinformatics*, *22*(2), 440–451.

Fan, F., Deng, Y., Hu, X., & Weng, Q. (2013). Estimating composite curve number using an improved scs-cn method with remotely sensed variables in guangzhou, china. *Remote Sensing*, *5*(3), 1425–1438.

Fitts, C. R. (2013). *Groundwater Science*. 225 Wyman Street, Waltham, MA 02451, USA: Elsevier.

Forkuor, G., Pavelic, P., Asare, E., & Obuobie, E. (2013). Modelling potential areas of groundwater development for agriculture in northern Ghana using GIS/RS. *Hydrological Sciences Journal*, *58*(2), 437–451. doi: 10.1080/02626667.2012.754101

Foster, S., & Chilton, P. (2003). Groundwater: the processes and global significance of aquifer degradation. *Philosophical Transactions of the Royal Society of London. Series B: Biological Sciences*, *358*(1440), 1957–1972.

Foster, S., Eichholz, M., Nlendc, B., & Gathu, J. (2020). Securing the critical role of groundwater for the resilient water-supply of urban Africa. *Water Policy*, *22*, 121–132. doi: 10.2166/wp.2020.177

Freitas, L., Afonso, M. J., Pereira, A. J. S. C., Delerue-Matos, C., & Chaminé, H. I. (2019). Assessment of sustainability of groundwater in urban areas (Porto, NW Portugal): a GIS mapping approach to evaluate vulnerability, infiltration and recharge. *Environmental Earth Sciences*, *78*(140), 1–17. doi: 10.1007/s12665-019-8167-6

Funk, C., Peterson, P., Landsfeld, M., Pedreros, D., Verdin, J., Shukla, S., ... others (2015). The climate hazards infrared precipitation with stations—a new environmental record for monitoring extremes. *Scientific data*, *2*(1), 1–21.

Garcia-Fresca, B. (2007). Urban-enhanced groundwater recharge: review and case study of austin, texas, usa. In *Urban groundwater, meeting the challenge* (pp. 19–34).

Gaye, C. B., & Tindimugaya, C. (2019). Challenges and opportunities for sustainable groundwater management in africa. *Hydrogeology Journal*, *27*(3), 1099–1110.

Gemitzi, A., Ajami, H., & Richnow, H.-H. (2017). Developing empirical monthly groundwater recharge equations based on modeling and remote sensing data – Modeling future groundwater recharge to predict potential climate change impacts. *Journal of Hydrology*, *546*, 1–13. doi: 10.1016/j.jhydrol.2017.01.005

Ghana MOE. (2018). *Education sector analysis.* Ghana Ministry of Education. (Accessed: 15-09-2021)

Ghana Statistical Service. (2013a). *2010 population and housing census: Kumasi metropolis district analytical report.* Ghana Statistical Service.

Ghana Statistical Service. (2013b). *2010 population and housing census: National analytical report.* Ghana Statistical Service.

Gleeson, T., Alley, W. M., Allen, D. M., Sophocleous, M. A., Zhou, Y., Taniguchi, M., & VanderSteen, J. (2012). Towards sustainable groundwater use: Setting long-term goals, backcasting, and managing adaptively. *Groundwater*, *50*(1), 19–26.

Google Earth Engine. (2020). *CHIRPS Daily: Climate Hazards Group InfraRed Precipitation with Station Data (version 2.0 final).* `https://developers.google.com/earth-engine/datasets/catalog/UCSB-CHG_CHIRPS_DAILY`. (Accessed: 16-06-2021)

Graaf, I. E. D., van Beek, R. L., Gleeson, T., Moosdorf, N., Schmitz, O., Sutanudjaja, E. H., & Bierkens, M. F. (2017). A global-scale two layer transient groundwater model: development and application to groundwater depletion. *Advances in Water Resources*, *102*(9), 53–67.

Guides: Supervised classification. (2021). `https://developers.google.com/earth-engine/guides/classification`. Google Earth Engine. (Accessed: 2021-05-31)

Gumma, M. K., & Pavelic, P. (2013). Mapping of groundwater potential zones across ghana using remote sensing, geographic information systems, and spatial modeling. *Environmental monitoring and assessment*, *185*(4), 3561–3579.

Han, D., Currell, M. J., Cao, G., & Hall, B. (2017). Alterations to groundwater recharge due to anthropogenic landscape change. *Journal of hydrology*, *554*, 545–557.

Hiscock, K. M., Rivett, M. O., & Davison, R. M. (2002). Sustainable groundwater development. *Geological Society, London, Special Publications*, *193*(1), 1–14.

Hong, Y., & Adler, R. (2008). Estimation of global scs curve numbers using satellite remote sensing and geospatial data. *International Journal of Remote Sensing*, *29*(2), 471–477.

IPCC. (2021). *IPCC Sixth Assessment Report Working Group I – The Physical Science Basis: Regional Fact Sheet - Africa.* Cambridge, United Kingdom: Cambridge University Press. Retrieved from `https://www.ipcc.ch/report/ar6/wg1/downloads/factsheets/IPCC_AR6_WGI_Regional_Fact_Sheet_Africa.pdf`

Jia, Z., Liu, S., Xu, Z., Chen, Y., & Zhu, M. (2012). Validation of remotely sensed evapotranspiration over the hai river basin, china. *Journal of Geophysical Research: Atmospheres*, *117*(D13).

Kabo-Bah, A. T., Diji, C., Nokoe, K., Mulugetta, Y., Obeng-Ofori, D., Akpoti, K., et al. (2016). Multiyear rainfall and temperature trends in the volta river basin and their potential impact on hydropower generation in ghana. *Climate*, *4*(4), 49.

Koranteng, A. (2017). Competitive land use/cover of kumasi and its environs based on satellite imagery studies. In *International conference on applied science and technology conference proceedings* (Vol. 1, pp. 208–219).

Kortatsi, B. (1994). Groundwater utilization in ghana. *IAHS Publications-Series of Proceedings and Reports-Intern Assoc Hydrological Sciences*, *222*, 149–156.

Krajewski, A., Sikorska-Senoner, A. E., Hejduk, A., & Hejduk, L. (2020). Variability of the initial abstraction ratio in an urban and an agroforested catchment. *Water*, *12*(2), 415.

Kuma, J. S., Owusu, R. O., & Gawu, S. K. Y. (2010). Evaluating the Water Supply System in Kumasi, Ghana. *European Journal of Scientific Research*, *40*(4), 506–514.

Kundu, S., Mondal, A., Khare, D., Hain, C., & Lakshmi, V. (2018). Projecting climate and land use change impacts on actual evapotranspiration for the narmada river basin in central india in the future. *Remote Sensing*, *10*(4), 578.

Kundzewicz, Z. W., Luis José Mata (Venezuela), N. A., Döll, P., Kabat, P., Jiménez, B., Miller, K., ... Shiklomanov, I. (2007). Groundwater. In *Climate change 2007: Impacts, adaptation and vulnerability. contribution of working group ii to the fourth assessment report of the* (chap. 3). Cambridge University Press.

Lapworth, D., MacDonald, A., Tijani, M., Darling, W., Gooddy, D., Bonsor, H., & Araguás-Araguás, L. (2013). Residence times of shallow groundwater in west africa: implications for hydrogeology and resilience to future changes in climate. *Hydrogeology Journal*, *21*(3), 673–686.

Lee, Y., & Kim, S. (2016). The modified sebal for mapping daily spatial evapotranspiration of south korea using three flux towers and terra modis data. *Remote Sensing*, *8*(12), 983.

Lerner, D. L. (1990). Groundwater recharge in urban areas. *Atmospheric Environment*, *24B*(1), 29-33.

Li, C., Wang, J., Wang, L., Hu, L., & Gong, P. (2014). Comparison of classification algorithms and training sample sizes in urban land classification with landsat thematic mapper imagery. *Remote sensing*, *6*(2), 964–983.

Liu, W., Hong, Y., Khan, S. I., Huang, M., Vieux, B., Caliskan, S., & Grout, T. (2010). Actual evapotranspiration estimation for different land use and land cover in urban regions using landsat 5 data. *Journal of Applied Remote Sensing*, *4*(1), 041873.

MacDonald, A. M., Lark, R. M., Taylor, R. G., Abiye, T., Fallas, H. C., Favreau, G., ... others (2021). Mapping groundwater recharge in africa from ground observations and implications for water security. *Environmental Research Letters*, *16*(3), 034012.

Maoulidi, M. (2010). A water and sanitation needs Assessment for Kumasi, Ghana. *MCI Social Sector Working Paper Series*, *16*.

Martin, N., & Giesen, N. V. D. (2005). Spatial Distribution of Groundwater Production and Development Potential in the Volta River basin of Ghana and Burkina Faso. *Water International*, *30*(2), 239–249. doi: 10.1080/02508060508691852

McGregor, D. F., Adam-Bradford, A., Thompson, D. A., & Simon, D. (2011). Resource management and agriculture in the periurban interface of kumasi, ghana: Problems and prospects. *Singapore Journal of Tropical Geography*, *32*(3), 382–398.

Meijerink, A. (2007). *Remote sensing applications to groundwater*. 7, Place de Fontenoy, 75352 Paris 07 SP (France): United Nations Educational, Scientific and Cultural Organization.

Midekisa, A., Holl, F., Savory, D. J., Andrade-Pacheco, R., Gething, P. W., Bennett, A., & Sturrock, H. J. W. (2017). Mapping land cover change over continental Africa using Landsat and Google Earth Engine cloud computing. *PLoS ONE*, *12*(9), 1–15. doi: 10.1371

Ministry of Foreign Affairs, N. (2019). Climate change profile: Ghana. Retrieved from `https://www.government.nl/documents/publications/2019/02/05/climate-change-profiles` (Accessed: 13-09-2021)

Mishra, S. K., & Singh, V. P. (2013). *Soil conservation service curve number (scs-cn) methodology* (Vol. 42). Springer Science & Business Media.

Modis land cover type/dynamics. (2021). `https://modis.gsfc.nasa.gov/data/dataprod/mod12.php`. NASA MODIS. (Accessed: 2021-08-10)

Monney, I., Donkor, E. A., & Buamah, R. (2020). Clean vehicles, polluted waters: empirical estimates of water consumption and pollution loads of the carwash industry. *Heliyon*, *6*(5), e03952.

Mu, Q., Zhao, M., & Running, S. W. (2013). *MODIS Global Terrestrial Evapotranspiration (ET) Product.* Numerical Terradynamic Simulation Group, College of Forestry and Conservation, The University of Montana, Missoula MT 59812: NASA.

Neitsch, S., Arnold, J., Kiniry, J., & Williams, J. (2009). *Soil and Water Assessment Tool: Theoretical Documentation Version 2009.* Texas Water Resources Institute.

O'Dochartaigh, B., Upton, K., MacDonald, A., Talbot, J., McKenzie, A., Abiye, T., ... Tindimugaya, C. (2019). User guide: Africa groundwater atlas country hydrogeology maps, version 1.1.

Owusu-Ansah, J. K. (2016). The influences of land use and sanitation infrastructure on flooding in kumasi, ghana. *GeoJournal*, *81*(4), 555–570.

Pal, M. (2005). Random forest classifier for remote sensing classification. *International journal of remote sensing*, *26*(1), 217–222.

Panagos, P., Jones, A., Bosco, C., & Senthil Kumar, P. (2011). European digital archive on soil maps (EuDASM): Preserving important soil data for public free access. *International Journal of Digital Earth*, *4*(5), 434-443.

Psomiadis, E., Soulis, K. X., & Efthimiou, N. (2020). Using scs-cn and earth observation for the comparative assessment of the hydrological effect of gradual and abrupt spatiotemporal land cover changes. *Water*, *12*(5), 1386.

Putra, D., & Baier, K. (2008). Impact of urbanization on groundwater recharge–the example of the indonesian million city yogyakarta. In *Un habitat-united nations settlement programs: Fourth session of the world urban forum, nanjing, china, documentations of germany's contribution to a sustainable urban future* (Vol. 2).

Rooyen, J. D. V., Watson, A. P., & Miller, J. A. (2020). Combining quantity and quality controls to determine groundwater vulnerability to depletion and deterioration throughout South Africa. *Environmental Earth Sciences*, *79*(255). doi: 10.1007/s12665-020-08998-1

Shapefiles of all districts in ghana (170 districts). (2019). `https://data.gov.gh/dataset/shapefiles-all-districts-ghana-170-districts`. Ghana Open Data Initiative. (Accessed: 01-03-2021)

Sisay, E., Halefom, A., Khare, D., Singh, L., & Worku, T. (2017). Hydrological modelling of ungauged urban watershed using SWAT model. *Modeling Earth Systems and Environment*, *3*, 696–702. doi: 10.1007/s40808-017-0328-6

Soulis, K. X. (2021). *Soil conservation service curve number (scs-cn) method: Current applications, remaining challenges, and future perspectives.* Multidisciplinary Digital Publishing Institute.

Szilagyi, J., Zlotnik, V. A., Gates, J. B., & Jozsa, J. (2011). Mapping mean annual groundwater recharge in the nebraska sand hills, usa. *Hydrogeology Journal*, *19*(8), 1503–1513.

Tang, J., & Di, L. (2019). Past and Future Trajectories of Farmland Loss Due to Rapid Urbanization Using Landsat Imagery and the Markov-CA Model: A Case Study of Delhi, India. *Remote Sensing*, *11*, 1–18. doi: 10.3390/rs11020180

Tassi, A., & Vizzari, M. (2020). Object-Oriented LULC Classification in Google Earth Engine Combining SNIC, GLCM, and Machine Learning Algorithms. *Remote Sensing*, *12*, 1–17. doi: 10.3390/rs12223776

Theis, C. (1940). The source of water derived from wells. *Civil Engineering*, *10*, 277–280.

UNESCO. (2007). *Groundwater resources sustainability indicators.* UNESCO-IHP.

USDA. (1986). *Urban Hydrology for Small Watersheds - TR 55.* US Department of Agriculture-Soil Conservation Service.

USGS. (2021). *Landsat missions: Landsat 7.* `https://www.usgs.gov/core-science-systems/nli/landsat/landsat-7`. U.S Geological Survey. (Accessed: 25-09-2021)

Vries, J. J. D., & Simmers, I. (2002). Groundwater recharge: an overview of processes and challenges. *Hydrogeology Journal*, *10*, 5–17. doi: 10.1007/s10040-001-0171-7

Vu, H. M., Shanafield, M., & Batelaan, O. (2018). Flux dynamics at the groundwater-surface water interface in a tropical catchment. *Limnologica*, *68*, 36–45.

Wada, Y., Van Beek, L. P., Van Kempen, C. M., Reckman, J. W., Vasak, S., & Bierkens, M. F. (2010). Global depletion of groundwater resources. *Geophysical research letters*, *37*(20).

Wakode, H. B., Baier, K., Jha, R., & Azzam, R. (2018). Impact of urbanization on groundwater recharge and urban water balance for the city of Hyderabad, India. *International Soil and Water Conservation Research*, *6*, 51–62. doi: 10.1016/j.iswcr.2017.10

World Bank. (2015). *Rising through cities in Ghana: Ghana urbanization review overview report.* World Bank Group.

WSUP. (2016). *Improving the quality of public toilet services in Kumasi.* Retrieved from `https://www.wsup.com/content/uploads/2017/08/PN027-Improving-the-quality-of-public-toilet-services-in-Kumasi.pdf` (Accessed: 15-09-2021)

Xie, S., Liu, L., Zhang, X., Yang, J., Chen, X., & Gao, Y. (2019). Automatic land-cover mapping using landsat time-series data based on google earth engine. *Remote Sensing*, *11*(24), 3023.

Yao, L., Wei, W., Yu, Y., Xiao, J., & Chen, L. (2018). Rainfall-runoff risk characteristics of urban function zones in beijing using the scs-cn model. *Journal of Geographical Sciences*, *28*(5), 656–668.

Yeleliere, E., Cobbina, S., & Duwiejuah, A. (2018). Review of ghana's water resources: the quality and management with particular focus on freshwater resources. *Applied Water Science*, *8*(3), 1–12.

Zarei, M., Ghazavi, R., Vali, A., & Abdollahi, K. (2016). Estimating groundwater recharge, evapotranspiration and surface runoff using land-use data: a case study in northeast iran. In *Biol. forum int. j* (Vol. 8, pp. 196–202).

A Appendix

A.1 Assumptions

Table A.1: Overview of all assumptions involved in this study.

Section	Assumption
Recharge using water balance	Groundwater recharge estimates allude to potential recharge: all water that infiltrates reaches the groundwater table (Vries & Simmers, 2002)˙ Groundwater flow is negligible when averaging over a longer time period (∼10y). Recharge is rain-dominated and groundwater-surface water negligible. Interaction cannot be quantified using water-balance approach. However,in dry months recharge can occur due to physical subsurface processes delaying water in the unsaturated zone from instantaneously recharging (Gemitzi et al., 2017; Bierkens & Wada, 2019). Only natural recharge is considered: recharge from irrigation, pipe leaks, sewage, etc. are not considered. Streams do not contribute to groundwater replenishment in the dry season as they are assumed to be gaining streams (i.e. streams are filled during the rainy season due to rain and drainage).
Curve numbers	Impervious area is connected to drainage system. Initial abstraction = $0.2S$ (Mishra & Singh, 2013) Bare land is in poor hydrologic condition (<50% grass cover), dense vegetated cover is in good hydrologic condition (>75% vegetated cover), sparse vegetation in fair condition (50-75% grass cover).
Runoff	Q_{in} = Q_{out} : effect of runoff on recharge from outside the urban boundary is not considered. Infiltration occurs instantaneously.
Evapotranspiration (modified estimate)	Intra-class differences in evapotranspiration between individual vegetation types, soil types, urban cover, etc. negligible. MODIS evapotranspiration is closer to potential ET during the rainy season and closer to actual ET during the dry season.
Groundwater abstraction	Population growth rate since 2010 = 5.5%. Drinking water consumption is substantially less than domestic water use, therefore the groundwater use percentage for domestic consumption (24%) is used to estimate groundwater use water totals. Groundwater consumption percentage and individual total water consumption is constant from 1986 to 2020. Household percentage consumption = individual consumption. 2021 non-domestic consumption results applicable to 2020.
Sustainability	Range in recharge values determined by using lower boundary of initial abstraction Ia = $0.1S$ instead of Ia = 0. This is assumed to be a more realistic value.

A.2 Soil maps

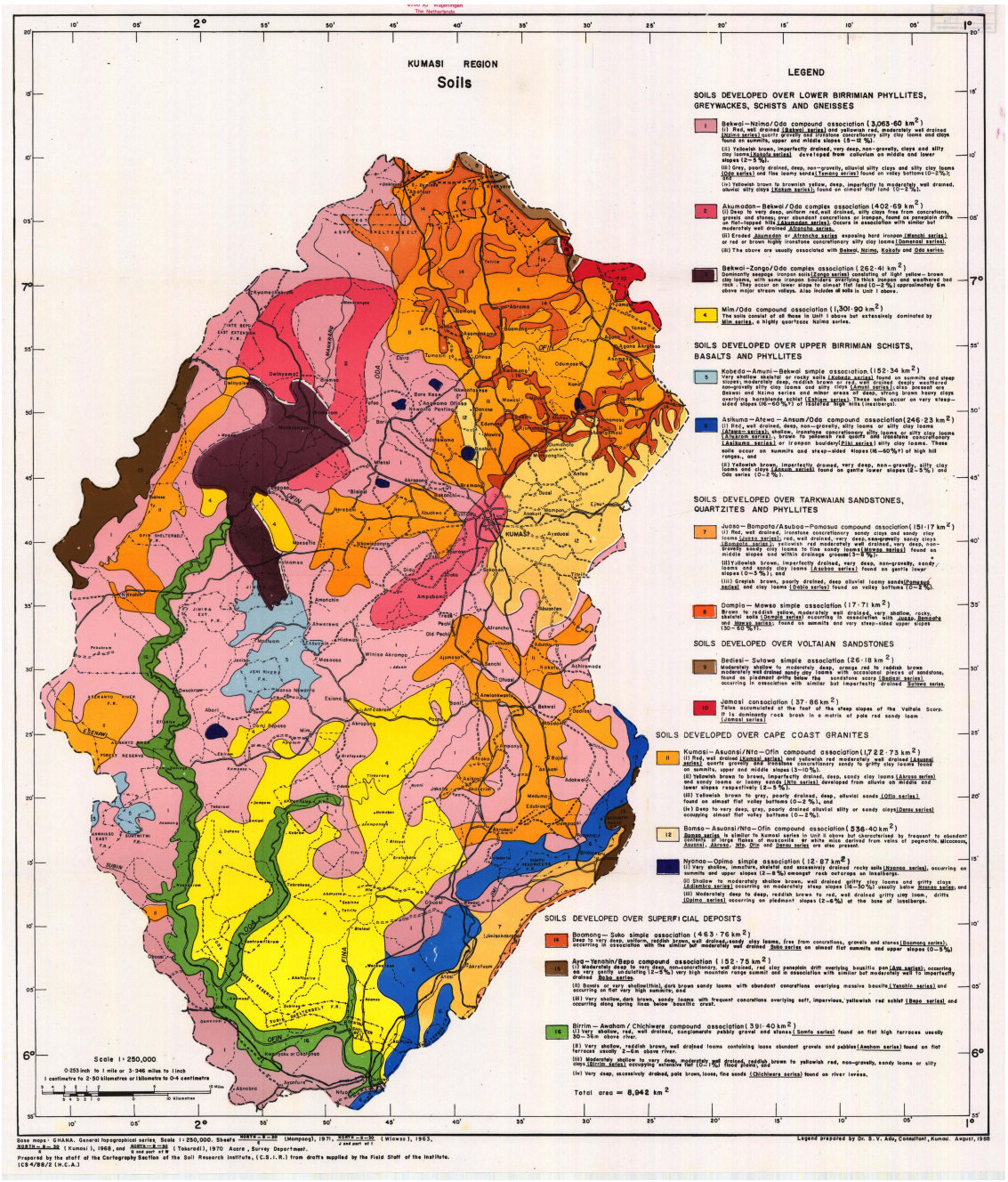

Figure A.1: Soil map used for HSG derivation including soil type and their properties in the region of Kumasi. Retrieved from Panagos et al. (2011).

A.3 Spectral ranges

Table A.2: Wavelength ranges for the different bands of surface reflectance products from Landsat 5, 7, 8, and Sentinel-2A. Landsat SR wavelengths retrieved from Earth Engine Data catalog and Sentinel-2 SR wavelengths retrieved from ESA (2020).

Band	Landsat 8	Landsat 5 & 7	Senintel 2A
	Wavelength range (μm)		
Blue	0.452-0.512	0.45-0.52	0.4594-0.5254
Green	0.533-0.590	0.52-0.60	0.5418-0.5778
Red	0.636-0.673	0.63-0.69	0.6491-0.6801
NIR	0.851-0.879	0.77-0.90	0.7798-0.8858
SWIR1	1.566-1.651	1.55-1.75	1.5682-1.6592
SWIR2	2.107-2.294	2.08-2.35	2.1149-2.899

A.4 Land cover classifications

Table A.3: Overview of areas (rounded to nearest km^2) covered by each land class for the different classifications and their corresponding accuracies.

Land class	Sentinel 2		Landsat		
	2020 (full bands)	**2020 (less bands)**	**2020**	**2013**	**1986**
Urban semipervious	166	164	164	113	38
Urban impervious	28	28	29	4	4
Bare land	3	3	5	2	3
Dense vegetation	7	6	8	40	118
Sparse vegetation	37	40	36	83	79
Water	0	0	0	0	0
Validation accuracy	*0.9*	*0.83*	*0.82*	*0.82*	*0.82* height

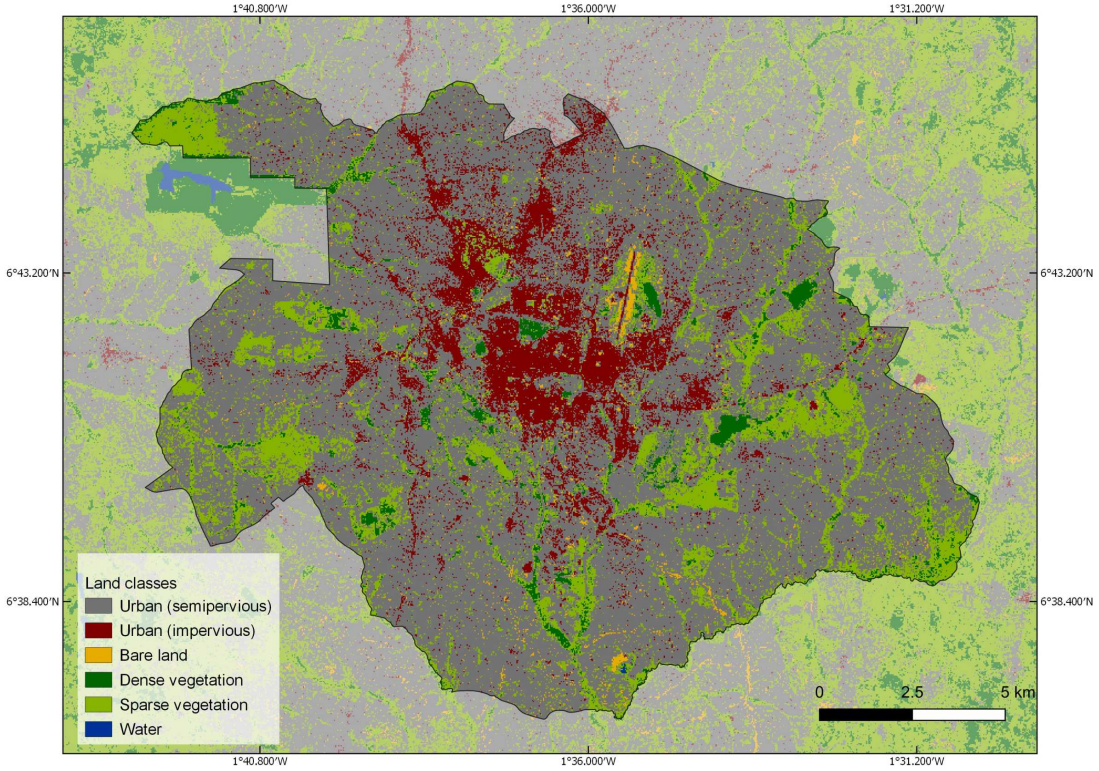

Figure A.2: 2020 land use map for Kumasi trained on Sentinel-2 2020 composite using RGB, Red edge bands, NIR, SWIR1, SWIR2 bands.

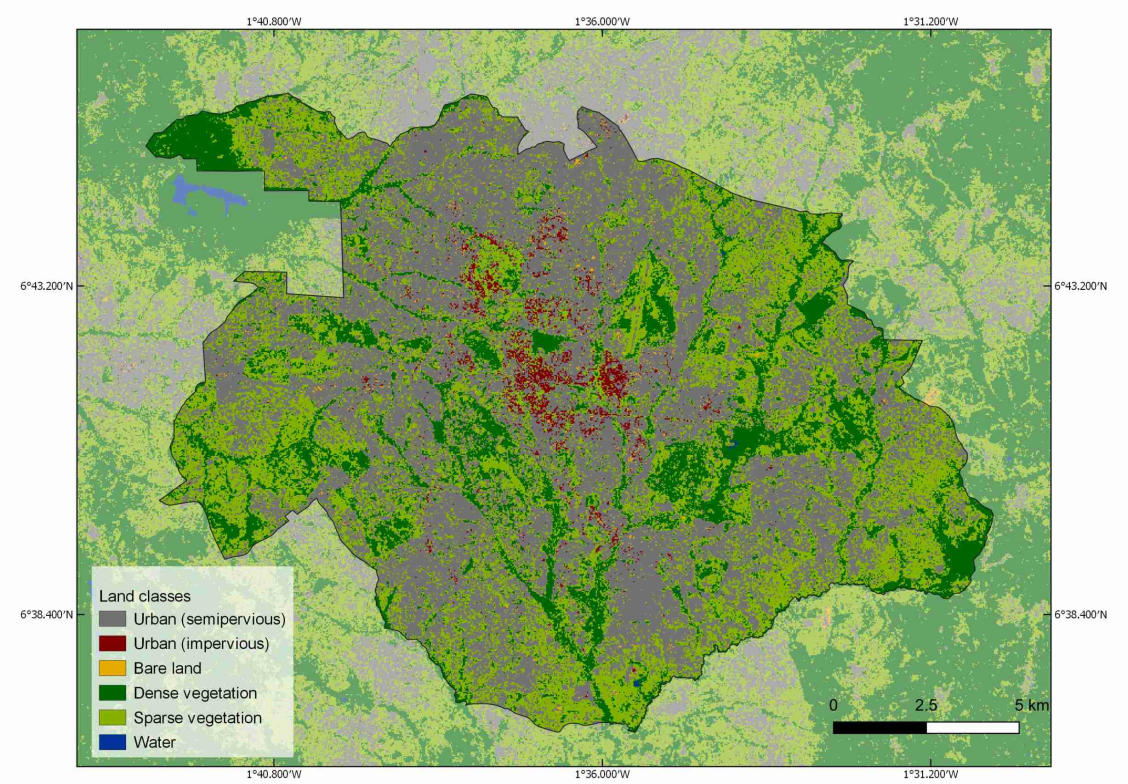

Figure A.3: 2013 land use map for Kumasi trained on Landsat 8 2020 composite using RGB, NIR, SWIR1, SWIR2 bands.

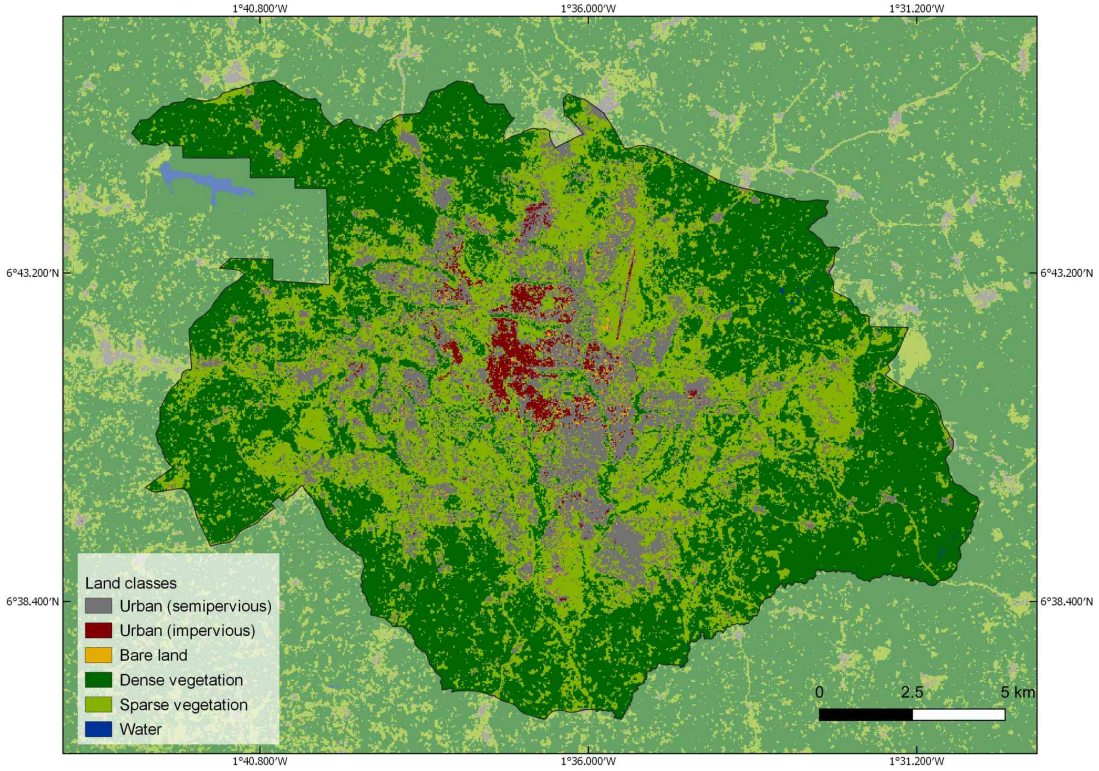

Figure A.4: 1986 land use map for Kumasi trained on Landsat 8 2020 composite using RGB, NIR, SWIR1, SWIR2 bands.

A.5 Selected Curve Numbers and their corresponding USDA (1986) definitions.

Table A.4: Detailed overview of the selected curve numbers for each class and their representative land cover descriptions from USDA

Cover type	**Corresponding cover type from USDA look-up tables**	**Hydrologic soil group**		
		A	**B**	**D**
Urban (impervious) *No grass cover, vegetation, only roofs, paved roads in area*	Paved lots, parking, driveways	98	98	98
Urban (semipervious) *Urban mixed with some vegetation, infiltration occurs on roads, non built-up areas (∼30% pervious)*	Streets: paved; open ditches	83	89	93
	Streets: dirt	72	82	89
	Streets: gravel	76	85	91
Bare land	Open space in poor condition (grass cover <50%)	68	79	89
Dense vegetation	Woods (no grass combination), assume good condition (woods protected from grazing, litter and brush adequately cover soil)	30	55	77
Sparse vegetation	Open spaces in good condition	39	61	80
	Meadow (continuous grass, protected from grazing, often mowed)	30	58	78
	Brush (weed and grass mixture) fair condition	35	56	77
	Woods with grass combination fair condition	43	65	82

A.6 Evapotranspiration initial results

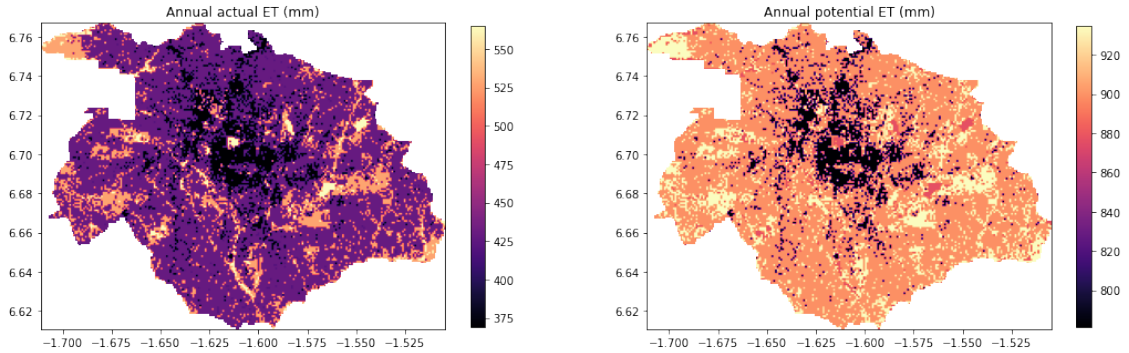

(a) Annual average evapotranspiration based on averages per land use class from 2020 classification.

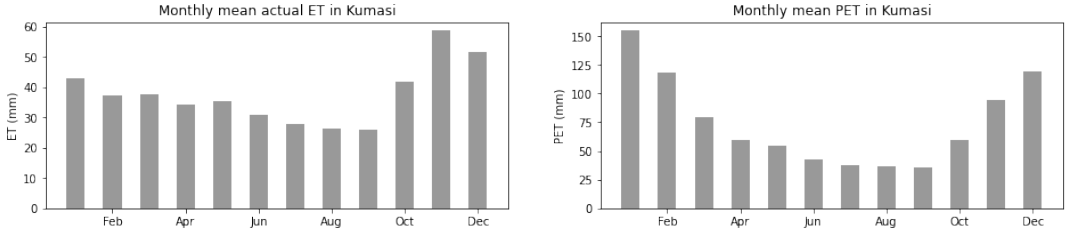

(b) Monthly average evapotranspiration based on averages per land use class from 2020 classification.

Figure A.5: Actual and potential evapotranspiration per land use class. Averages are taken from the extent of the classification and re-applied to the area of Kumasi. This was done on a monthly basis for the period of 2001-2020. Mean annual actual ET is 443mm and mean annual PET is 891mm.

A.7 Groundwater recharge

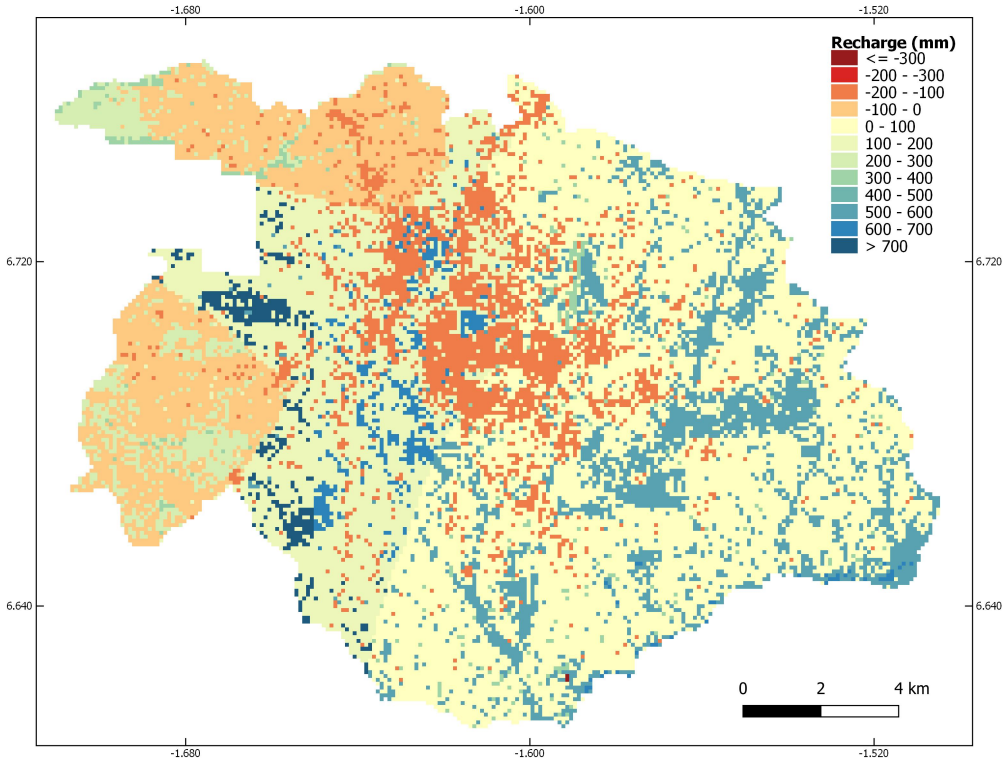

Figure A.6: Raw, non-filtered groundwater recharge results for 2020 land use map and 2001-2020 forcing data.

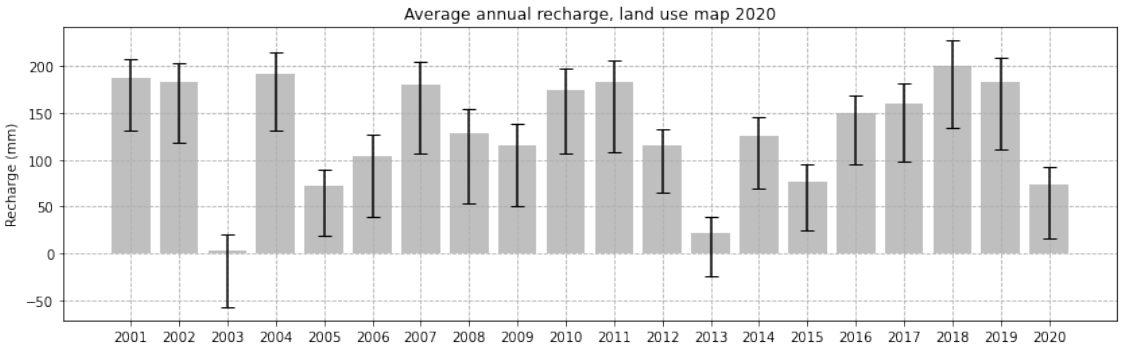

Figure A.7: Uncertainties in annual recharge totals based on sensitivity scenarios.

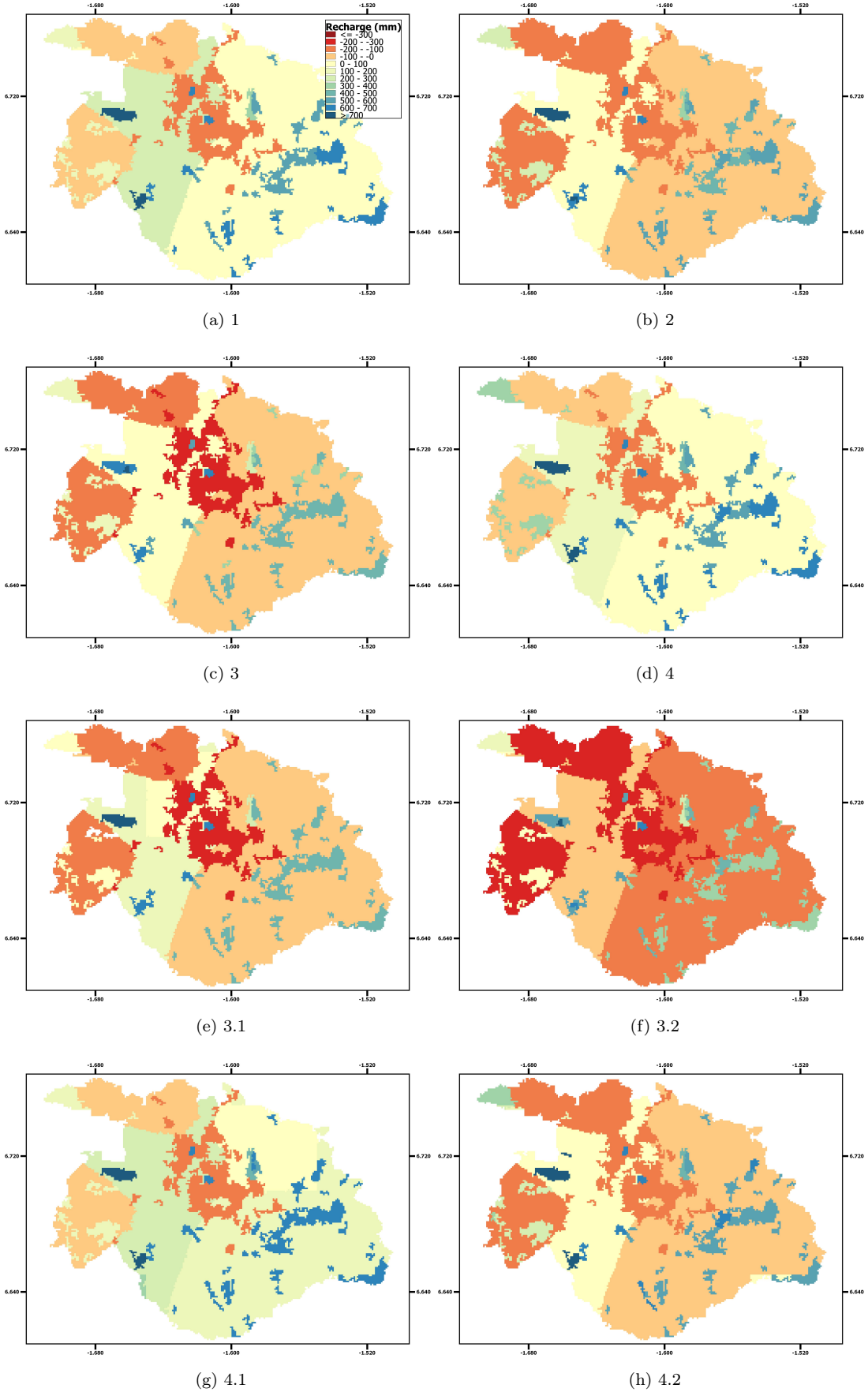

(a) 1 (b) 2

(c) 3 (d) 4

(e) 3.1 (f) 3.2

(g) 4.1 (h) 4.2

Figure A.8: Average annual recharge per sensitivity scenario. See Table 7.2 for sensitivity parameters. Legend in (a) applies to all maps.

A.8 TAHMO station locations

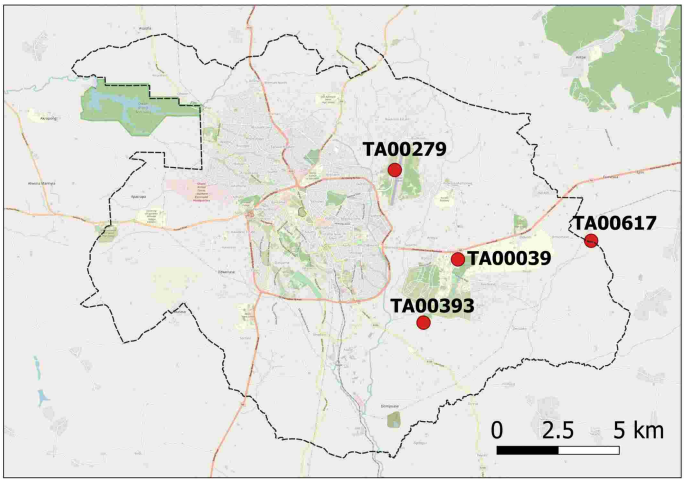

Figure A.9: Locations of four TAHMO stations in Kumasi.

A.9 Population

Table A.5: Population numbers from 1960 to 2010. Prediction for 2020 based on 5.5% growth rate since 2010.

Year	Population	Source
1960	100,584	Kuma (et.al)
1970	346,336	Ghana Statistical Service (2013b)
1984	496,628	
2000	1,170,270	
2010	2,035,064	
2020	3,476,183	Apply annual growth rate of 5.5% Ghana Statistical Service (2013a)

A.10 Water consumption

Table A.6: Principal sources of water for drinking and domestic purposes in Kumasi. Data summarised from Ghana Statistical Service (2013a).

	Drinking	**Domestic**
Source of water	**% of households**	**% of households**
Pipe borne (inside and outside dwelling)	66.5	67.2
Public tap (pipe)	7.6	7.7
Borehole/pump/tube well	12.6	14.7
Protected well	6.4	8.6
Bottled water	0.4	-
Protected spring	0.4	0.3
Sachet water	5.2	-
Tanker supply/vendor	0.3	0.3
Unprotected well	0.2	0.5
River/stream	0.1	0.3
% groundwater source	**19.2**	**23.8**

Table A.7: Survey results (n = 52 locations) for non-domestic groundwater consumption in Kumasi.

Type of facility	n	%
Hotel & restaurant	13	25
Sachet water	1	2
Car wash	20	38
Laundry	1	2
Private Hospital	1	2
Restaurant	4	8
School	1	2
Public toilet	5	10
Hostel	4	8
Public tap	2	4
Has the water source dried up before?		
Never dried up	47	90
Never dried up (low yield in dry	3	6
Yes (dry season)	2	4
Usage period (years)		
1 to 9	35	67
10 to 19	12	23
20 to 30	5	10
Purpose		
All purpose	2	4
Don't drink	19	37
Drinking	21	40
Washing cars	9	17
Flushing toilet	1	2
Water quality issues		
None	50	96
Colour issues	2	4
Water used per day (L)		
1000-5000	24	46
5000-8000	16	31
8000-12000	8	15
12000-16000	4	8

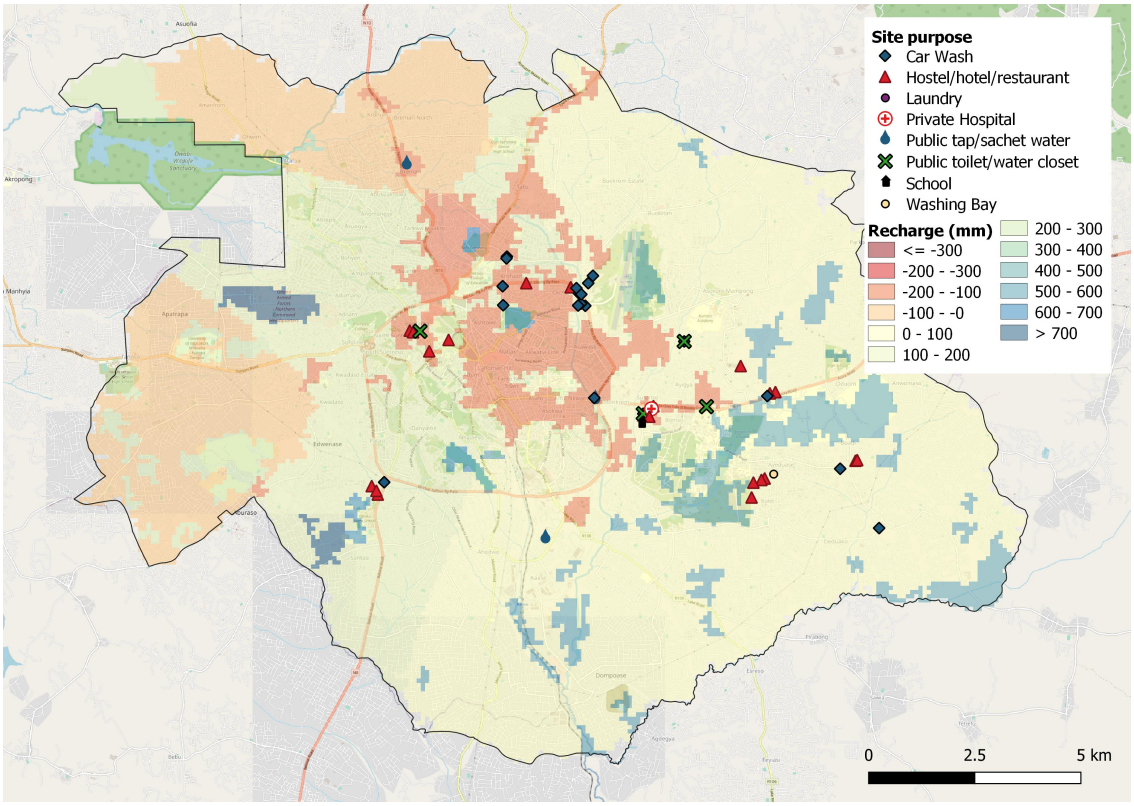

Figure A.10: Survey locations and corresponding non-domestic functions of each point.

B Google Earth Engine script

Google Earth Engine access is only possible is users are registered. Once this is done, supplementary material to run the scripts should be downloaded from `http://repository.tudelft.nl/`. This includes the following files:

1. 2020 classification map over Kumasi: "classification2020_S2.tif"
2. 2013 classification map over Kumasi: "classification2013_L8.tif"
3. 2003 classification map over Kumasi: "classification2003.tif" (optional)
4. 1986 classification map over Kumasi: "classification1986_L5.tif"
5. Hydrological soil groups: "HSG.kumasi.tif"
6. Kumasi outline: "Kumasioutline.zip"

Groundwater recharge: `https://code.earthengine.google.com/e2777cbfd10b4e65d278c9d2456f9ae8`
Land use classification: `https://code.earthengine.google.com/354e640cbbce643507af82463dd7cf88`